Applications of Evolutionary Modeling to the Study of Drug Resistance in Cancer

A DISSERTATION
SUBMITTED TO THE FACULTY OF THE GRADUATE SCHOOL
OF THE UNIVERSITY OF MINNESOTA
BY

Danika Gray Lindsay

IN PARTIAL FULFILLMENT OF THE REQUIREMENTS
FOR THE DEGREE OF
DOCTOR OF PHILOSOPHY

Jasmine Foo

July, 2018

Acknowledgements

I am eternally grateful to those who have supported me on my journey through graduate school, both professionally and personally.

First, I would like to thank my committee members for taking the time to read my thesis and provide me with their feedback. In particular, I want to thank my advisor, Jasmine Foo, for everything I have learned over the past four years about cancer modeling and how to be a successful mathematician. I also want to thank Dick McGehee for his professional guidance and support throughout my graduate school career.

I would like to acknowledge the support of the National Science Foundation under grant numbers DMS-00039202 and DMS-1349724. In addition, I want to thank my collaborators, Shannon Mumenthaler and Colleen Garvey, as well as my professional mentors. I especially want to extend my sincerest gratitude to Cynthia Wyels for her continued support, advice, guidance, feedback, and mentorship over the course of the past decade.

The completion of this thesis would never have been possible without the constant love and support of my family and friends. To Mom, Dad, Kira, and Grammy: Thank you for always cheering me on and making me feel loved, even when you were 1,529 miles away. I am also very grateful to have had you as my own personal team of editors this year during my job search. To the Kibby family: Thank you for accepting me into your family and for your understanding and patience during the countless hours I spent working on research in your guest room. To Sam, Katie, Will, and Daniel: The highlight of my experience in graduate school is, without a doubt, the lifelong friendships I have made with each one of you. Thank you for your continued support and for sharing in this experience with me in a way no one else quite could. I never would have made it

through the past six years without our little friend group.

Finally, I want to thank my best friend and the love of my life: Blake Kibby. You have been my partner in this adventure and my rock every step of the way – from helping me with my applications when graduate school was just a distant dream to moving across the country and making a life with me in Minnesota to now and everything in between. Thank you for everything you have done to take care of me over the past six years when I was too busy or stressed to take care of myself. Your endless love, support, and encouragement are what made my dream a reality and, for that, I will be forever grateful. I love you so much. Here's to our next chapter!

Dedication

This thesis is dedicated to my mom, Cathy, whose battle with cancer inspired me to study mathematical biology and cancer modeling.

Abstract

The evolution of resistance to therapy remains a significant challenge to the clinical treatment of cancer. As a tumor evolves, new genetic variants possessing a fitness advantage over normal cancer cells may be produced, thus leading to the development of resistance. Because the underlying biological processes driving this evolution are inherently random, they may be modeled using stochastic processes. This thesis consists of two main projects in which branching process models are employed to study the evolution of resistance to cancer therapy.

In the first project, we develop a stochastic model of a non-small cell lung tumor undergoing treatment with a combination of two drugs. One drug is the current standard therapy used in the clinic to treat this disease, which has proven to be ineffective in the long term due to the inevitable development of resistance. The other is a novel drug specifically aimed at targeting oxygen-deprived regions in tumors. Using this model, we show that a therapeutic regimen in which both drugs are given may greatly improve patient outcomes over the current standard monotherapy. We also use our model to predict the optimal combination treatment protocol.

The goal of the second project is to understand the impact of different resistance mechanisms on tumor recurrence. We define two separate branching process models to compare the case in which resistance arises via a single gene mutation with the case in which resistance arises via a gradual gene amplification process. We prove law of large numbers results regarding the convergence of the stochastic tumor recurrence times in both models and use these results to compare the two resistance mechanisms.

Contents

List of Tables

List of Figures

Chapter 1

Introduction

Cancer is a leading cause of death worldwide, and many cancer-related deaths can be attributed to the development of resistance to therapy. Traditionally, cancer has been treated using a variety of chemotherapeutic agents. However, recent efforts to better understand the specific molecular processes underlying the growth and spread of cancer have led to the development of a new treatment modality known as "targeted therapy" [1]. This term refers to any anticancer therapy designed to act on a specific molecular target believed to play a critical role in cancer progression. The invention and widespread clinical use of these targeted therapies has significantly impacted the way in which certain cancers are treated [2]. Tyrosine kinase inhibitors such as imatinib, gefitinib, and erlotinib represent a primary example of this shift in approaches to treatment [3]. Imatinib is currently used in the clinic as a first-line treatment for chronic myelogenous leukemia (CML). Additionally, non-small cell lung cancers (NSCLCs) driven by mutations in the epidermal growth factor receptor (EGFR) are very responsive to both gefitinib and erlotinib. In contrast with traditional cytotoxic chemotherapy, these drugs stop the growth and spread of NSCLC by preventing the cancer cells from multiplying.

Although initially hypothesized to revolutionize the treatment of cancer, targeted therapies have some very significant drawbacks, the most notable of which is the development of resistance. The evolution of drug resistance is evident in virtually all patients who undergo therapy with one of these targeted drugs [4]. For example, despite initial responses to therapy, NSCLC patients taking erlotinib eventually experience disease progression, usually within a period of 12 to 18 months after starting treatment [5]. This

development of resistance to targeted therapies remains a significant challenge to the clinical treatment of cancer. Acquiring a more complete understanding of the evolution of resistant cancer cell populations during therapy may be the key to designing more effective therapeutic regimens capable of preventing or delaying disease progression due to resistance.

A significant amount of research effort has been dedicated to gaining insights into the development of resistance via mathematical modeling. Some of these models have focused on answering questions regarding the case of pre-existing resistance, in which resistant cells arise prior to the beginning of treatment. Other models have been developed to address the problem of resistance emerging during the course of treatment. In this thesis, we will focus on the second case, in which a patient who is initially sensitive to therapy acquires resistance.

Goldie and Coldman used a stochastic mathematical model to examine the probability of resistance arising during therapy, and concluded that both early initiation of therapy and the use of multiple drugs in combination can reduce the risk of resistance [6, 7]. Later on, using a multi-type pure birth process, Coldman and Murray found that early intensification of therapy maximizes the product of the probability of cure and the probability of no toxicity [8]. More recently, Iwasa et al. used a mutli-type branching process to model a heterogeneous population of cells and found that the probability of cure is largest when many different drugs are used since the cancer cells cannot escape extinction unless they evolve mutations that confer resistance to all of the drugs [9].

Komarova and Wodarz developed a stochastic model to study multi-drug resistance, where resistance to each drug is driven by an independent mutation [10]. They then defined another stochastic model to examine the effect of cancer stem cell quiescence on the development of resistance [11]. Using the model previously defined by Komarova in [12] together with a computational approach, Komarova et al. found that the use of two drugs increases the probability of treatment success in CML, but additional drugs provide no additional advantage [13].

In order to reflect the anti-proliferative effect of many targeted therapies, Foo and Michor constructed a non-homogeneous multi-type birth-death process model of resistance in which birth and death rates of both sensitive and resistant cells vary with drug concentration [14, 15]. They developed an approach to identify optimal dosing

strategies, given drug concentration-dependent birth and death rates. Specifically in the context of EGFR-mutant NSCLC, Chmielecki et al. and Foo et al. used evolutionary modeling to identify optimal dosing strategies to either prevent or delay resistance to erlotinib [16, 17]. Later on, Foo and Leder used a similar branching process model to characterize the time during treatment at which the tumor population begins expanding as well as the time at which the resistant cells begin to dominate the tumor [18].

The remainder of this thesis builds on this body of work and is divided into two main parts. Chapter 2 employs a computational approach to solve a more applied problem, whereas Chapter 3 utilizes an analytical approach to solve a more theoretical problem. In Chapter 2, we use a stochastic model of EGFR-mutant NSCLC to understand the impact of tumor heterogeneity on the evolution of resistance to erlotinib. This model suggests that, by combining erlotinib with a second drug specifically designed to target oxygen-deprived regions within the tumor, patient outcomes may be significantly improved. Furthermore, we optimize combination treatment protocols to minimize tumor burden and risk of resistance. The work in Chapter 2 was completed in collaboration with Shannon Mumenthaler and Colleen Garvey at the University of Southern California. In Chapter 3, we study the stochasticity of the tumor recurrence time in two different models in which resistance arises via two separate biological mechanisms. We prove law of large numbers results for both of these stochastic times and use our results to compare the impacts of these two resistance mechanisms on tumor recurrence.

Chapter 2

Understanding the Impact of the Tumor Microenvironment

2.1 Background

Solid tumor vasculature is characterized by a disorganized, aberrant network structure of tortuous, hyperpermeable blood vessels [19]. These characteristics lead to nonuniform spatial distributions of drug and oxygen (as well as other nutrients and growth factors) throughout tumors, which in turn have been implicated in the emergence and evolution of resistance [20, 21, 22, 23, 24, 25]. Indeed, several recent studies have demonstrated that the presence of spatial gradients of drug in an environment can accelerate the emergence of antibiotic resistance in bacteria [26, 27]. One explanation for this phenomenon is that regions of low drug concentration generate local niches where sustained cell proliferation drives the production of new genetic variants. These spatial regions often coincide with hypoxic (low oxygen) conditions where drug-resistant variants may possess a survival advantage over drug-sensitive cells [28, 20, 29, 30, 31], thus enabling the establishment of stable pockets of drug resistance in tumor regions not easily accessible by drugs. In light of these observations, one strategy proposed is to design therapy regimens that exploit the interaction between tumor cell populations and their environments to achieve long-term tumor eradication or control.

Hypoxia is defined as reduced levels of molecular oxygen (typically less than 1%) in tissue. In contrast, ambient air exists at approximately 21% and most human organs

have oxygen levels in the range of 2% to 9% [32]. The prevalence of hypoxic regions in solid tumors has led to the development of hypoxia-activated prodrugs (HAPs), which are compounds designed to metabolize into active drugs upon entry into hypoxic environments [33, 34, 35, 36]. For example, one such compound, evofosfamide, consists of a radical anion linked to a potent DNA-alkylating agent which penetrates effectively through tissues under normoxic (normal oxygen) conditions. Under hypoxic conditions, however, the radical anion undergoes irreversible fragmentation and releases the activated drug into the tumor [37, 36]. This type of novel action allows evofosfamide to penetrate and target cancer cells within hypoxic regions of a tumor, unlike standard therapies whose range is often confined to well-vascularized, normoxic regions.

Currently, several HAPs are in clinical trials [38]. Tirapazamine was the first HAP to be tested in the clinic, in combination with both chemotherapy and radiotherapy; however, results did not show any significant therapeutic benefit. It was thought that off-target toxicity and insufficient tissue penetration were the primary contributing factors to this result. More recently, evofosfamide, which has a superior tissue-penetration ability, underwent Phase III testing in combination with chemotherapies for pancreatic cancer and soft tissue sarcoma. Neither of these trials demonstrated a significant survival benefit. However, given the response kinetics of hypoxic cancer cells to these therapies in preclinical studies, we hypothesize that the potential of HAPs has not yet been fully realized in previous clinical trials, and that mathematical modeling may be beneficial in identifying the combination treatment strategies that lead to survival benefit. It has been demonstrated in previous work that identifying the right dosing schedule is important in improving cancer treatment outcomes, and further that mathematical modeling is an effective tool to help identify optimal administration strategies [16, 17, 39]. In particular, it was demonstrated in [39] that altering the timing of treatment periods in sequential combination therapies may prevent or delay the emergence of drug resistance.

This work builds upon a large body of literature on evolutionary modeling of drug resistance in cancer (see, e.g. the review [40] and references therein). Here we discuss a few recent contributions to modeling combination therapies in cancer. For example, Komarova et al. [13] utilized a stochastic birth-death process model to study the impact of combination therapies in Chronic Myeloid Leukemia, finding that a combination of

two but not three drugs should be used in the prevention of drug resistance. In a later work by the same authors, Katouli et al. [41] designed a general algorithm to compare combination treatment protocols in Chronic Myeloid Leukemia according to their cross-resistance properties, and to identify the protocols with the highest probability of treatment success. Most recently, Bozic et al. [42] developed a mathematical model that predicts responses to combinations of targeted inhibitors in melanoma patients. Using this model, the author predicted that combinations of two or three drugs will be far more effective than sequential treatment with the same agents, with the potential for complete cure.

Here we will focus our modeling efforts on designing HAP-targeted combination treatment strategies for NSCLC. Erlotinib is a tyrosine kinase inhibitor commonly used to treat EGFR-mutant NSCLC [43, 44, 45]. However, most patients develop resistance and disease progression within 12-18 months of starting treatment [5]. Consequently, novel approaches to prevent, or at least delay, the onset of resistance to erlotinib are of great clinical importance. A significant amount of research has been dedicated to improving treatment of NSCLC. Several studies have shown that it may be beneficial to continue therapy with tyrosine kinase inhibitors such as erlotinib even after the point of disease progression [46, 47, 48]. Previous work has focused on the use of mathematical models of tumor growth and resistance during erlotinib treatment to optimize therapeutic strategies and minimize a patient's risk of resistance [17, 16]. Another approach that has been extensively studied is the use of combination therapy to mitigate resistance to erlotinib [39, 49, 50]. However, these studies lack a consideration for the heterogeneous oxygen and drug distributions throughout the tumor, and in particular their role in mediating tumor response to therapy and the emergence of drug resistance. Recently, Mumenthaler et al. demonstrated through modeling efforts that the consideration of heterogeneous tumor oxygenation and drug concentration reveals dramatically different treatment outcomes and evolutionary responses to therapy when compared to models under homogeneous environmental conditions [20].

In this work, we investigate the potential benefits of using a HAP in combination with standard therapy to prevent the emergence of resistance to erlotinib in NSCLC. We design a stochastic mathematical model, with parameters informed by experimental

data, to describe the evolutionary dynamics of a cancer cell population within a heterogeneous tumor microenvironment during treatment with erlotinib and evofosfamide. Using this model, we show that a combination treatment strategy results in treatment outcomes preferable to those resulting from monotherapy with either of these drugs alone. We also use a novel approach to define toxicity constraints for this combination therapy, which allows us to optimize treatment strategies over the space of tolerated dosing schedules using both drugs in order to minimize tumor burden and probability of resistance. Determining toxicity constraint profiles for combination therapies could have significant clinical implications as severe toxicity issues is one of the major reasons that HAP combinations have not been successful in clinical trials.

2.2 Methods

In the following we describe an evolutionary mathematical modeling approach to evaluate the impact of combination erlotinib-evofosfamide therapy on a NSCLC tumor cell population, in which each tumor cell response is dependent upon local environmental concentrations of oxygen and drug. The pseudo-spatial model is comprised of a weighted series of environmental compartments whose oxygen and drug profiles mirror tumor physiologic data. The model is parameterized using (i) experimentally calculated growth rates under a spectrum of environmental perturbations of oxygen and erlotinib concentration, (ii) published experimental results on cell viability in response to evofosfamide therapy, (iii) tumor oxygenation measurements, and (iv) pharmacokinetic data mapping evofosfamide and erlotinib dose to plasma concentration. We also utilize clinical trial data for both therapies to design a methodology for inferring toxicity constraints on the space of possible combination treatment strategies.

2.2.1 Evolutionary Model

In order to model tumor evolution within an environment with heterogeneous oxygen and drug concentrations, we consider a stochastic population dynamic process in which the cell population is distributed amongst a series of habitats with varying oxygen and drug profiles. Oxygen concentration within the tumor decays exponentially as a function of distance from the nearest blood vessel. This decay rate is parameterized in the model

based on estimates of the half-length away from the blood vessel [20]. This is used to define the oxygen concentration in each microenvironmental compartment; hence every compartment corresponds to a volume some distance from the nearest blood vessel. To estimate the relative contributions of each of these compartments to the tumor microenvironment, we utilize experimental data capturing relative frequencies of a spectrum of oxygen partial pressures throughout solid tumors [51]. We consider a total of 32 environmental compartments in which compartment i has an oxygen partial pressure of $2.5 \cdot i$ mmHg to mirror this data. We then construct a mixture model of compartments in which the weighting of each compartment is determined based on the relative frequency of its corresponding oxygen partial pressure in the experimental profile. A schematic of this process is depicted in Figure 2.1.

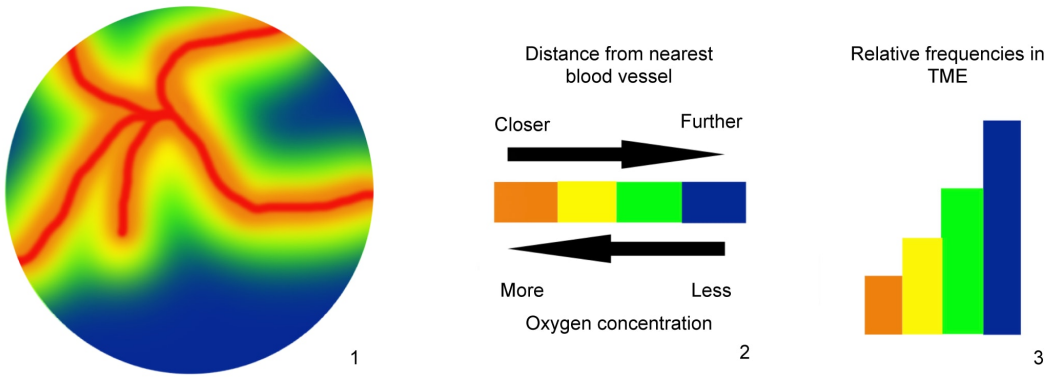

Figure 2.1: **Tumor microenvironment modeling process.** This schematic shows the process used to model the tumor microenvironment as a set of discrete compartments. A series of compartments is defined based on various distances from the nearest blood vessel, and the oxygen concentration in each compartment is calculated accordingly. The relative weights of the compartments are determined based on experimental observations of oxygen partial pressure distribution in solid tumors.

Within each compartment, we use a multi-type, non-homogeneous, continuous-time birth-death process to model the population of cancer cells during treatment. We assume for now that the evolutionary dynamics within each microenvironmental compartment are independent. (This assumption will be relaxed later, see Section 2.5.) The number of erlotinib-sensitive cells in compartment i at time t is denoted by $X_i(t)$, and the number of erlotinib-resistant cells in compartment i at time t is given by $Y_i(t)$. The joint process

$\mathbf{X}_i(t) = (X_i(t), Y_i(t))$ represents the combined state of the sensitive and resistant cell populations in compartment i at time t. In compartment i, erlotinib-sensitive cells proliferate and die with rates $\lambda_{X,i}(t)$ and $\mu_{X,i}(t)$, respectively, while erlotinib-resistant cells proliferate and die with rates $\lambda_{Y,i}(t)$ and $\mu_{Y,i}(t)$. These birth and death rates reflect the effect of treatment on the cancer cell population in an environmental compartment i, and therefore depend on the concentrations of oxygen and both drugs found in that compartment at time t. During every sensitive cell division, a mutation may arise with some small probability u, giving rise to a new resistant cell. This mutation rate falls in the range between 10^{-8} and 10^{-6} [17, 52, 53]. Here we use $u = 10^{-7}$. We consider an initial population of $M = 1.6 \cdot 10^6$ erlotinib-sensitive cancer cells and zero resistant cells. The number of sensitive cells M_i initially in compartment i is calculated using the relative compartment weights.

The evolutionary dynamics within each microenvironmental compartment can be described using analytic approximations for the probability of resistance and means of the sensitive and resistant cell populations. The derivations of these analytic expressions are outlined elsewhere [15]. Because u is very small, we approximate $1 - u \approx 1$ in the following. Then the population of sensitive cells $X_i(t)$ in compartment i can be described using a simple birth-death process. Hence the mean number of sensitive cells at time t in this compartment is

$$\mathbb{E}[X_i(t)] = M_i \exp\left[\int_0^t (\lambda_{X,i}(\tau) - \mu_{X,i}(\tau))\, d\tau\right]. \tag{2.1}$$

The mean number of resistant cells in this compartment at time t is

$$\mathbb{E}[Y_i(t)] = \int_0^t b_i(\tau) \exp\left[\int_0^{t-\tau} (\lambda_{Y,i}(\tau + \eta) - \mu_{Y,i}(\tau + \eta))\, d\eta\right] d\tau, \tag{2.2}$$

where $b_i(t)$, the rate of production at time t of the resistant cells from the sensitive cell population in compartment i, is given by the formula

$$b_i(t) = M_i \exp\left[\int_0^t (\lambda_{X,i}(\tau) - \mu_{X,i}(\tau))\, d\tau\right] \lambda_{X,i}(t) u.$$

Lastly, the probability of resistance in compartment i at time t is

$$\mathbb{P}[Y_i(t) > 0] = 1 - \exp\left[\int_0^t -b_i(T)\left(1 - P_i^{ext}(T,t)\right) dT\right]. \tag{2.3}$$

$P_i^{ext}(T,t)$ represents the probability that a group of resistant cells originating from a single resistant cell produced at time T in compartment i is completely extinct by time t, and is given by the formula

$$P_i^{ext}(T,t) = \frac{\int_0^{t-T} \mu_{Y,i}(\tau+T)\omega_i(\tau,T)d\tau}{1+\int_0^{t-T} \mu_{Y,i}(\tau+T)\omega_i(\tau,T)d\tau},$$

where

$$\omega_i(\tau,T) = \exp\left[\int_0^{\tau} \left(\mu_{Y,i}(\eta+T) - \lambda_{Y,i}(\eta+T)\right) d\eta\right].$$

Now we calculate the probability of resistance and means of the sensitive and resistant cell populations in the entire tumor at time t. We can obtain the means at time t of the sensitive cell population $X(t)$ and the resistant cell population $Y(t)$ in the entire tumor by summing over all compartments:

$$\mathbb{E}[X(t)] = \sum_i \mathbb{E}[X_i(t)],$$
$$\mathbb{E}[Y(t)] = \sum_i \mathbb{E}[Y_i(t)].$$

Here, $\mathbb{E}[X_i(t)]$ and $\mathbb{E}[Y_i(t)]$ are given by equation (2.1) and equation (2.2), respectively. The mean tumor size at time t is given by

$$\mathbb{E}[X(t) + Y(t)] = \mathbb{E}[X(t)] + \mathbb{E}[Y(t)].$$

The probability that there exists one or more resistant cells in compartment i at time t is $\mathbb{P}[Y_i(t) > 0]$. Then $1 - \mathbb{P}[Y_i(t) > 0]$ is the probability of having zero resistant cells in this compartment at time t. Since we assume independence of the microenvironmental compartments, this implies the probability of having no resistant cells in the entire tumor at time t is given by $\prod_i (1 - \mathbb{P}[Y_i(t) > 0])$. Therefore, the probability of resistance at time t is

$$\mathbb{P}[Y(t) > 0] = 1 - \prod_i \left(1 - \mathbb{P}[Y_i(t) > 0]\right),$$

where $\mathbb{P}[Y_i(t) > 0]$ is given by equation (2.3).

2.2.2 Model Parameterization

The evolutionary dynamics of the tumor cell population depend on the birth and death rates of sensitive and resistant cells in each microenvironmental compartment. These rates, in turn, vary as the concentrations of both drugs change over time. To reflect this variation, we first define distinct functions describing the individual effects of erlotinib and evofosfamide on these birth and death rates. The growth kinetics of the cancer cell population during treatment by each of these drugs are estimated using a combination of pharmacokinetic and experimental cell viability data. In the following sections, functions pertaining to erlotinib are denoted with 1's and functions pertaining to evofosfamide are denoted using 2's. We note that the birth and death rates used in this parameterization are taken from *in vitro* data. Thus the specific time scale and cell population sizes of the model predictions are relevant to the *in vitro* setting.

Effect of Erlotinib and Oxygen on Growth Kinetics

Recent experimental results have demonstrated that the response of NSCLC tumor cells to erlotinib is dependent on the tumor microenvironment and, in particular, oxygen concentration. In [20], this dependence was quantified by obtaining live/dead cell counts for isogenic HCC827 sensitive and resistant (harboring the T790M resistance mutation) cell lines *in vitro* at varying concentrations of oxygen and drug. We then calculated birth and death rates of erlotinib-sensitive and erlotinib-resistant cells in terms of oxygen concentration x and erlotinib concentration c_1 using an exponential growth model. Given an erlotinib concentration of c_1 μM, let the index $I(c_1)$ be given by $I(c_1) = \left\lfloor 10c_1 + \frac{1}{2} \right\rfloor + 1$. Then the birth and death rate functions approximating the experimental data are defined as follows:

$$\lambda_X^1(x, c_1) = SB_{I(c_1),1} + x \cdot SB_{I(c_1),2} + 1.217 \cdot SB_{I(c_1),3},$$
$$\mu_X^1(x, c_1) = SD_{I(c_1),1} + x \cdot SD_{I(c_1),2} + 1.217 \cdot SD_{I(c_1),3},$$
$$\lambda_Y^1(x, c_1) = RB_{I(c_1),1} + x \cdot RB_{I(c_1),2} + 1.217 \cdot RB_{I(c_1),3},$$
$$\mu_Y^1(x, c_1) = RD_{I(c_1,1} + x \cdot RD_{I(c_1),2} + 1.217 \cdot RD_{I(c_1),3},$$

where SB, SD, RB, and RD are given by the matrices in Section 2.7. The "control" birth and death rates in the absence of drug in compartment i with oxygen concentration x_i are then given by:

$$\lambda_{X,i}^c = \lambda_X^1(x_i, 0), \tag{2.4}$$
$$\mu_{X,i}^c = \mu_X^1(x_i, 0), \tag{2.5}$$
$$\lambda_{Y,i}^c = \lambda_Y^1(x_i, 0), \tag{2.6}$$
$$\mu_{Y,i}^c = \mu_Y^1(x_i, 0). \tag{2.7}$$

For each compartment, by setting the oxygen concentration in these functions equal to the oxygen concentration in that compartment, we obtain birth and death rates of sensitive and resistant cells as functions of erlotinib concentration. For example, Figure 2.2 shows the net growth rates of sensitive and resistant cells as functions of erlotinib concentration at a low oxygen concentration (0.33%) as well as a high oxygen concentration (10.5%). These values correspond to the concentrations of oxygen in the compartment furthest from the blood vessel and closest to the blood vessel, respectively. We observe that overall drug response for both cell types is more pronounced in high oxygen compartments than in low oxygen compartments, which actually comprise the tumor bulk. Strikingly, the resistant cells display essentially complete resistance under low oxygen levels but only partial resistance under high oxygen levels, whereas the sensitive cells exhibit only a minor increase in drug tolerance under low-oxygen levels. During the course of treatment with erlotinib, we let the birth and death rates of the sensitive cell population in compartment i be denoted by $\lambda_{X,i}^1(t)$ and $\mu_{X,i}^1(t)$, and we let $\lambda_{Y,i}^1(t)$ and $\mu_{Y,i}^1(t)$ represent the birth and death rates of the resistant cell population in

compartment i.

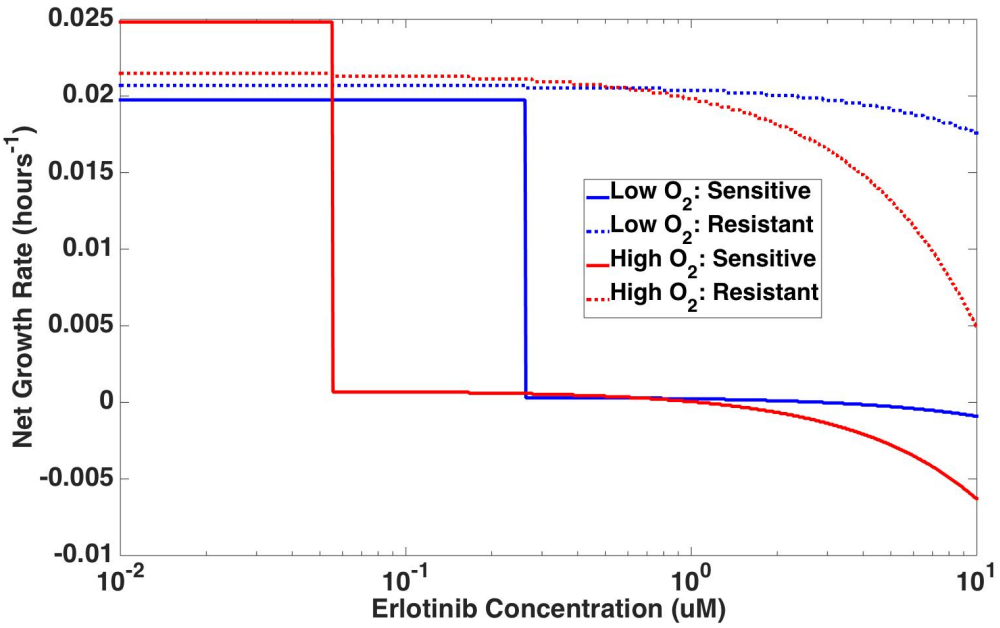

Figure 2.2: **Net growth rates as functions of erlotinib concentration.** Examples of net growth rates of sensitive and resistant cells are shown as functions of erlotinib concentration. These rates are shown in blue for a low oxygen concentration (0.33%), corresponding to that which is found in the compartment furthest from the blood vessel, as well as in red for a high oxygen concentration (10.5%), corresponding to that which is found in the compartment closest to the blood vessel. Solid lines represent sensitive cell growth rates, and dotted lines represent resistant cell growth rates.

Analysis of erlotinib pharmacokinetic data. During treatment, the concentration of erlotinib within each compartment fluctuates in time, according to the dosing schedule. Assume erlotinib is administered in doses of D_1 mg every T_1 hours. We first determine how the drug concentration varies at the blood vessel over the course of treatment. To define the plasma concentration over time after one dose of D_1 mg erlotinib, we assume this quantity decays exponentially as a function of time and let $\rho_1(t) = c_1^{max} e^{-k_1 t}$ describe this exponential decay, where c_1^{max} is the maximum plasma concentration achieved after one dose of erlotinib and k_1 is the rate of decay. Using the clinical pharmacokinetic data in [17, 54, 55], we acquire pairs of best-fit parameters for this function at a variety of doses between 100 and 300 mg. The values obtained for k_1 are averaged to

produce $k_1 = 0.0307$, and a linear function $c_1^{max}(D_1) = 7D_1 + 365$ is defined to reflect the relationship between dose and maximum plasma concentration. Hence we define erlotinib plasma concentration after one dose, given an initial dose D_1, as a function of time:

$$\rho_1(t) = (7D_1 + 365)e^{-0.0307t}. \tag{2.8}$$

Using this function for plasma concentration after one dose of erlotinib, we define a function to describe plasma concentration over time for the entire course of treatment with erlotinib. The concentration of erlotinib at the blood vessel at some time $t \in [nT_1, (n+1)T_1)$ for $n = 0, 1, 2, ...$ is given by

$$C_1(t) = \sum_{i=0}^{n} \rho_1(t - iT_1). \tag{2.9}$$

Erlotinib concentration decays spatially away from the vessel exponentially. Since experimental characterization of erlotinib drug penetration in solid tumors in unavailable currently, this decay rate is parameterized based on the decay rate of doxorubicin, which has a similar molecular weight to erlotinib [21]; in [20], a range of decay rates was investigated to account for differences in cellular uptake rate between these two molecules. Combining this decay rate with $C_1(t)$ fully specifies a new function $C_{1,i}(t)$ for the concentration of erlotinib in each compartment i at time t. For example, the concentration of erlotinib over time, given a standard dosing schedule of 150 mg erlotinib daily, is plotted for two different compartments (the compartments closest to and furthest from the nearest blood vessel) in Figure 2.3.

By substituting $C_{1,i}(t)$ into these expressions, we obtain functions describing the birth and death rates of sensitive and resistant cells in compartment i at any time t during treatment:

$$\begin{aligned} \lambda_{X,i}^1(t) &= \lambda_{X,i}^1(C_{1,i}(t)), \\ \mu_{X,i}^1(t) &= \mu_{X,i}^1(C_{1,i}(t)), \\ \lambda_{Y,i}^1(t) &= \lambda_{Y,i}^1(C_{1,i}(t)), \\ \mu_{Y,i}^1(t) &= \mu_{Y,i}^1(C_{1,i}(t)). \end{aligned} \tag{2.10}$$

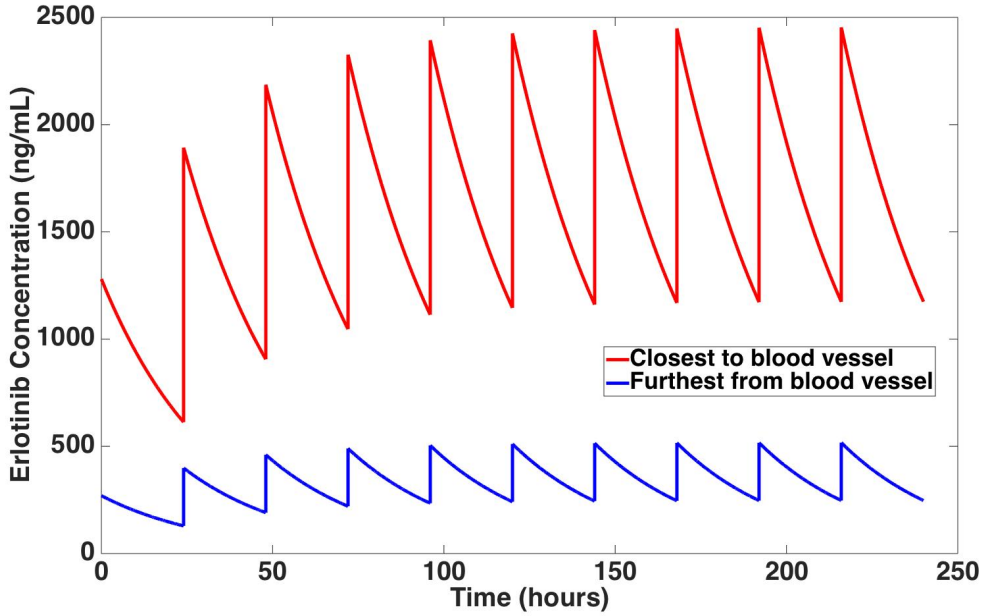

Figure 2.3: **Example of erlotinib concentration over time.** Examples of plasma concentration functions over time are shown for erlotinib. Given a standard dosing schedule of 150 mg erlotinib administered daily, the red curve shows the concentration of erlotinib found in the compartment closest to the nearest blood vessel, and the blue curve shows the erlotinib concentration found in the compartment furthest from the nearest blood vessel.

Effect of Evofosfamide and Oxygen on Growth Kinetics

Next, we consider the effect of evofosfamide on the erlotinib-sensitive and erlotinib-resistant cell populations in each microenvironmental compartment. Note that the mechanisms of action differ greatly between erlotinib and evofosfamide. In particular, the mutation conferring resistance to erlotinib occurs in the EGFR kinase domain, which is independent of the action of evofosfamide; thus the presence of this mutation is not thought to impact evofosfamide response. So we assume the same response of erlotinib-sensitive and erlotinib-resistant cells to evofosfamide.

We start by defining the percent of viable cells $V_i(C_2)$ in compartment i as a function of evofosfamide concentration. Suppose that, for a fixed concentration of oxygen, cell viability behaves as a logistic function with respect to drug concentration. Let $V(C_2) =$

$100 - \frac{A}{1+e^{-\alpha/\beta}} + \frac{A}{1+e^{(C_2-\alpha)/\beta}}$, with A, α, and β unknown parameters, to reflect the fact that cells are 100% viable in the absence of drug ($V(0) = 100$). We fit this logistic function to to multiple experimentally-derived data sets for cell viability in [37], each at a different fixed oxygen concentration between 0% and 21%, to obtain values for A, α, and β. The estimates of A are averaged to yield $A = 88.5983$, and the relationship between α and β for compartment i and x_i, the oxygen concentration in compartment i, is described as follows:

$$\alpha_i = \begin{cases} (1.937 \cdot 10^{-7})x_i^3 - (2.932 \cdot 10^{-6})x_i^2 + (1.252 \cdot 10^{-5})x_i + 3.97 \cdot 10^{-7} & x_i < 10\% \\ (2.613 \cdot 10^{-6})x_i - 4.727 \cdot 10^{-8} & x_i \geq 10\%, \end{cases}$$

$$\beta_i = \begin{cases} (6.389 \cdot 10^{-8})x_i^3 - (9.284 \cdot 10^{-7})x_i^2 + (3.87 \cdot 10^{-6})x_i + 3.792 \cdot 10^{-8} & x_i < 10\% \\ (6.366 \cdot 10^{-7})x_i - 3.421 \cdot 10^{-6} & x_i \geq 10\%. \end{cases}$$

Therefore, for compartment i, the percent of viable cells at an evofosfamide concentration of C_2 is expressed as

$$V_i(C_2) = 100 - \frac{A}{1 + e^{-\alpha_i/\beta_i}} + \frac{A}{1 + e^{(C_2-\alpha_i)/\beta_i}},$$

where A, α_i, and β_i are all defined as above. Figure 2.4 shows a plot of this function together with the corresponding data points at the seven fixed oxygen concentrations examined in the cell viability experiments.

We now use the experimental cell viability data in [37] together with the cell viability function to derive expressions $N_{X,i}(C_2)$ and $N_{Y,i}(C_2)$ for net growth rates of sensitive and resistant cells in compartment i as functions of evofosfamide concentration C_2. Let the fraction of viable cells in compartment i as a function of evofosfamide concentration be denoted by $v_i(C_2) = \frac{1}{100}V_i(C_2)$. Since we assume evofosfamide has the same effect on the sensitive and resistant cells, we need only define one function for net growth rate in compartment i in terms of evofosfamide concentration which we can then apply to both the sensitive and resistant cell populations. Let $N(x, d)$ represent the net growth rate of cells in an environment with oxygen concentration x (written as a percentage) and

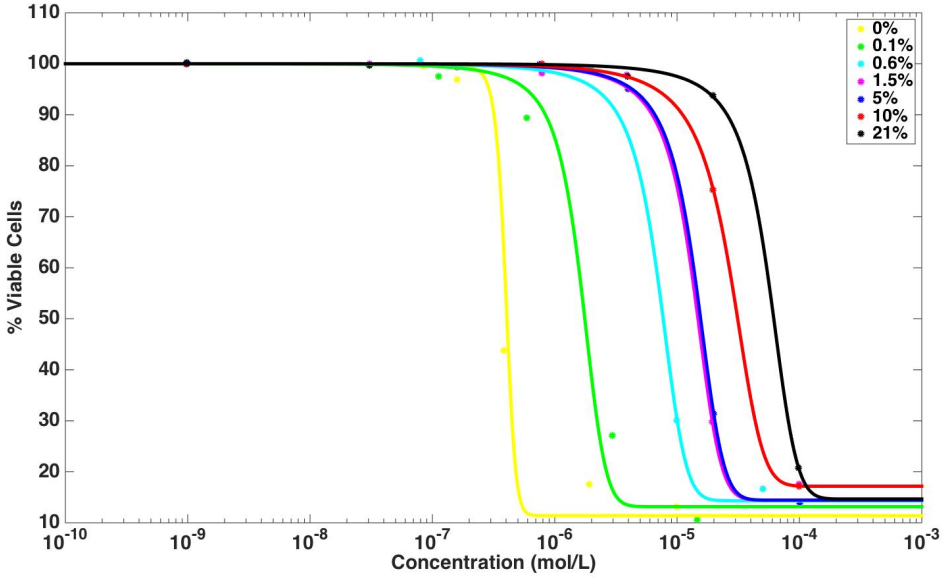

Figure 2.4: **Cell viability fit.** Percent of viable cells as a function of evofosfamide concentration. The points represent data from the cell viability experiments, and the curves show the fitted cell viability function at the fixed oxygen concentrations corresponding to the data.

evofosfamide concentration d. We define this function by writing out explicit expressions for the number of cells in the treated and control groups at certain points in time according to the details of the cell viability experiments and comparing this with the cell viability function.

Let group A represent the control group in the cell viability experiments from [37] and let group B denote the group of cells treated with evofosfamide concentration C_2 at an oxygen concentration of x_i, corresponding to the oxygen concentration expected to coincide with compartment i of the tumor microenvironment. Use $n_A(t)$ and $n_B(t)$ to represent the number of cells in each of these groups at time t. Then for all t,

$$v_i(C_2) = \frac{n_B(t)}{n_A(t)}. \tag{2.11}$$

We use the detailed process followed in [37] to write explicit expressions for the number of cells in groups A and B at certain points in time. At time $t = 0$, there are $n_A(0) = n_B(0)$

cells in each group. According to [37], exponentially growing cells were seeded 24 hours before the addition of test compounds. We express the number of cells present in each group at $t = 24$ by

$$n_A(24) = n_A(0)e^{24N(21,0)},$$
$$n_B(24) = n_B(0)e^{24N(21,0)}.$$

After the addition of evofosfamide, the plates were incubated for 2 hours under the altered oxygen concentration. The number of cells in each group at $t = 26$ is then given by

$$n_A(26) = n_A(24)e^{2N(x_i,0)},$$
$$n_B(26) = n_B(24)e^{2N(x_i,C_2)}.$$

Lastly, cells were cultured for 72 hours after washing under normoxic conditions. We can express the number of cells in each group at time $t = 98$ as

$$n_A(98) = n_A(26)e^{72N(21,0)},$$
$$n_B(98) = n_B(26)e^{72N(21,0)}.$$

By repeated substitution using the above equations, $n_A(98)$ and $n_B(98)$ can be written as follows:

$$\begin{aligned} n_A(98) &= n_A(0)e^{24N(21,0)}e^{2N(x_i,0)}e^{72N(21,0)}, \\ n_B(98) &= n_B(0)e^{24N(21,0)}e^{2N(x_i,C_2)}e^{72N(21,0)}. \end{aligned} \tag{2.12}$$

We proceed by relating the above equations to cell viability. Setting $t = 98$ in equation (2.11) yields

$$v_i(C_2) = \frac{n_B(98)}{n_A(98)}. \tag{2.13}$$

By substituting the equations in (2.12) into equation (2.13) and simplifying, keeping in mind that $n_A(0) = n_B(0)$, we obtain

$$v_i(C_2) = e^{2[N(x_i,C_2)-N(x_i,0)]}.$$

Taking the natural log of both sides, dividing by 2, and solving for $N(x_i, C_2)$ yields

$$N(x_i, C_2) = N(x_i, 0) + \frac{1}{2}\ln[v_i(C_2)].$$

We can rewrite this, applying the above results to both sensitive and resistant cells, to express net growth rates in compartment i as functions of evofosfamide concentration C_2:

$$N_{X,i}(C_2) = N_{X,i}(0) + \frac{1}{2}\ln[v_i(C_2)],$$
$$N_{Y,i}(C_2) = N_{Y,i}(0) + \frac{1}{2}\ln[v_i(C_2)].$$

Note that in the above equations, $N_{X,i}(0)$ and $N_{Y,i}(0)$ are simply the net growth rates of sensitive and resistant cells in the absence of drug. In other words,

$$N_{X,i}(0) = \lambda^c_{X,i} - \mu^c_{X,i},$$
$$N_{Y,i}(0) = \lambda^c_{Y,i} - \mu^c_{Y,i},$$

where the superscript c denotes the control growth rates in the absence of drug, as defined previously. The functions for net growth rate dependence on evofosfamide concentration are plotted in Figure 2.5 for a low oxygen concentration (0.33%) and a high oxygen concentration (10.5%).

However, having explicitly defined functions for net growth rates of the sensitive and resistant cell populations is not quite enough; we must define their respective birth and death rates as well. Since evofosfamide releases a cytotoxic agent in hypoxic regions, we assume that its primary effect is to increase cellular death rates rather than to decrease cellular birth rates. Hence the birth rates of cells under any concentration of

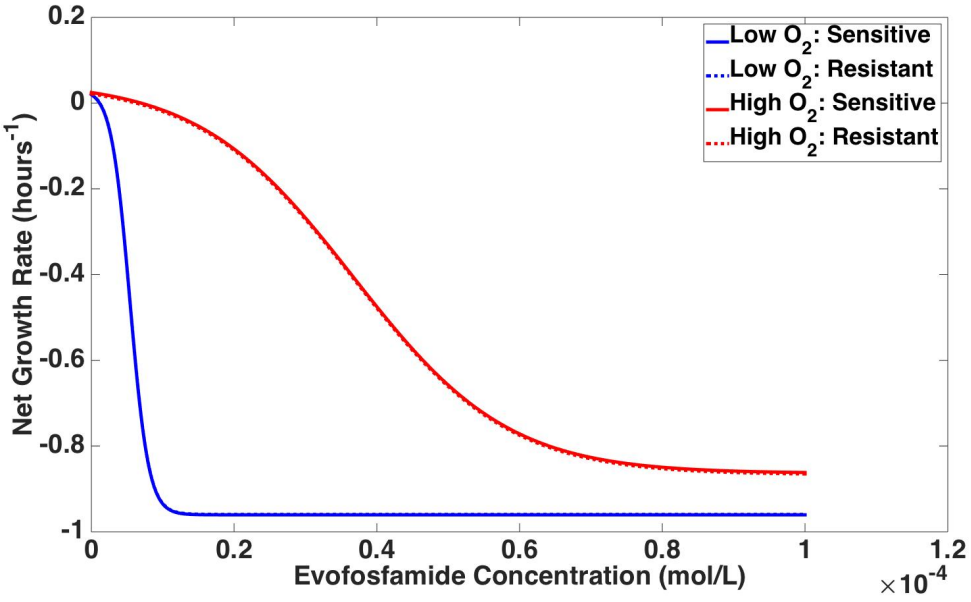

Figure 2.5: **Net growth rates as functions of evofosfamide concentration.** Examples of net growth rates of sensitive and resistant cells are shown as functions of evofosfamide concentration. These rates are shown in blue for a low oxygen concentration (0.33%), corresponding to that which is found in the compartment furthest from the blood vessel, as well as in red for a high oxygen concentration (10.5%), corresponding to that which is found in the compartment closest to the blood vessel. Solid lines represent sensitive cell growth rates, and dotted lines represent resistant cell growth rates.

evofosfamide are equal to those in the absence of drug. Thus we define birth rates of sensitive and resistant cells in compartment i due to evofosfamide by

$$\lambda^2_{X,i}(t) = \lambda^c_{X,i},$$
$$\lambda^2_{Y,i}(t) = \lambda^c_{Y,i}.$$

Using the fact that net growth rates are differences between birth and death rates along with a series of substitutions of the above equations followed by algebraic simplification

yields the following functions for death rates of sensitive and resistant cells in compartment i:

$$\mu^2_{X,i}(t) = \mu^c_{X,i} - \frac{1}{2}\ln[v_i(C_2(t))],$$
$$\mu^2_{Y,i}(t) = \mu^c_{Y,i} - \frac{1}{2}\ln[v_i(C_2(t))].$$

Analysis of evofosfamide pharmacokinetic data. Next, we consider how the concentration of evofosfamide changes during treatment. Using pharmacokinetic data from a phase 1 clinical trial [56], we define a function $\rho_2(t)$ for plasma concentration over time after one dose of D_2 mg/m^2 evofosfamide. Unlike with erlotinib, we cannot simply approximate the plasma concentration of evofosfamide using only exponential decay because doing this would force the maximum concentration to be artificially high since evofosfamide decays so quickly with respect to time. This does not present a problem in the erlotinib plasma concentration function because the decay rate of erlotinib is much lower than that of evofosfamide. From the clinical data in [56], we estimate the time at which maximum plasma concentration is achieved to be $t = \frac{1}{2}$ (30 minutes after the initial dose is administered). We approximate the plasma concentration for $t \geq \frac{1}{2}$ as exponential decay using $\rho_2(t) = c_2^{max} e^{-k_2(t-1/2)}$, where c_2^{max} is the maximum plasma concentration achieved after one dose and k_2 is the decay rate of evofosfamide. We acquire pairs of best-fit parameters for this function at a variety of doses between 7.5 and 940 mg/m^2 using the clinical trial data. Cubic functions are defined for both c_2^{max} and k_2 to describe the relationship between dose D_2 and maximum concentration and decay rate as follows:

$$c_2^{max}(D_2) = (2.008 \cdot 10^{-7})D_2^3 - 0.0003276D_2^2 + 0.1753D_2 - 12.54,$$
$$k_2(D_2) = (1.302 \cdot 10^{-7})D_2^3 - 0.0002043D_2^2 + 0.08873D_2 - 5.829.$$

To estimate the plasma concentration for $t < \frac{1}{2}$, we define a linear function connecting $(0, 0)$ with $\left(\frac{1}{2}, c_2^{max}(D_2)\right)$. We can now define evofosfamide plasma concentration after one dose as a function of time as follows:

$$\rho_2(t) = \begin{cases} 2c_2^{max}(D_2)t & t < \frac{1}{2} \\ c_2^{max}(D_2)e^{-k_2(D_2)(t-1/2)} & t \geq \frac{1}{2}, \end{cases} \tag{2.14}$$

where $c_2^{max}(D_2)$ and $k_2(D_2)$ are each defined as in the above equations.

Since evofosfamide is very quickly eliminated from the blood stream (half-life of 0.81 hours [56]), for treatment schedules where doses are spaced at least 6 hours apart, the plasma concentration over the course of treatment $\rho_2(t)$ can be approximated as a periodic function. Then for $n = 0, 1, 2, ...$ and $t \in [nT_2, (n+1)T_2)$, the concentration of evofosfamide at the blood vessel at time t is given by

$$C_2(t) = \rho_2(t - nT_2). \tag{2.15}$$

Figure 2.6 shows the plasma concentration function corresponding to a dosing schedule of 575 mg/m^2 evofosfamide given every week.

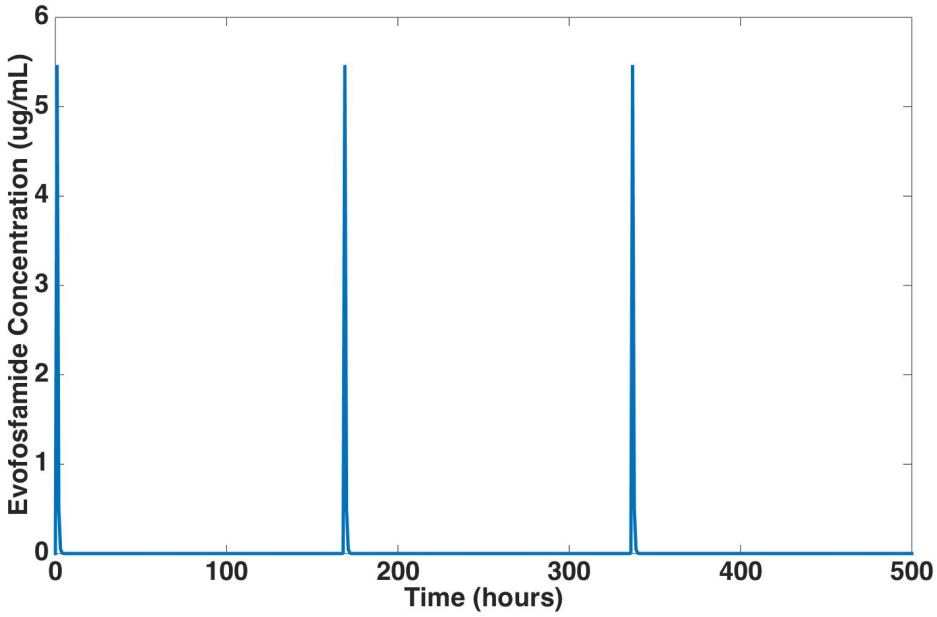

Figure 2.6: **Example of evofosfamide concentration over time.** Example of a period function for evofosfamide plasma concentration over time, given a dosing schedule of 575 mg/m^2 administered weekly.

Next we consider how the birth and death rates of sensitive and resistant cells change across environmental compartments at various oxygen levels. Experimental studies have quantified the distribution of apoptotic and proliferative markers within tumor tissue after treatment with evofosfamide and showed relatively uniform expression levels with respect to distance from the nearest blood vessel [57]. This suggests that cell birth and death are also approximately uniform in these compartments until one reaches the more hypoxic regions of the tumor where apoptosis and DNA damage levels increase. Therefore, unlike with erlotinib, we assume the concentration of evofosfamide in every compartment of the tumor microenvironment at any given time is equal to the concentration $C_2(t)$ at the blood vessel at that time.

Finally, using $C_2(t)$ we obtain birth and death rates of sensitive and resistant cells in each compartment i at any time t during treatment:

$$\begin{aligned} \lambda^2_{X,i}(t) &= \lambda^c_{X,i}, \\ \mu^2_{X,i}(t) &= \mu^c_{X,i} - \frac{1}{2}\ln[v_i(C_2(t))], \\ \lambda^2_{Y,i}(t) &= \lambda^c_{X,i}, \\ \mu^2_{Y,i}(t) &= \mu^c_{Y,i} - \frac{1}{2}\ln[v_i(C_2(t))]. \end{aligned} \tag{2.16}$$

In the above equations, the superscript c denotes the control growth rates in the absence of drug, as defined previously. v_i is the function describing cell viability in terms of evofosfamide concentration, as previously defined.

Growth Kinetics During Combination Therapy

Consider a combination dosing regimen consisting of some number of identical cycles, each of length $t_1 + t_2$ hours. During each cycle, assume the first t_1 hours are dedicated to treatment with erlotinib, whereas the last t_2 hours are used for evofosfamide treatment. For the reasons discussed above, given a sufficient amount of time between the last dose of evofosfamide in one cycle and the first dose of erlotinib in the next cycle, we may assume that during the erlotinib treatment phase there is no residual evofosfamide. Therefore the birth and death rates during the first t_1 hours in every cycle are governed by erlotinib response kinetics. Since erlotinib has a much longer half-life than evofosfamide, during the last t_2 hours of evofosfamide treatment it is possible that some

erlotinib will remain in the blood stream by the beginning of this period. Therefore the cellular birth and death rates must reflect responses to both drugs. However, since erlotinib is primarily cytostatic while evofosfamide is primarily cytotoxic, we assume that during this period of time, cellular birth rates reflect the response to erlotinib while cellular death rates reflect the response to evofosfamide.

Since cycles are identical, functions describing birth and death rates over the course of treatment are periodic with period $t_1 + t_2$. Using the equations in (2.10) and (2.16), we define birth and death rates of the sensitive and resistant cell populations in compartment i at time $t \in [0, t_1 + t_2)$ by

$$\begin{aligned}
\lambda_{X,i}(t) &= \lambda^1_{X,i}(C_{1,i}(t)), \\
\mu_{X,i}(t) &= \begin{cases} \mu^1_{X,i}(C_{1,i}(t)) & t \in [0, t_1) \\ \mu^c_{X,i} - \frac{1}{2}\ln[v_i(C_2(t))] & t \in [t_1, t_1 + t_2), \end{cases} \\
\lambda_{Y,i}(t) &= \lambda^1_{Y,i}(C_{1,i}(t)), \\
\mu_{Y,i}(t) &= \begin{cases} \mu^1_{Y,i}(C_{1,i}(t)) & t \in [0, t_1) \\ \mu^c_{Y,i} - \frac{1}{2}\ln[v_i(C_2(t))] & t \in [t_1, t_1 + t_2). \end{cases}
\end{aligned} \tag{2.17}$$

These functions are used in equation (2.1), equation (2.2), and equation (2.3) to predict tumor evolutionary dynamics over the course of treatment.

Model Parameter Notations

We have summarized the parameters used in our model in Table 2.1. These parameters are listed in order of appearance in the chapter. The first column in this table provides a variable name (if given in the chapter) for the parameter and the second column provides its biological meaning. The third column gives the value of the constant parameters in the model.

2.3 Results

Using the stochastic model, we examined the evolutionary dynamics of a tumor undergoing therapy with a wide variety of dosing regimens using erlotinib and evofosfamide, both

Name	Biological Meaning	Value and Units
–	oxygen decay rate (spatial)	-0.0385
$\lambda_{X,i}(t)$	sensitive cell birth rate	hours^{-1} (see equation (2.17))
$\mu_{X,i}(t)$	sensitive cell death rate	hours^{-1} (see equation (2.17))
$\lambda_{Y,i}(t)$	resistant cell birth rate	hours^{-1} (see equation (2.17))
$\mu_{Y,i}(t)$	resistant cell death rate	hours^{-1} (see equation (2.17))
u	mutation rate	10^{-7}
M	initial number of sensitive cells in tumor	$1.6 \cdot 10^6$
M_i	initial number of sensitive cells	(from compartment weights)
$\lambda^1_{X,i}(t)$	sensitive cell birth rate due to erlotinib	hours^{-1} (see equation (2.10))
$\mu^1_{X,i}(t)$	sensitive cell death rate due to erlotinib	hours^{-1} (see equation (2.10))
$\lambda^1_{Y,i}(t)$	resistant cell birth rate due to erlotinib	hours^{-1} (see equation (2.10))
$\mu^1_{Y,i}(t)$	resistant cell death rate due to erlotinib	hours^{-1} (see equation (2.10))
D_1	dose of erlotinib	mg
T_1	time between erlotinib doses	hours
$\rho_1(t)$	plasma concentration after one dose erlotinib	ng/mL (see equation (2.8))
$C_1(t)$	plasma concentration during erlotinib treatment	ng/mL (see equation (2.9))
–	erlotinib decay rate (spatial)	-0.0173
$C_{1,i}(t)$	erlotinib concentration in compartment i	μM (calculated using $C_1(t)$ and i)
$\lambda^2_{X,i}(t)$	sensitive cell birth rate due to evofosfamide	hours^{-1} (see equation (2.16))
$\mu^2_{X,i}(t)$	sensitive cell death rate due to evofosfamide	hours^{-1} (see equation (2.16))
$\lambda^2_{Y,i}(t)$	resistant cell birth rate due to evofosfamide	hours^{-1} (see equation (2.16))
$\mu^2_{Y,i}(t)$	resistant cell death rate due to evofosfamide	hours^{-1} (see equation (2.16))
D_2	dose of evofosfamide	mg/m^2
T_2	time between evofosfamide doses	hours
$\rho_2(t)$	plasma concentration after one dose evofosfamide	μg/mL (see equation (2.14))
$C_2(t)$	evofosfamide plasma concentration	μg/mL (see equation (2.15))
$\lambda^c_{X,i}$	sensitive cell control birth rate	hours^{-1} (see equation (2.4))
$\mu^c_{X,i}$	sensitive cell control death rate	hours^{-1} (see equation (2.4))
$\lambda^c_{Y,i}$	resistant cell control birth rate	hours^{-1} (see equation (2.4))
$\mu^c_{Y,i}$	resistant cell control death rate	hours^{-1} (see equation (2.4))
$v_i(C_2)$	cell viability due to evofosfamide	(see equation (2.11))
t_1	duration of erlotinib treatment	hours
t_2	duration of evofosfamide treatment	hours

Table 2.1: **Model parameter notations.** The parameters used in our model are summarized in the table below, in order of appearance in the chapter. The first column contains the variable name of the parameter, if applicable. The second column summarizes the biological meaning of this parameter. The third column gives the units as well as values for any parameters which are constant in the model. The subscript i represents quantities in compartment i.

separately and in combination. We first developed a model for the toxicity constraints governing both single-agent and combination therapies, based on reported toxicities and side effects of the two drugs in Phase I/II trials. We then optimized combination treatment strategies in order to predict which types of dosing strategies could lead to the

best treatment outcomes for patients diagnosed with NSCLC.

2.3.1 Toxicity Constraints

We defined the space of all tolerated single-agent and combination therapy dosing schedules using clinical trial data on drug tolerability. For each single-agent treatment we defined a toxicity constraint curve representing the relationship between frequency of drug administration and maximum tolerated dose. In addition, we analyzed the overlapping toxicities between the two drugs as well as each drug elimination rate to determine the necessary conditions for safely administering both drugs in succession. This combination therapy constraint, together with the toxicity constraint curves corresponding to each of the monotherapies, defines the space of all tolerated dosing schedules.

Monotherapy Toxicity Constraints

For each drug, we derive a toxicity constraint curve such that all points on and below the curve correspond to tolerated dosing schedules, whereas all points above the curve correspond to dosing schedules which lead to dose-limiting toxicities. These curves are constructed using data from clinical trials on the tolerability and toxicity of each drug. For each dosing schedule tested in clinical trials, we convert the schedule to an ordered pair describing the relationship between frequency of drug administration and dose as follows: the first coordinate is defined to be the number of times the drug is administered in a 3-week period, and the second coordinate is given by the corresponding dose. The location of each ordered pair relative to the toxicity constraint curve is determined based on whether or not that dosing schedule was tolerated in clinical trials. Each of these clinically tested dosing schedules is listed in Table 2.2, along with its corresponding ordered pair and location relative to the toxicity constraint curve. Note that in order to handle the discrepancy between clinical trial data sets for the 200 mg/day erlotinib dosing schedule, we err on the side of caution and assume this dosing schedule is not tolerated.

Using the data from Table 2.2, we construct toxicity constraint curves for erlotinib and evofosfamide. For each drug, we define a function to describe the relationship between maximum tolerated dose and frequency of drug administration such that the criteria in the last two columns of Table 2.2 are satisfied. The erlotinib toxicity constraint

Erlotinib				
Dose (mg)	Schedule	Tolerated?	(n, D_1)	Location
25	daily for 3 days/week	yes [58]	$(9, 25)$	below curve
50	daily for 3 days/week	yes [58]	$(9, 50)$	below curve
50	daily	yes [58]	$(21, 50)$	below curve
100	daily for 3 days/week	yes [58]	$(9, 100)$	on/below curve
100	daily	yes [54, 58]	$(21, 100)$	below curve
100	twice daily	no [58]	$(42, 100)$	above curve
150	daily	yes [54, 58]	$(21, 150)$	on/below curve
200	daily	yes [54], no [58]	$(21, 200)$	above curve
250	daily	no [54]	$(21, 250)$	above curve
1200	weekly	yes [59]	$(3, 1200)$	below curve
1600	weekly	yes [59]	$(3, 1600)$	below curve
2000	weekly	yes [59]	$(3, 2000)$	on/below curve
Evofosfamide				
Dose (mg/m^2)	Schedule	Tolerated?	(n, D_2)	Location
7.5	weekly	yes [56]	$(3, 7.5)$	below curve
15	weekly	yes [56]	$(3, 15)$	below curve
30	weekly	yes [56]	$(3, 30)$	below curve
60	weekly	yes [56]	$(3, 60)$	below curve
120	weekly	yes [56]	$(3, 120)$	below curve
120	5 days every 3 weeks	yes [60]	$(5, 120)$	below curve
170	5 days every 3 weeks	yes [60]	$(5, 170)$	below curve
240	weekly	yes [56]	$(3, 240)$	below curve
240	5 days every 3 weeks	yes [60]	$(5, 240)$	below curve
330	5 days every 3 weeks	yes [60]	$(5, 330)$	below curve
460	5 days every 3 weeks	yes [60]	$(5, 460)$	on/below curve
480	weekly	yes [56]	$(3, 480)$	below curve
550	5 days every 3 weeks	no [60]	$(5, 550)$	above curve
575	weekly	yes [56]	$(3, 575)$	on/below curve
670	weekly	no [56]	$(3, 670)$	above curve
670	once every 3 weeks	yes [56]	$(1, 670)$	on/below curve
940	once every 3 weeks	no [56]	$(1, 940)$	above curve

Table 2.2: **Drug tolerability data from clinical trials.** Details regarding erlotinib and evofosfamide dosing schedules tested in clinical trials and how this data informs the construction of the toxicity constraint curve for each drug. The dose administered is shown in the first column, and the corresponding dosing schedule is shown in the second column. The third column shows whether or not this particular dosing schedule was tolerated in the clinical trial. The fourth column shows the ordered pair this dosing schedule corresponds to, and the last column shows the location of this point relative to the toxicity constraint curve. We assume that any point corresponding to a maximum tolerated dosing schedule tested in a clinical trial can either lie on or below the toxicity constraint curve to account for the possibility that a higher dose (which was not tested in the trial) is tolerated.

curve is defined as follows, where n is the number of times erlotinib is administered in a 3-week period and D_1 represents the maximum tolerated erlotinib dose (in mg) corresponding to that particular dosing schedule:

$$D_1(n) = \begin{cases} 2000 & n \leq 3 \\ 2000e^{-0.1439(n-3)} & n \geq 3. \end{cases}$$

The toxicity constraint curve for evofosfamide is given by the following function, where n represents the number of times evofosfamide is administered in a 3-week period and D_2 is the maximum tolerated dose of evofosfamide (in mg/m^2) associated to the dosing schedule defined by the value of n:

$$D_2(n) = \begin{cases} 670 & n \leq 1 \\ 670e^{-0.076454(n-1)} & n \geq 1. \end{cases}$$

These curves, along with the corresponding data points from Table 2.2, are shown in Figure 2.7.

Combination Therapy Toxicity Constraints

To characterize the toxicity constraints relevant for considering alternating dosing combination strategies, we study the minimum length of time that should pass between the last dose of one drug and the first dose of the other drug. Since evofosfamide is eliminated from the blood stream in a matter of a few hours, we assume that as long as six or more hours have elapsed since the last dose of evofosfamide, a patient can safely take a dose of erlotinib without the worry of compounding side effects from the two drugs.

Next, we aim to determine the necessary waiting time between a last dose of erlotinib and a first dose of evofosfamide. Since the half-life of erlotinib is much longer than that of evofosfamide, it may not be reasonable to wait until erlotinib has been completely eliminated from the blood stream before administering evofosfamide, as waiting this long with so little drug in the blood stream could allow the cancer cells to rapidly proliferate. Analysis of clinical trial data for both drugs indicates that erotinib and

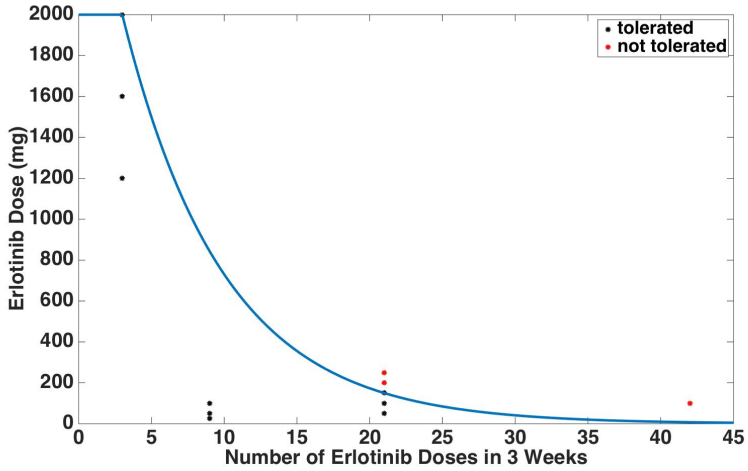

(a) Erlotinib toxicity constraint curve

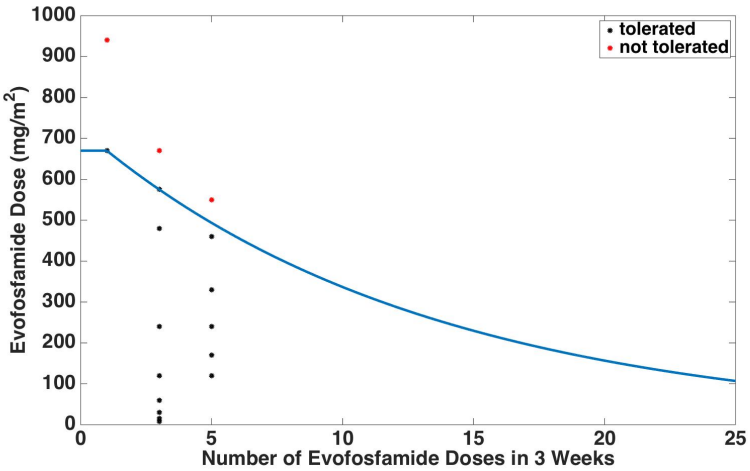

(b) Evofosfamide toxicity constraint curve

Figure 2.7: **Toxicity constraint curves for erlotinib and evofosfamide.** These curves depict the maximum tolerated doses for erlotinib (a) and evofosfamide (b) as functions of frequency of dose administration. The black points are the coordinates from Table 2.2 corresponding to tolerated dosing schedules, and the red points are the ordered pairs associated to dosing schedules that were not tolerated in clinical trials. All points contained in the areas on and below these two curves make up the space of tolerated monotherapy dosing schedules, and all points contained in the areas above these two curves make up the space of dosing schedules which lead to dose-limiting toxicities.

evofosfamide can both cause skin and mucosal toxicities, but there are no other overlapping toxicities reported. When erlotinib is administered three days every week, skin toxicities are observable at a dose of 50 mg, but not a dose of 25 mg [58]. Similarly, when erlotinib is given daily, mucosal toxicities are observable at a dose of 150 mg, but not at 100 mg [58]. Hence we assume that a patient taking 25 mg erlotinib three days every week experiences neither skin nor mucosal toxicities. Given this dosing schedule, a maximum plasma concentration of 2.357 μM is achieved, according to the previously defined erlotinib plasma concentration function. Thus we assume that once erlotinib plasma concentration has fallen to 2.357 μM or lower, it is safe to administer evofosfamide since this concentration of erlotinib will not cause any side effects overlapping with those caused by evofosfamide. Although this is most likely a simplification of the true combination toxicity constraints, we feel it is a realistic assumption based on the single-agent toxicity data available.

2.3.2 Comparison of Combination Therapy with Standard Monotherapy

To investigate the potential of combination therapies, we first compare treatment outcomes resulting from several combination therapies with the monotherapy schedules currently in clinical use. The standard dosing schedule for erlotinib is 150 mg/day. Two evofosfamide dosing schedules have been tested in a clinical trial and designated as maximum tolerated dosing schedules: 670 mg/m^2 given every 3 weeks and 575 mg/m^2 given weekly. We consider combination schedules which are clinically feasible and satisfy the toxicity constraints described in the previous section. Table 2.3 provides an overview of all of these dosing schedules. Schedule A is the standard erlotinib dosing schedule, and schedules B and C are the two evofosfamide dosing schedules. The remaining schedules (D through J) represent all combination therapies considered in this analysis. Since the toxicity constraints for erlotinib and evofosfamide are formulated in terms of the number of doses administered in a 3-week period, we define these schedules based on 3-week cycles, and hence only show dosing protocols for the first 21 days since this pattern repeats every 3 weeks for each schedule. Entries in Table 2.3 represent doses of either erlotinib in mg (subscript 1) or evofosfamide in mg/m^2 (subscript 2). For a fixed schedule (column) and day (row), a single entry represents the one dose scheduled for

that day, and the lack of an entry indicates that no drugs are administered on that day. Two entries on a single day for a given schedule represent the scheduling of two doses on the same day.

Day	A	B	C	D	E	F	G	H	I	J
1	150_1	670_2	575_2	150_1	150_1	7_1 7_1	7_1 7_1	150_1	150_1	150_1 145_2
2	150_1			150_1	150_1	7_1 7_1	7_1 7_1	150_1	150_1	150_1 145_2
3	150_1			150_1	150_1	7_1 7_1	7_1 7_1	150_1	150_1	150_1 145_2
4	150_1			150_1	150_1	7_1 7_1	7_1 7_1	150_1	150_1	150_1 145_2
5	150_1			150_1	150_1	7_1 7_1	7_1 7_1	150_1	150_1	150_1 145_2
6	150_1			150_1		7_1 7_1	7_1 7_1	150_1	150_1	150_1 145_2
7	150_1			150_1	575_2	7_1 7_1	575_2	150_1	575_2	150_1 145_2
8	150_1		575_2	150_1	150_1	7_1 7_1	7_1 7_1	150_1	150_1	150_1 145_2
9	150_1			150_1	150_1	7_1 7_1	7_1 7_1	150_1	150_1	150_1 145_2
10	150_1			150_1	150_1	7_1 7_1	7_1 7_1	150_1	150_1	150_1 145_2
11	150_1			150_1	150_1	7_1 7_1	7_1 7_1	150_1	150_1	150_1 145_2
12	150_1			150_1	150_1	7_1 7_1	7_1 7_1	150_1	150_1	150_1 145_2
13	150_1			150_1		7_1 7_1	7_1 7_1	150_1	150_1	150_1 145_2
14	150_1			150_1	575_2	7_1 7_1	575_2	150_1	575_2	150_1 145_2
15	150_1		575_2	150_1	150_1	7_1 7_1	7_1 7_1	150_1	150_1	150_1 145_2
16	150_1			150_1	150_1	7_1 7_1	7_1 7_1	150_1	150_1	150_1 145_2
17	150_1			150_1	150_1	7_1 7_1	7_1 7_1	150_1	150_1	150_1 145_2
18	150_1			150_1	150_1	7_1 7_1	7_1 7_1	150_1	150_1	150_1 145_2
19	150_1			150_1	150_1	7_1 7_1	7_1 7_1	150_1	150_1	150_1 145_2
20	150_1					7_1	7_1 7_1	150_1	150_1	150_1 145_2
21	150_1			670_2	575_2	670_2	575_2	670_2	575_2	150_1 145_2

Table 2.3: **Dosing schedules considered in the comparison of single-agent and combination therapies.** Each lettered column denotes a distinct dosing schedule containing repeating 3-week cycles defined by the dosing protocols in that column. The entries with subscripts of 1 are doses of erlotinib in mg and the entries with subscripts of 2 are doses of evofosfamide in mg/m^2. For a fixed schedule (column) and day (row), a single entry represents the one dose of either erlotinib or evofosfamide scheduled for that day. A missing entry for a fixed schedule and day corresponds to a day with neither erlotinib nor evofosfamide. Two entries for a given schedule on a single day represent the scheduling of two doses, either one dose of each drug or two doses of the same drug.

For each of the ten dosing schedules in Table 2.3, the mean tumor size and probability of resistance over the course of treatment are predicted using the model. The results of these calculations up to recurrence time (the time at which the cancer cell population reaches its initial size once again) are plotted in Figure 2.8a and Figure 2.8b, respectively. The red curves show the evolutionary dynamics of a tumor during treatment with erlotinib alone, the blue curves show the dynamics during monotherapy with evofosfamide, and the green curves show the evolutionary dynamics of the cancer

cell population during combination therapy. The label on each curve indicates which dosing schedule from Table 2.3 corresponds to those results. The means of the sensitive and resistant cell populations are shown separately in Figure 2.8c for one of each type of dosing schedule: erlotinib alone, evofosfamide alone, and combination therapy. Figure 2.8d shows the mean tumor size for the combination schedules, averaged only over those that develop resistance.

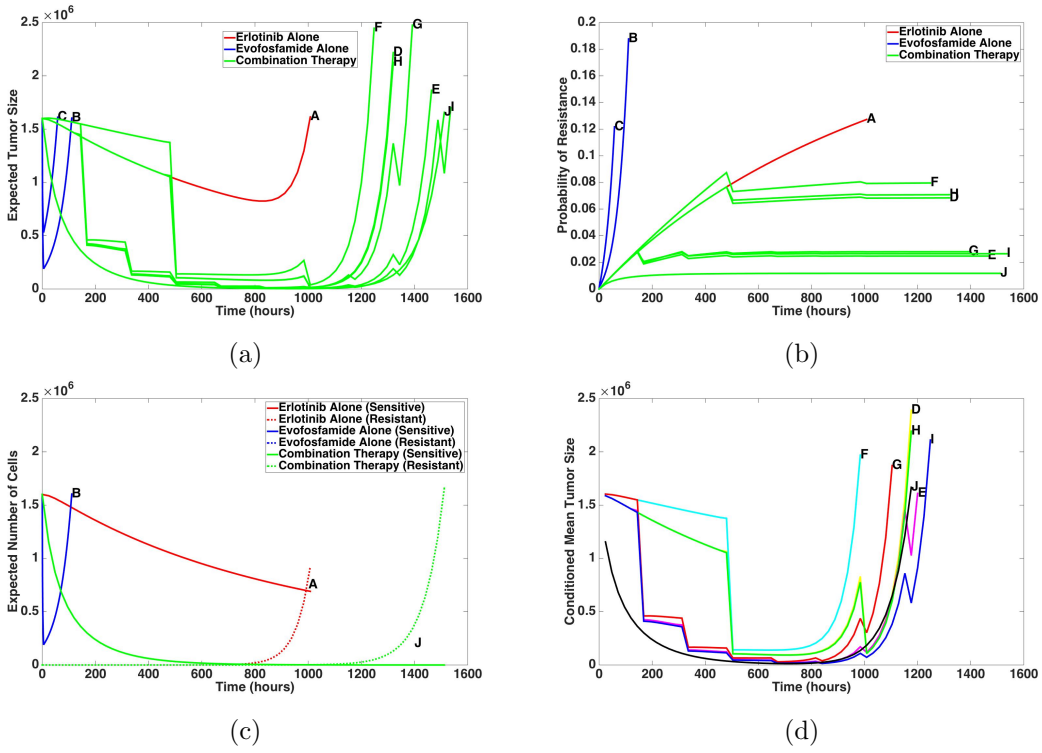

Figure 2.8: **Tumor evolutionary dynamics over time, given a variety of single-agent and combination therapies.** Mean tumor size (a) and probability of resistance (b) are calculated up to recurrence time for a tumor with an initial population of $1.6 \cdot 10^6$ sensitive cells undergoing treatment with each of the ten dosing schedules defined in Table 2.3. Each labeled curve corresponds to the dosing schedule with the matching letter in Table 2.3. For the sake of comparison, results due to dosing schedules using erlotinib alone are shown in red, results due to dosing schedules using evofosfamide alone are shown in blue, and results due to combination therapies are shown in green. Mean tumor size for one of each of these three types of dosing schedules is broken down into the means of sensitive and resistant cells in (c). (d) shows the expected tumor size for combination strategies, conditioned upon the event of developing resistance.

We find that all the combination therapies considered produce treatment outcomes superior to the standard monotherapy schedules. Figure 2.8a demonstrates that the combination schedules result in lower average tumor sizes over the course of treatment than those resulting from either of the monotherapies. Even more significantly, Figure 2.8b shows that the probability of developing resistance decreases dramatically with the use of combination therapy. Under monotherapy with either drug, the probability of resistance eventually reaches one (in agreement with clinical results); this is due to the fact that sensitive cell division is not sufficiently inhibited by therapy to prevent the emergence of resistance before eradication of the tumor. However the model predicts that for a significant fraction of patients tumor eradication is possible under combination therapy.

The breakdown of sensitive and resistant cell populations under therapy is shown in Figure 2.8c. Erlotinib monotherapy yields a steady but slow decline of the sensitive cell population, due to the fact that the tumor oxygen distribution consists primarily of hypoxic regions and erlotinib does not penetrate well to these areas. On the other hand, treatment with evofosfamide alone targets hypoxic regions which comprise the majority of the cell population, leading to an initial steep decline of the sensitive cell population. However, due to the toxicity constraint during the subsequent break in treatment the mean of the sensitive cells quickly surpasses the initial population size and drives the production of erlotinib-resistant mutants. During combination therapy, however, the cancer cell population demonstrates an initial steep decline due to evofosfamide, followed by a long-term controlled phase due to the combination of evofosfamide and erlotinib. This tight control over the sensitive cell population during combination therapy is possible due to the fact that cancer cells close to blood vessels are receiving lethal concentrations of erlotinib while cancer cells in hypoxic regions are targeted by evofosfamide. Figure 2.8d demonstrates that for the patients who develop resistance, the average length of time until tumor recurrence is longer for all of the combination therapy dosing schedules than it is for either of the standard monotherapies. For example, it takes patients who develop resistance 40.54% longer to rebound on Schedule I compared with standard erlotinib therapy. However, the length of time until recurrence as well as the overall probability of resistance varies between specific combination schedules; this serves as motivation for identifying the optimal timing and dosage sequence for

combination schedules in the following section. Finally, we note that the combination strategies were also compared to optimized monotherapies (subject to the toxicity constraints developed in the previous section), and we found that no tolerated monotherapy schedule could outperform combinations in delaying or preventing resistance.

2.3.3 Optimized Combination Strategies

We next utilize the mathematical model to optimize over the space of tolerated combination treatment strategies (constrained by toxicity constraints derived in the previous section) to minimize the probability of developing resistance or maximally delay recurrence.

We consider three distinct classes of combination therapies. Class 1 investigates schedules created by systematically combining standard erlotinib monotherapy with a variety of evofosfamide dosing schedules. However, the amount of time between administration of different drugs can play an important role in the degree to which therapy affects the cancer cell population. Thus the rationale for defining the other two classes are to investigate schedules decreasing the amount of time after erlotinib but before evofosfamide dosing (Class 2), and after evofosfamide but before erlotinib dosing (Class 3).

For each class, we start with a base erlotinib dosing schedule complying with the monotherapy toxicity constraint curve in Figure 2.7a. Modifications to this schedule are then made to incorporate n doses of evofosfamide, where n varies from 0 (corresponding to erlotinib monotherapy) to a maximal value N (corresponding to evofosfamide monotherapy), in a three-week period. The dose of evofosfamide is determined by the toxicity constraint curve in Figure 2.7b. Whenever necessary, the minimum number of erlotinib doses are removed to comply with the combination toxicity constraint described in the previous section.

To define each combination schedule, we begin by defining a single cycle, consisting of the base erlotinib dosing schedule and a single dose of evofosfamide. We start by calculating the length L of the cycle, given n. Since n is the number of evofosfamide doses given in 3 weeks and there are 504 hours in 3 weeks, $L = 504/n$. Next we calculate the maximum tolerated dose of evofosfamide, given n, from the evofosfamide toxicity constraint curve. This dose of evofosfamide is administered at time $t = L - 24$ for

Classes 1 and 2, and $t = L - 6$ for Class 3. The remaining time in the cycle, starting at $t = 0$ and going up to the time of the evofosfamide infusion, is then filled with the fixed erlotinib dosing schedule associated with the given optimization class. If necessary, doses of erlotinib are then removed, beginning with the dose immediately before evofosfamide is administered and working backward, until there is enough time between the last dose of erlotinib and the first dose of evofosfamide for the erlotinib plasma concentration to fall below 2.357 μM so as to not violate the combination toxicity constraint. These cycles are then repeated some finite number of times to form complete dosing schedules.

In Class 1, we use the standard erlotinib monotherapy schedule of 150 mg/day, and the evofosfamide dose in each cycle is given 24 hours before the start of the next cycle. In Class 2, we use a low-dose erlotinib schedule of 7 mg twice daily, which allows for a shorter waiting period after erlotinib doses and before evofosfamide doses. Class 3 uses the same standard erlotinib monotherapy as in Class 1; however, the evofosfamide dose in each cycle is given 6 hours before the start of the next cycle instead of 24, which decreases the amount of time after evofosfamide doses and before erlotinib doses.

Figure 2.9 shows an example depicting dose schedule definition for one cycle of treatment for all three optimization classes when $n = 3$. For the reasons stated in the above paragraph, a cycle in Class 1 or 3 contains a standard erlotinib dosing schedule, whereas a cycle in Class 2 contains a low-dose erlotinib schedule. When $n = 3$, each cycle is one week. So for Classes 1 and 2, the evofosfamide dose in each cycle is given 24 hours before the end of the week, and for Class 3 the evofosfamide dose in each cycle is given 6 hours before the end of the week. This information is all depicted in step 1 (the top row) of Figure 2.9. In step 2 (the bottom row), the necessary number of erlotinib doses leading up to the evofosfamide infusion is removed in order to satisfy the combination toxicity constraint. In Classes 1 and 3, the last dose of erlotinib shown in step 1 is removed in step 2 to allow the erlotinib concentration to fall sufficiently low before the evofosfamide infusion. Note that in Class 2 the removal of erlotinib is not necessary due to the already low erlotinib concentration.

Combination schedules outperform monotherapy endpoints. We calculated the means of the sensitive and resistant cells as well as the probability of resistance, after nine weeks of treatment for every dosing schedule in each optimization class. Table 2.4 demonstrates that the tumor population size under $n = 0$ or N (i.e. the monotherapies) after 9

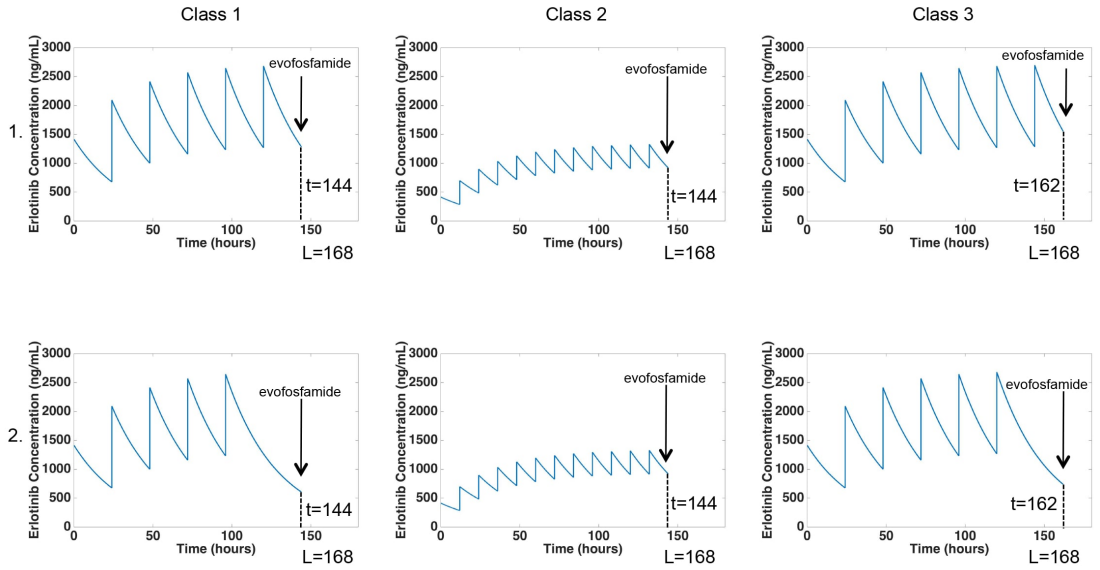

Figure 2.9: **Example depicting dose schedule definition for one cycle of treatment with $n = 3$ for all optimization classes.** This schematic shows the process by which one cycle of treatment is defined for each optimization class with $n = 3$. A cycle in Class 1 or 3 contains a standard erlotinib dosing schedule of 150 mg/day, whereas a cycle in Class 2 contains a low-dose erlotinib schedule of 7 mg twice daily. When $n = 3$, each cycle has length $L = 168$ (one week). For Classes 1 and 2, the evofosfamide dose in each cycle is given 24 hours before the end of the week, and for Class 3 the evofosfamide dose in each cycle is given 6 hours before the end of the week. This is all depicted in step 1. Step 2 shows the removal of erlotinib doses required to satisfy the combination toxicity constraint. Each of these cycles is then repeated to form the entire dosing schedule.

weeks is $O(10^{10})$ for any optimization class or either drug type, whereas Figure 2.10 demonstrates that each of the combination therapies considered yields a total population size of $O(10^7)$ or less. In fact, when comparing Table 2.4 to Figure 2.10 we observe that all of the combination therapies we have investigated yield a considerable benefit (in terms of tumor population sizes as well as probability of resistance) over any of the optimal monotherapies in each dosing class. Thus we do not include the endpoints corresponding to monotherapies in Figure 2.10 due to the large disparity in the sizes of these results. Furthermore, at the end of treatment with evofosfamide, the tumor primarily consists of sensitive cells, which agrees with our previous observation that

evofosfamide is unable to control the sensitive cell population without erlotinib. Note that some of the means are unrealistically high for an *in vivo* setting ($> 10^{12}$), due to the fact that the model is parameterized using *in vitro* growth rates.

Class 1				
	$\mathbb{E}[X]$	$\mathbb{E}[Y]$	$\mathbb{E}[X+Y]$	$\mathbb{P}[Y>0]$
Erlotinib	$5 \cdot 10^5$	10^{10}	10^{10}	0.16
Evofosfamide	$9 \cdot 10^{15}$	$7 \cdot 10^9$	$9 \cdot 10^{15}$	1
Class 2				
	$\mathbb{E}[X]$	$\mathbb{E}[Y]$	$\mathbb{E}[X+Y]$	$\mathbb{P}[Y>0]$
Erlotinib	10^6	$4 \cdot 10^{10}$	$4 \cdot 10^{10}$	0.22
Evofosfamide	$3 \cdot 10^{17}$	$3 \cdot 10^{11}$	$3 \cdot 10^{17}$	1
Class 3				
	$\mathbb{E}[X]$	$\mathbb{E}[Y]$	$\mathbb{E}[X+Y]$	$\mathbb{P}[Y>0]$
Erlotinib	$5 \cdot 10^5$	10^{10}	10^{10}	0.16
Evofosfamide	$6 \cdot 10^{18}$	10^{13}	$6 \cdot 10^{18}$	1

Table 2.4: **Probability of resistance and means of sensitive and resistant cells at the end of treatment with monotherapy.** Means of the sensitive cells ($\mathbb{E}[X]$), resistant cells ($\mathbb{E}[Y]$), and total tumor size ($\mathbb{E}[X+Y]$), as well as the probability of resistance ($\mathbb{P}[Y>0]$), are calculated for a tumor with an initial population of $1.6 \cdot 10^6$ sensitive cells at the end of nine weeks of treatment. The dosing schedules depicted here include both types of monotherapies (erlotinib alone and evofosfamide alone) from all three optimization classes.

Means of the sensitive and resistant cell populations for $n = 1, ..., N-1$ (true combination therapies) are plotted in Figure 2.10a and Figure 2.10b, respectively. The sums of these means, or the mean tumor sizes, are plotted in Figure 2.10c. The probability of resistance for each dosing schedule is plotted in Figure 2.10d. All four panels include results for Class 1 in blue, results for Class 2 in red, and results for Class 3 in yellow. Note that in these figures, every integer on the x-axis corresponds to a combination dosing schedule given by the number of evofosfamide doses in a 3-week period, as defined in the previous paragraph.

One interesting characteristic of the means of the sensitive and resistant cells in Figure 2.10 is the presence of two local minima. It turns out that this phenomenon is due to the variability in timing between the last dose of erlotinib and the first dose of evofosfamide in each cycle.

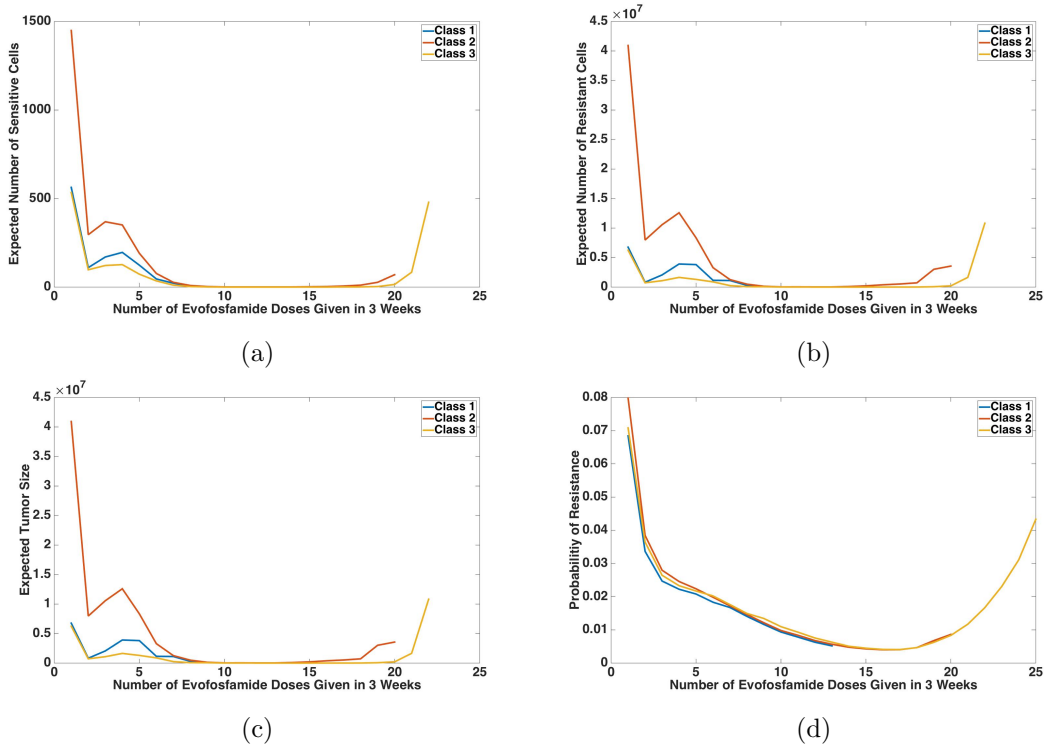

Figure 2.10: **Probability of resistance and means of sensitive and resistant cells at the end of treatment with combination therapy.** For every dosing schedule in each optimization class, means of the sensitive cells (a), resistant cells (b), and total tumor size (c), as well as probability of resistance (d), are calculated according to the model at the end of nine weeks of treatment for a tumor initially consisting of $1.6 \cdot 10^6$ sensitive cells. The results shown here only include dosing schedules from Class 1 (blue), Class 2 (red), and Class 3 (yellow) which use a combination of both erlotinib and evofosfamide. Every integer on the x-axis represents a combination dosing schedule defined by the number of evofosfamide doses administered in three weeks.

To eliminate the variation in timing between doses, we re-define all dosing schedules in Class 1 so that either erlotinib or evofosfamide is administered every day with no additional doses in between. After calculating the length L of one cycle, we round $L - 24$ to the nearest 24 hours and define that to be the time of the evofosfamide infusion. Then, ignoring combination toxicity constraints solely for the purpose of this argument, we schedule erlotinib doses every 24 hours prior to the evofosfamide infusion. After re-defining dosing schedules in this manner, there no longer exists variability in

the time between drug administrations since there is always a 24-hour waiting period between any two doses.

Originally, because the n evofosfamide doses were evenly divided into every three weeks, the end of treatment (at nine weeks) was also the end of a treatment cycle for every dosing schedule. However, that is no longer the case for these new daily dosing schedules since doses are forced to occur every 24 hours and only every 24 hours. Thus there are now two options for what to consider as the end of treatment. We may define the end of treatment to be exactly nine weeks from the treatment start date, but this introduces variability in the position within the cycle at which the resistance dynamics are calculated. The other option is to define the end of treatment to be the end of the cycle closest to nine weeks, but this will be at different times for different dosing schedules.

We examine both of these possibilities by re-calculating the means of the sensitive and resistant cells at both of these times for Class 1 under these new daily dosing schedules, shown in Figure 2.11a and Figure 2.11b, respectively. For the sake of comparison, the optimization results from the original dosing schedules in Class 1 are shown in blue. For each daily dosing schedule, the means of the sensitive and resistant cells are calculated at two different times: nine weeks from the start of treatment (yellow) and the end of the cycle closest to nine weeks after treatment begins (red). During the creation of the daily dosing schedules, the rounding of $L - 24$ to the nearest 24 hours leads to multiple dosing schedules with the same dose timing but different doses. To simplify the analysis, we only include one dosing schedule with each particular schedule of doses in Figure 2.11, chosen based on which n yields the value of $L - 24$ closest to the common rounded value.

Let us now compare the results from the original dosing schedules with those from the daily dosing schedules. The elimination of the variability in time between doses causes the first local minimum to become less pronounced for both the mean of the sensitive cells and the mean of the resistant cells, regardless of how the end of treatment is defined. Although the first local minimum still exists, its existence can now be easily explained in every case based on the different types of variation that have been introduced.

When the end of treatment is defined to be nine weeks after the treatment start date, this introduces variability in the relative position within the cycle at which the

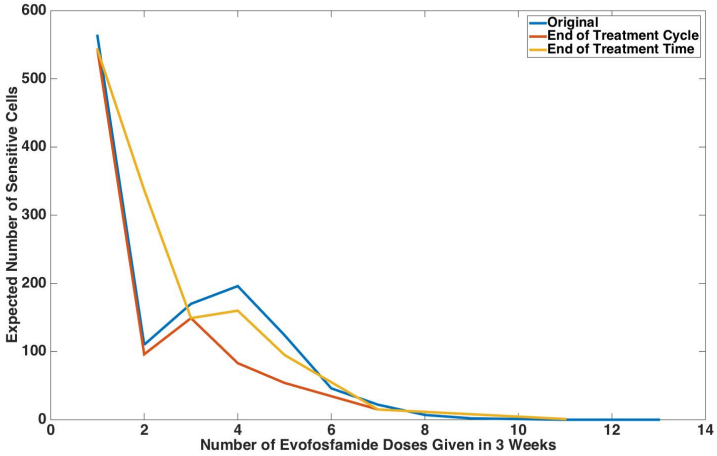

(a)

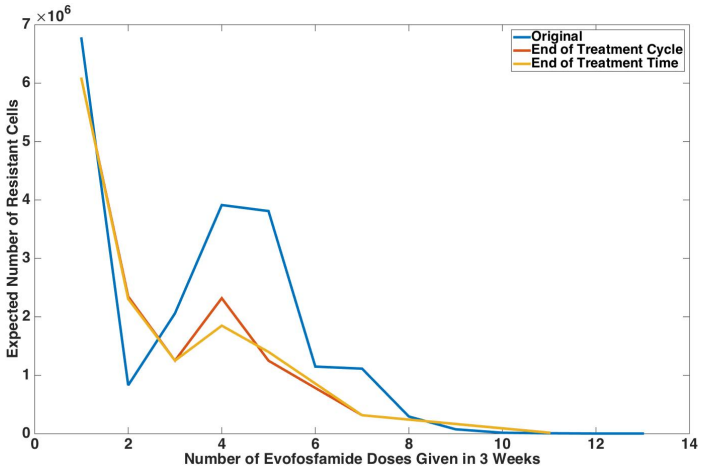

(b)

Figure 2.11: **A comparison of means of sensitive and resistant cells for dosing schedules with and without variation in amount of time between doses.** The means of the sensitive (a) and resistant (b) cell populations at the end of treatment for a tumor initially consisting of $1.6 \cdot 10^6$ sensitive cells are plotted for the original dosing schedules with variation in time between doses from Class 1 (blue) as well as the newly-defined daily dosing schedules, which eliminate this variation. For each daily dosing schedule, these means are calculated at two different times: nine weeks from the start of treatment (yellow) and the end of the cycle closest to nine weeks after treatment begins (red).

evolutionary dynamics are calculated. Specifically, the point at which this calculation occurs during treatment for $n = 3$ is at the very end of a cycle (after a large decline in the cancer cell population due to evofosfamide), whereas the point at which this calculation occurs for $n = 2$ and $n = 4$ is right before a dose of evofosfamide. This explains the existence of a local minimum at $n = 3$ for both means when the end of treatment is defined to be nine weeks after the start of treatment.

On the other hand, when the end of treatment is defined to be the end of a cycle, this introduces variability in the actual time at which the recurrence dynamics are calculated, and hence variability in the total treatment time. Specifically, the total treatment time for $n = 2$ is quite high relative to other values of n. Since the sensitive cell population is in a constant state of decline during treatment, this explains the existence of a local minimum at $n = 2$ for the mean of the sensitive cell population when the end of treatment is defined as the end of a cycle. Additionally, the total treatment time for $n = 3$ is quite low relative to other values of n. Since the resistant cell population is steadily growing by the end of treatment, this explains the existence of a local minimum at $n = 3$ for the mean of the resistant cells when the end of treatment is defined as the end of a cycle.

Note that for the mean of the sensitive cells, by following the curve for which the end of treatment is defined to be at nine weeks up to $n = 3$ and then the curve for which the end of treatment is defined to be the end of a cycle, the first local minimum is completely eliminated. This is a reasonable comparison to make because for $n = 3$, nine weeks after the start of treatment is the end of a treatment cycle. Together, all of the above evidence shows that the first local minimum is due to the variability in timing between the last dose of erlotinib and the first dose of evofosfamide in each cycle.

Minimize treatment break after evofosfamide dosing. Next consider the results due to combination therapy shown in Figure 2.10. We note that all three classes lead to similar results, which suggests that our findings regarding the characteristics of optimal combination dosing strategies are quite robust. Upon closer examination, Figure 2.10 demonstrates that the tumor population sizes under the Class 3 schedules are generally less than half the population sizes under Class 1, and also less than those under Class 2. This suggests that designing schedules that minimize the amount of time after a dose of evofosfamide and before a dose of erlotinib may lead to better control of the tumor

population. This finding is in agreement with our previous observations that the tumor population response to evofosfamide is strong but short-lived; hence quickly intervening in the subsequent population growth phase is important.

As we move along the spectrum of combination densities (horizontal axis) from monotherapy with erlotinib to monotherapy with evofosfamide, there is a clear region in the interior (approximately $n = 9$–17 evofosfamide doses) where the tumor size and sensitive and resistant population size are minimized. This region also contains the region minimizing the probability of developing resistance. To investigate this further, Table 2.5 shows the specific n which optimizes the given characteristic (means of sensitive, resistant, and total cancer cells as well as probability of resistance are all minimized). In addition, the bottom row of Table 2.5 indicates the best overall dosing schedule among all three classes which minimizes the particular value that column represents.

	$\mathbb{E}[X]$	$\mathbb{E}[Y]$	$\mathbb{E}[X+Y]$	$\mathbb{P}[Y>0]$
Class 1	$n = 13$	$n = 13$	$n = 13$	$n = 13$
Class 2	$n = 12$	$n = 12$	$n = 12$	$n = 16$
Class 3	$n = 14$	$n = 14$	$n = 14$	$n = 17$
Best Overall	Class 3, $n = 14$	Class 3, $n = 14$	Class 3, $n = 14$	Class 2, $n = 16$

Table 2.5: **Optimal dosing schedules for each class.** For each class, this table shows the values of n for which the means of sensitive, resistant, and total cancer cells, as well as probability of resistance, are each minimized. For each column, the bottom row indicates which of the three classes produces the best overall result for that characteristic of the cancer cell population at the end of treatment.

Sequential alternating sequences are optimal. From Table 2.5 we observe that all optimal dosing schedules correspond to values of n between 12 and 17. This implies that combination therapies incorporating more frequent, smaller doses of evofosfamide result in better treatment outcomes. Even more interestingly, all values of n in Table 2.5 correspond to the same type of dosing schedule. Besides $n = 12$ in Class 2, every other optimal n corresponds to a dosing schedule which alternates between a single dose of erlotinib and a single dose of evofosfamide. We call these alternating dosing schedules. The dosing schedule corresponding to $n = 12$ in Class 2 consists of two low doses of erlotinib for every dose of evofosfamide, which is still quite similar to the alternating dosing schedules. Thus, even though the optimization ranged over a full spectrum of

treatment schedules incorporating variable dose densities for each drug, the optimal therapies were those that utilized close to an equal number of doses of evofosfamide and erlotinib in a sequential alternating fashion.

2.4 Discussion

In this work, we considered an approach to investigate the use of hypoxia-activated prodrugs (HAPs) to enhance the effectiveness of targeted therapies and, in particular, prevent the (usually inevitable) emergence of drug resistance. To this end, we developed a model reflecting the heterogeneity of oxygen and drug concentrations throughout a tumor to describe the evolutionary dynamics of resistance emerging under combination HAP-targeted therapy strategies. The model was parameterized using experimental and clinical pharmacokinetic data to investigate potential combinations of the HAP evofosfamide with the targeted tyrosine kinase inhibitor erlotinib against EGFR-activated NSCLC. Our model predictions are useful in comparing the outcomes of a spectrum of dosing schedules in the *in vitro* setting, and provide a means to use available experimental data to help inform and guide future clinical studies *in vivo*.

We investigated combinations in which doses were not given simultaneously (to avoid toxicities) and our model predicted that the complementary action of evofosfamide and erlotinib results in a combined ability to control the tumor's evolution and growth. In particular:

(i) Combination therapies outperform standard clinical monotherapies. This is most significantly realized in reduction of the probability of developing resistance. The time to progression, for those who develop resistance, is 40.54% longer using an optimal combination therapy rather than standard monotherapy with erlotinib.

(ii) Sequentially alternating single doses of each drug leads to minimal tumor burden and maximal reduction in probability of developing resistance. Deviating significantly from an equal number of evofosfamide and erlotinib doses leads to an increase in both average tumor burden and the probability of developing resistance.

(iii) Strategies minimizing the length of time after an evofosfamide dose and before

erlotinib confer further benefits in reduction of tumor burden. The tumor population response to evofosfamide is strong but short-lived; hence quickly intervening in the subsequent population growth phase is important.

These alternating dosing schedules (and other similar dosing schedules) are likely the most effective because the constant switching between erlotinib and evofosfamide allows the strengths of these drugs to complement one another. Too much time spent taking erlotinib without evofosfamide allows the sensitive cell population to remain quite substantial for a long period of time (due to the lack of targeting the hypoxic regions), which, in turn, leads to a high probability of a resistance mutation arising. On the other hand, too much time spent on evofosfamide without erlotinib allows the sensitive cell population to expand drastically since evofosfamide is unable to control its long-term growth. Alternating between these two drugs allows each one to provide the necessary control over the cancer cell population the other one is lacking. In addition, it is important to consider the subpopulation of cancer cells each drug acts on. Erlotinib acts primarily on portions of the tumor microenvironment close to blood vessels, whereas evofosfamide acts primarily on hypoxic regions that are further from the blood stream. Because of this, alternating frequently between the two drugs allows the entire population of cancer cells in the tumor microenvironment to be constantly controlled by the drugs. This same phenomenon has recently been observed with a different combination therapy utilizing evofosfamide in neuroblastoma and rhabdomyosarcoma preclinical models [61].

These results demonstrate that incorporating HAPs in combination with targeted therapies may be an effective tool in preventing resistance, and suggest an alternative use for HAPs. Current clinical trials have combined HAPs not with targeted therapies but with chemotherapies to control tumor growth. In addition, these trials used dosing strategies involving simultaneous drug administration rather than sequential administration, as is used in our model. It is difficult to draw conclusions about the outcome of these clinical trials using our model since this would require growth rate parameterizations and pharmacokinetics for the chemotherapies utilized in the combination treatment (gemcitabine and doxorubicin) in different cell types (pancreatic cancers and soft tissue sarcomas). However, we did observe that the reduction in probability of developing resistance is dependent on the exact timing and sequence of the combination

therapy. This highlights the importance of using mathematical modeling to predict treatment outcomes and inform decisions regarding schedules to be tested in clinical trials.

In addition to its promising clinical implications, this work provides insight into the biological factors which can cause a treatment strategy to either succeed or fail. Specifically, analysis and comparison of the tumor evolutionary dynamics during single-agent and combination therapy suggests that erlotinib and evofosfamide may be effective together because they target separate subpopulations within the tumor microenvironment and on much different scales of time with differing degrees of strength. This theory can be generalized to predict which types of drugs have the potential to be strong partners in combination therapy; specifically, this methodology can be applied to determine the biological and pharmacokinetic parameters that may lead to treatment success or failure with monotherapy or combination therapy. These findings highlight the importance of designing combination therapies with drugs whose strengths complement each other in order to maximize the therapeutic benefits. Another important implication of this work, and something to consider when designing combination dosing regimens using two or more drugs, is the role that variability in timing between the dosing of different drugs plays in treatment outcomes.

This work gave rise to multiple promising improvements that could be made in the treatment of NSCLC. However, the dosing strategies proposed here need to be tested *in vivo* to verify these model predictions. In addition, this work provided a novel framework for defining drug toxicity constraints, which is sufficiently general to be extended to any drug or combination of drugs. One planned extension of this work is to further study the implications of cellular migration within the microenvironment on the evolutionary dynamics of the tumor. An initial investigation into this impact is shown in Section 2.5. For this study, experimental work investigating the details of the migration patterns and quantification of migration rates in this system are necessary. In addition, since evofosfamide is hypoxia-activated and birth and death rates due to erlotinib are microenvironment-dependent, there is good reason to suspect that alterations to the tumor microenvironment would have a large impact on the treatment outcomes with both single-agent and combination therapy. In Section 2.6, we provide some preliminary results to support this hypothesis. Other extensions of this work include considering

the possibility of pre-existing resistance as well as modeling the bystander effect, which refers to the idea that evofosfamide, once activated in a hypoxic region of the tumor, diffuses outward and affects cancer cells in normoxic regions as well [34, 37]. In addition, it would be useful to explore the effect of HAPs other than evofosfamide on the probability of developing resistance in order to determine whether the results presented here are specific to evofosfamide or rather are a general phenomenon of HAPs used in combination with tyrosine kinase inhibitors.

2.5 Impact of Migration

To investigate the impact of migration on our model predictions, we relaxed the assumption that the evolutionary dynamics within each microenvironmental compartment are independent by introducing a migration term that allows cells to move between compartments. In addition to proliferating and dying, suppose cells in compartment i migrate to compartment j with rate $\rho(i,j)$. Assume that cells in compartment i can only migrate to compartment $i+1$ or $i-1$ at a given point in time. Then the means of the sensitive and resistant cells in each compartment are governed by a system of 64 ODE's. For $i = 1, 2, ..., 32$, we have

$$\begin{aligned}
\frac{d}{dt}\mathbb{E}[X_i(t)] = &\Big(\lambda_{X,i}(t) - \mu_{X,i}(t) - \rho(i,i-1) - \rho(i,i+1)\Big)\mathbb{E}[X_i(t)] \\
&+ \rho(i-1,i)\mathbb{E}[X_{i-1}(t)] + \rho(i+1,i)\mathbb{E}[X_{i+1}(t)], \\
\frac{d}{dt}\mathbb{E}[Y_i(t)] = &\Big(\lambda_{Y,i}(t) - \mu_{Y,i}(t) - \rho(i,i-1) - \rho(i,i+1)\Big)\mathbb{E}[Y_i(t)] \\
&+ \lambda_{X,i}(t)u\mathbb{E}[X_i(t)] + \rho(i-1,i)\mathbb{E}[Y_{i-1}(t)] + \rho(i+1,i)\mathbb{E}[Y_{i+1}(t)].
\end{aligned}$$

In the above equations, let $\rho(1,0) = \rho(0,1) = 0$ and $\rho(32,33) = \rho(33,32) = 0$ to account for the fact that there are only 32 compartments.

We defined the migration rate $\rho(i,j)$ using three different methods. Let the rates defined by these methods be denoted as $\rho_A(i,j)$, $\rho_B(i,j)$, and $\rho_C(i,j)$. For each compartment, by using the decay rate of oxygen away from the blood vessel together with the range of oxygen concentrations in that compartment, we estimated the range of distances from the blood vessel that correspond to the given compartment. We then used

the minimum and maximum distances for each compartment to estimate a measurement of "width" - call this w_i for compartment i. To estimate w_i for the compartment furthest from the nearest blood vessel, we used the fact that the mean inter-capillary distance in tumor tissue is approximately 300 μm, so the point furthest from the nearest blood vessel in this compartment is at a distance of approximately 150 μm [62, 63]. We assume that cells travel at a rate of $r = 0.3$ μm/min [64]. The first method we used to define $\rho_A(i, j)$ assumes that cells only migrate toward the nearest blood vessel. So the migration rate is given by

$$\rho_A(i,j) = \begin{cases} \frac{r}{w_i} & i < j \\ 0 & i \geq j. \end{cases} \tag{2.18}$$

The second method we used assumes that cells only migrate away from the nearest blood vessel. Then the migration rate is given by

$$\rho_B(i,j) = \begin{cases} \frac{r}{w_i} & i > j \\ 0 & i \leq j. \end{cases} \tag{2.19}$$

For the third method, we allowed cells to migrate both toward and away from the nearest blood vessel with a constant migration rate of $\rho_C(i, j) = 0.1$. This is a reasonable estimate since the order of magnitude of r is -1 and for most compartments, w_i has order of magnitude 0.

To examine the impact of migration on the mean tumor size, we calculated mean tumor size over time for two different combination dosing schedules using migration defined in each of the three methods described above as well as without migration. Figure 2.12a shows the results of this calculation for a dosing schedule that combines a standard 150 mg daily erlotinib schedule with a standard 575 mg/m^2 weekly evofosfamide schedule. Figure 2.12b shows the results for the combination dosing schedule given by $n = 14$ in Class 3, which was found to be the optimal dosing schedule to minimize mean tumor size in the previous section.

We find that migration does have an impact on our model predictions with regards to mean tumor size. Since the majority of the cancer cells are initially in hypoxic regions of the tumor microenvironment, allowing migration between compartments governed

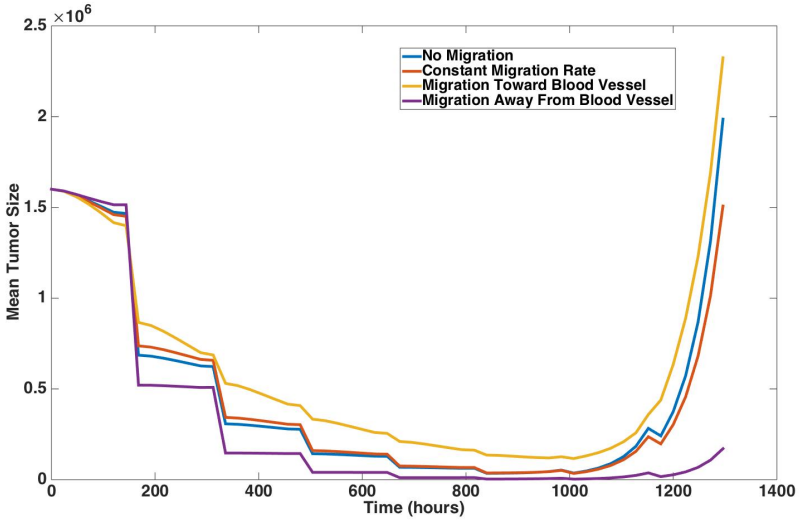

(a)

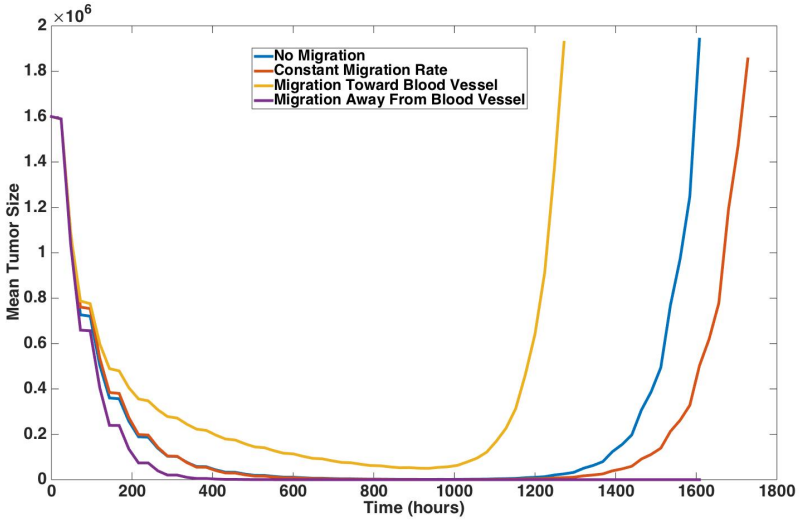

(b)

Figure 2.12: **A comparison of mean tumor size with and without migration.** Mean tumor size over time is plotted for two different combination dosing schedules in (a) and (b) using no migration (blue curves), a constant migration rate (red curves), a migration rate in which cells can only move toward the nearest blood vessel (yellow curves), and a migration rate in which cells can only move away from the nearest blood vessel (purple curves).

by a constant migration rate leads to a more well-mixed population. Therefore, with a constant migration rate incorporated into the model, erlotinib has more of an effect on the population while evofosfamide has less of an effect since the cells are more evenly distributed throughout the tumor microenvironment. This can be seen in Figure 2.12a and Figure 2.12b. This same phenomenon can be observed in the case where cells only migrate toward the blood vessel, although it is more pronounced in this situation since cells are only allowed to move away from the hypoxic regions of the tumor microenvironment. On the other hand, by incorporating migration such that cells may only move away from the blood vessel, the observed shift in mean tumor size is likely due to a decreased response to erlotinib and an increased response to evofosfamide due to the fact that the cancer cells are even more concentrated in hypoxic regions.

These results indicate that unidirectional migration of cell populations either towards or away from blood vessels have more of an impact on the model-predicted mean tumor evolution than bidirectional migration rates. However, the migration rates chosen here fell on the higher end of literature-reported values, and it is likely that migration patterns found *in vivo* are multidirectional, heterogeneous and dependent upon cellular density in local and surrounding compartments. In addition, it is possible that sensitive and resistant cells may have different migration speeds or capabilities. To better quantify the impact of migration on the evolutionary dynamics of the tumor population, further experimental investigation is needed to quantify migration rates and develop a more refined mathematical model of local migration between compartments.

2.6 Impact of Tumor Oxygenation

Here, we extend our model to study the effect of changing the tumor microenvironment on response to treatment with erlotinib and evofosfamide. Since erlotinib response is microenvironment-dependent and evofosfamide is hypoxia-activated, it may be possible to improve predicted treatment outcomes even further by manipulating the state of the tumor microenvironment. We compare predicted treatment outcomes using a standard tumor microenvironment with those using tumor microenvironments where the overall oxygen concentration throughout the tumor has been either increased or decreased. This comparison provides insight into how alterations to the tumor microenvironment could

be leveraged to maximize the therapeutic benefit of these drugs. The addition of this work contributes to a more complete understanding of the interactions between cancer cells and their microenvironments as well as provides a potentially improved strategy for optimal tumor control in NSCLC patients.

We predict the evolutionary dynamics of three different tumors (one well-oxygenated, one poorly-oxygenated, and one whose oxygen profile mirrors standard tumor physiologic data) undergoing therapy with two separate combination dosing regimens. For each of these tumors and each of the two therapies, the predicted mean tumor size and probability of resistance up to recurrence time (the time at which the cancer cell population reaches its initial size once again) are plotted in Figure 2.13. The blue curves show the evolutionary dynamics of a tumor with a 13.16% oxygen concentration at the blood vessels, which matches tumor physiologic data [51]. The red curves show the dynamics of a more well-oxygenated tumor (26.32% at the blood vessels) and the yellow curves show the dynamics of a more poorly-oxygenated tumor (6.58% at the blood vessels). Predictions for a dosing schedule in which the patient is given 150 mg erlotinib daily on the first 5 days of each week and 575 mg/m^2 evofosfamide on the last day of each week are shown in Figure 2.13a and Figure 2.13b. Predictions for a dosing schedule in which the patient receives one dose of 150 mg erlotinib and one dose of 248 mg/m^2 evofosfamide in every 36-hour period (the optimal dosing schedule identified in Subsection 2.3.3) are shown in Figure 2.13c and Figure 2.13d.

These results suggest that treatment with a combination of erlotinib and evofosfamide may be more effective on poorly-oxygenated tumors and less effective on well-oxygenated tumors. Although we observe a benefit to poorly-oxygenated tumors during therapy with each drug since cellular growth rates are reduced as oxygen levels are lowered, changes in tumor oxygenation play a larger role in response to evofosfamide than to erlotinib. This is because evofosfamide is hypoxia-activated, and hence more effective at lower oxygen concentrations. Thus tumor oxygenation differences lead to a more dramatic difference in response during the dosing schedule used in Figure 2.13c compared with the dosing schedule used in Figure 2.13a. In light of these observations, we conclude that the optimal treatment strategies proposed in Subsection 2.3.3 may be improved further by decreasing the oxygen throughout the tumor and maximizing the number of evofosfamide doses.

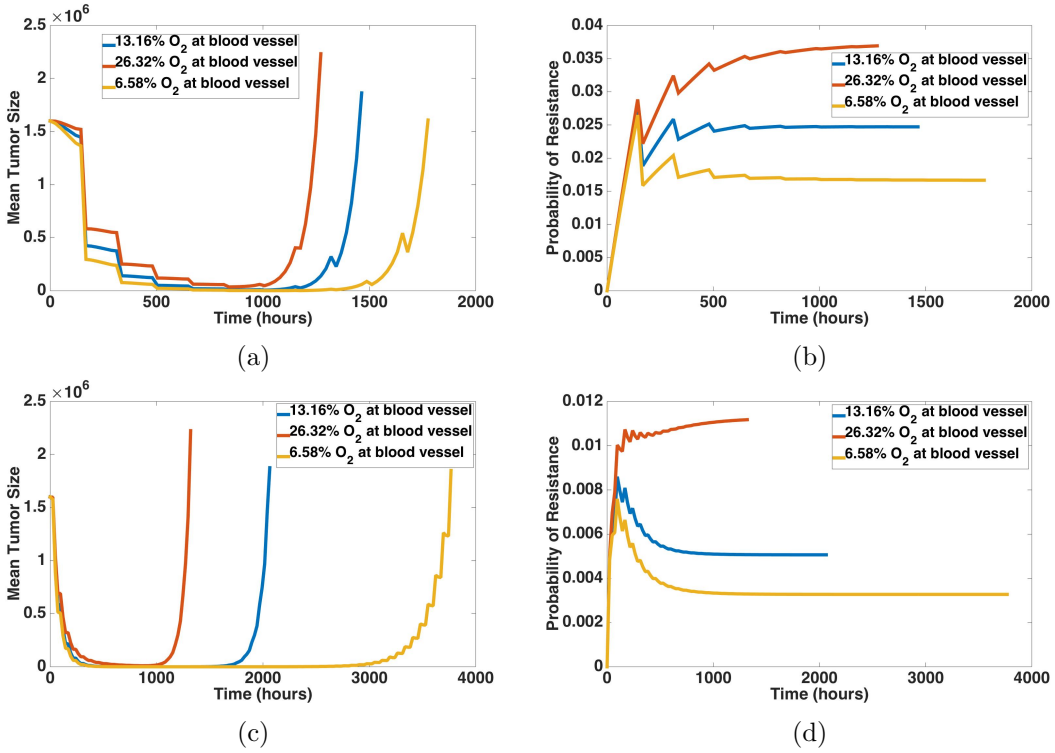

Figure 2.13: **Comparison of evolutionary dynamics over time for tumors with varying oxygen profiles.** Mean tumor size (a) and probability of resistance (b) are calculated up to recurrence time for a dosing schedule consisting of 150 mg erlotinib daily for days 1–5 and 575 mg/m^2 evofosfamide given on day 7 of every week. Mean tumor size (c) and probability of resistance (d) are plotted for a dosing schedule consisting of one dose of 150 mg erlotinib and one dose of 248 mg/m^2 evofosfamide given every 36 hours. Results are shown for a tumor with a concentration of 13.16% oxygen at the blood vessels in blue, 26.32% oxygen in red, and 6.58% oxygen in yellow.

The addition of this work suggests another approach with the potential to further improve treatment outcomes for patients with NSCLC. In Subsection 2.3.2, our model predicted that, while the emergence of resistance is inevitable during monotherapy with erlotinib, the addition of evofosfamide may result in tumor eradication for a significant fraction of patients. Here we have shown that this combination strategy may be improved upon even further with the addition of therapy aimed at decreasing tumor oxygenation. Given the correct timing and dosing sequence of erlotinib and evofosfamide,

the combination of these two drugs, together with additional therapy to decrease oxygen concentration throughout tumors, may have the potential to significantly improve treatment outcomes for NSCLC patients.

2.7 Supplementary Matrices

Here we show the matrices SB, SD, RB, and RD used to calculate the birth and death rate functions of erlotinib-sensitive and erlotinib-resistant cells, defined in Subsection 2.2.2.

$$SB = \begin{bmatrix} 1.1053393e{-}02 & 4.7156432e{-}04 & 7.7651360e{-}03 \\ 5.4991358e{-}04 & 1.1535643e{-}05 & 5.9142865e{-}04 \\ 5.4989360e{-}04 & 1.1528540e{-}05 & 5.9146688

$$SD = \begin{bmatrix}
1.4792648e{-}03 & -2.7085135e{-}05 & -4.5609723e{-}04 \\
1.5481068e{-}03 & -2.5930657e{-}05 & -4.5845635e{-}04 \\
1.6169489e{-}03 & -2.4776179e{-}05 & -4.6081546e{-}04 \\
1.6857909e{-}03 & -2.3621701e{-}05 & -4.6317457e{-}04 \\
1.7546330e{-}03 & -2.2467222e{-}05 & -4.6553369e{-}04 \\
1.8234750e{-}03 & -2.1312744e{-}05 & -4.6789280e{-}04 \\
1.8923170e{-}03 & -2.0158266e{-}05 & -4.7025192e{-}04 \\
1.9611591e{-}03 & -1.9003788e{-}05 & -4.7261103e{-}04 \\
2.0300011e{-}03 & -1.7849310e{-}05 & -4.7497014e{-}04 \\
2.0988432e{-}03 & -1.6694831e{-}05 & -4.7732926e{-}04 \\
2.1676852e{-}03 & -1.5540353e{-}05 & -4.7968837e{-}04 \\
2.2365272e{-}03 & -1.4385875e{-}05 & -4.8204748e{-}04 \\
2.3053693e{-}03 & -1.3231397e{-}05 & -4.8440660e{-}04 \\
2.3742113e{-}03 & -1.2076919e{-}05 & -4.8676571e{-}04 \\
2.4430534e{-}03 & -1.0922440e{-}05 & -4.8912483e{-}04 \\
2.5118954e{-}03 & -9.7679622e{-}06 & -4.9148394e{-}04 \\
2.5807374e{-}03 & -8.6134840e{-}06 & -4.9384305e{-}04 \\
2.6495795e{-}03 & -7.4590058e{-}06 & -4.9620217e{-}04 \\
2.7184215e{-}03 & -6.3045276e{-}06 & -4.9856128e{-}04 \\
2.7872635e{-}03 & -5.1500494e{-}06 & -5.0092040e{-}04 \\
2.8561056e{-}03 & -3.9955712e{-}06 & -5.0327951e{-}04 \\
2.9249476e{-}03 & -2.8410930e{-}06 & -5.0563862e{-}04 \\
2.9937897e{-}03 & -1.6866148e{-}06 & -5.0799774e{-}04 \\
3.0626317e{-}03 & -5.3213659e{-}07 & -5.1035685e{-}04 \\
3.1314737e{-}03 & 6.2234162e{-}07 & -5.1271597e{-}04 \\
3.2003158e{-}03 & 1.7768198e{-}06 & -5.1507508e{-}04 \\
3.2691578e{-}03 & 2.9312980e{-}06 & -5.1743419e{-}04 \\
3.3379999e{-}03 & 4.0857762e{-}06 & -5.1979331e{-}04 \\
3.4068419e{-}03 & 5.2402544e{-}06 & -5.2215242e{-}04 \\
3.4756839e{-}03 & 6.3947326e{-}06 & -5.2451154e{-}04 \\
3.5445260e{-}03 & 7.5492109e{-}06 & -5.2687065e{-}04 \\
3.6133680e{-}03 & 8.7036891e{-}06 & -5.2922976e{-}04 \\
3.6822101e{-}03 & 9.8581673e{-}06 & -5.3158888e{-}04 \\
3.7510521e{-}03 & 1.1012645e{-}05 & -5.3394799e{-}04 \\
3.8198941e{-}03 & 1.2167124e{-}05 & -5.3630711e{-}04 \\
3.8887362e{-}03 & 1.3321602e{-}05 & -5.3866622e{-}04 \\
3.9575782e{-}03 & 1.4476080e{-}05 & -5.4102533e{-}04 \\
4.0264203e{-}03 & 1.5630558e{-}05 & -5.4338445e{-}04 \\
4.0952623e{-}03 & 1.6785036e{-}05 & -5.4574356e{-}04 \\
4.1641043e{-}03 & 1.7939515e{-}05 & -5.4810267e{-}04 \\
4.2329464e{-}03 & 1.9093993e{-}05 & -5.5046179e{-}04 \\
4.3017884e{-}03 & 2.0248471e{-}05 & -5.5282090e{-}04 \\
4.3706305e{-}03 & 2.1402949e{-}05 & -5.5518002e{-}04 \\
4.4394725e{-}03 & 2.2557428e{-}05 & -5.5753913e{-}04 \\
4.5083145e{-}03 & 2.3711906e{-}05 & -5.5989824e{-}04 \\
4.5771566e{-}03 & 2.4866384e{-}05 & -5.6225736e{-}04 \\
4.6459986e{-}03 & 2.6020862e{-}05 & -5.6461647e{-}04 \\
4.7148406e{-}03 & 2.7175340e{-}05 & -5.6697559e{-}04 \\
4.7836827e{-}03 & 2.8329819e{-}05 & -5.6933470e{-}04 \\
4.8525247e{-}03 & 2.9484297e{-}05 & -5.7169381e{-}04 \\
4.9213668e{-}03 & 3.0638775e{-}05 & -5.7405293e{-}04 \\
4.9902088e{-}03 & 3.1793253e{-}05 & -5.7641204e{-}04 \\
5.0590508e{-}03 & 3.2947731e{-}05 & -5.7877116e{-}04 \\
5.1278929e{-}03 & 3.4102210e{-}05 & -5.8113027e{-}04 \\
5.1967349e{-}03 & 3.5256688e{-}05 & -5.8348938e{-}04 \\
5.2655770e{-}03 & 3.6411166e{-}05 & -5.8584850e{-}04 \\
5.3344190e{-}03 & 3.7565644e{-}05 & -5.8820761e{-}04 \\
5.4032610e{-}03 & 3.8720122e{-}05 & -5.9056673e{-}04 \\
5.4721031e{-}03 & 3.9874601e{-}05 & -5.9292584e{-}04 \\
5.5409451e{-}03 & 4.1029079e{-}05 & -5.9528495e{-}04 \\
5.6097872e{-}03 & 4.2183557e{-}05 & -5.9764407e{-}04 \\
5.6786292e{-}03 & 4.3338035e{-}05 & -6.0000318e{-}04 \\
5.7474712e{-}03 & 4.4492513e{-}05 & -6.0236230e{-}04 \\
5.8163133e{-}03 & 4.5646992e{-}05 & -6.0472141e{-}04 \\
5.8851553e{-}03 & 4.6801470e{-}05 & -6.0708052e{-}04 \\
5.9539974e{-}03 & 4.7955948e{-}05 & -6.0943964e{-}04 \\
6.0228394e{-}03 & 4.9110426e{-}05 & -6.1179875e{-}04 \\
6.0916814e{-}03 & 5.0264904e{-}05 & -6.1415786e{-}04 \\
6.1605235e{-}03 & 5.1419383e{-}05 & -6.1651698e{-}04 \\
6.2293655e{-}03 & 5.2573861e{-}05 & -6.1887609e{-}04 \\
6.2982076e{-}03 & 5.3728339e{-}05 & -6.2123521e{-}04 \\
6.3670496e{-}03 & 5.4882817e{-}05 & -6.2359432e{-}04 \\
6.4358916e{-}03 & 5.6037295e{-}05 & -6.2595343e{-}04 \\
6.5047337e{-}03 & 5.7191774e{-}05 & -6.2831255e{-}04 \\
6.5735757e{-}03 & 5.8346252e{-}05 & -6.3067166e{-}04 \\
6.6424177e{-}03 & 5.9500730e{-}05 & -6.3303078e{-}04 \\
6.7112598e{-}03 & 6.0655208e{-}05 & -6.3538989e{-}04 \\
6.7801018e{-}03 & 6.1809687e{-}05 & -6.3774900e{-}04 \\
6.8489439e{-}03 & 6.2964165e{-}05 & -6.4010812e{-}04 \\
6.9177859e{-}03 & 6.4118643e{-}05 & -6.4246723e{-}04 \\
6.9866279e{-}03 & 6.5273121e{-}05 & -6.4482635e{-}04 \\
7.0554700e{-}03 & 6.6427599e{-}05 & -6.4718546e{-}04 \\
7.1243120e{-}03 & 6.7582078e{-}05 & -6.4954457e{-}04 \\
7.1931541e{-}03 & 6.8736556e{-}05 & -6.5190369e{-}04 \\
7.2619961e{-}03 & 6.9891034e{-}05 & -6.5426280e{-}04 \\
7.3308381e{-}03 & 7.1045512e{-}05 & -6.5662192e{-}04 \\
7.3996802e{-}03 & 7.2199990e{-}05 & -6.5898103e{-}04 \\
7.4685222e{-}03 & 7.3354469e{-}05 & -6.6134014e{-}04 \\
7.5373643e{-}03 & 7.4508947e{-}05 & -6.6369926e{-}04 \\
7.6062063e{-}03 & 7.5663425e{-}05 & -6.6605837e{-}04 \\
7.6750483e{-}03 & 7.6817903e{-}05 & -6.6841749e{-}04 \\
7.7438904e{-}03 & 7.7972381e{-}05 & -6.7077660e{-}04 \\
7.8127324e{-}03 & 7.9126860e{-}05 & -6.7313571e{-}04 \\
7.8815745e{-}03 & 8.0281338e{-}05 & -6.7549483e{-}04 \\
7.9504165e{-}03 & 8.1435816e{-}05 & -6.7785394e{-}04 \\
8.0192585e{-}03 & 8.2590294e{-}05 & -6.8021306e{-}04 \\
8.0881006e{-}03 & 8.3744772e{-}05 & -6.8257217e{-}04 \\
8.1569426e{-}03 & 8.4899251e{-}05 & -6.8493128e{-}04 \\
8.2257846e{-}03 & 8.6053729e{-}05 & -6.8729040e{-}04 \\
8.2946267e{-}03 & 8.7208207e{-}05 & -6.8964951e{-}04 \\
8.3634687e{-}03 & 8.8362685e{-}05 & -6.9200862e{-}04
\end{bmatrix}$$

$$RB = \begin{bmatrix}
1.0085430e{-}02 & 1.0771499e{-}04 & 8.7460853e{-}03 \\
1.0022742e{-}02 & 1.0536662e{-}04 & 8.6793665e{-}03 \\
9.9600535e{-}03 & 1.0301824e{-}04 & 8.6126477e{-}03 \\
9.8973651e{-}03 & 1.0066987e{-}04 & 8.5459288e{-}03 \\
9.8346767e{-}03 & 9.8321502e{-}05 & 8.4792100e{-}03 \\
9.7719883e{-}03 & 9.5973131e{-}05 & 8.4124912e{-}03 \\
9.7092999e{-}03 & 9.3624760e{-}05 & 8.3457724e{-}03 \\
9.6466115e{-}03 & 9.1276388e{-}05 & 8.2790536e{-}03 \\
9.5839231e{-}03 & 8.8928017e{-}05 & 8.2123348e{-}03 \\
9.5212347e{-}03 & 8.6579646e{-}05 & 8.1456160e{-}03 \\
9.4585463e{-}03 & 8.4231275e{-}05 & 8.0788971e{-}03 \\
9.3958579e{-}03 & 8.1882904e{-}05 & 8.0121783e{-}03 \\
9.3331695e{-}03 & 7.9534532e{-}05 & 7.9454595e{-}03 \\
9.2704811e{-}03 & 7.7186161e{-}05 & 7.8787407e{-}03 \\
9.2077927e{-}03 & 7.4837790e{-}05 & 7.8120219e{-}03 \\
9.1451043e{-}03 & 7.2489419e{-}05 & 7.7453031e{-}03 \\
9.0824159e{-}03 & 7.0141048e{-}05 & 7.6785843e{-}03 \\
9.0197275e{-}03 & 6.7792676e{-}05 & 7.6118654e{-}03 \\
8.9570391e{-}03 & 6.5444305e{-}05 & 7.5451466e{-}03 \\
8.8943507e{-}03 & 6.3095934e{-}05 & 7.4784278e{-}03 \\
8.8316623e{-}03 & 6.0747563e{-}05 & 7.4117090e{-}03 \\
8.7689739e{-}03 & 5.8399191e{-}05 & 7.3449902e{-}03 \\
8.7062855e{-}03 & 5.6050820e{-}05 & 7.2782714e{-}03 \\
8.6435971e{-}03 & 5.3702449e{-}05 & 7.2115526e{-}03 \\
8.5809087e{-}03 & 5.1354078e{-}05 & 7.1448337e{-}03 \\
8.5182203e{-}03 & 4.9005707e{-}05 & 7.0781149e{-}03 \\
8.4555319e{-}03 & 4.6657335e{-}05 & 7.0113961e{-}03 \\
8.3928435e{-}03 & 4.4308964e{-}05 & 6.9446773e{-}03 \\
8.3301551e{-}03 & 4.1960593e{-}05 & 6.8779585e{-}03 \\
8.2674667e{-}03 & 3.9612222e{-}05 & 6.8112397e{-}03 \\
8.2047783e{-}03 & 3.7263850e{-}05 & 6.7445209e{-}03 \\
8.1420899e{-}03 & 3.4915479e{-}05 & 6.6778020e{-}03 \\
8.0794015e{-}03 & 3.2567108e{-}05 & 6.6110832e{-}03 \\
8.0167131e{-}03 & 3.0218737e{-}05 & 6.5443644e{-}03 \\
7.9540247e{-}03 & 2.7870366e{-}05 & 6.4776456e{-}03 \\
7.8913363e{-}03 & 2.5521994e{-}05 & 6.4109268e{-}03 \\
7.8286479e{-}03 & 2.3173623e{-}05 & 6.3442080e{-}03 \\
7.7659595e{-}03 & 2.0825252e{-}05 & 6.2774892e{-}03 \\
7.7032711e{-}03 & 1.8476881e{-}05 & 6.2107703e{-}03 \\
7.6405827e{-}03 & 1.6128510e{-}05 & 6.1440515e{-}03 \\
7.5778943e{-}03 & 1.3780138e{-}05 & 6.0773327e{-}03 \\
7.5152059e{-}03 & 1.1431767e{-}05 & 6.0106139e{-}03 \\
7.4525175e{-}03 & 9.0833959e{-}06 & 5.9438951e{-}03 \\
7.3898291e{-}03 & 6.7350247e{-}06 & 5.8771763e{-}03 \\
7.3271407e{-}03 & 4.3866534e{-}06 & 5.8104575e{-}03 \\
7.2644523e{-}03 & 2.0382822e{-}06 & 5.7437387e{-}03 \\
7.2017639e{-}03 & -3.1008899e{-}07 & 5.6770198e{-}03 \\
7.1390755e{-}03 & -2.6584602e{-}06 & 5.6103010e{-}03 \\
7.0763871e{-}03 & -5.0068314e{-}06 & 5.5435822e{-}03 \\
7.0136987e{-}03 & -7.3552026e{-}06 & 5.4768634e{-}03 \\
6.9510103e{-}03 & -9.7035739e{-}06 & 5.4101446e{-}03 \\
6.8883219e{-}03 & -1.2051945e{-}05 & 5.3434258e{-}03 \\
6.8256335e{-}03 & -1.4400316e{-}05 & 5.2767070e{-}03 \\
6.7629451e{-}03 & -1.6748688e{-}05 & 5.2099881e{-}03 \\
6.7002567e{-}03 & -1.9097059e{-}05 & 5.1432693e{-}03 \\
6.6375683e{-}03 & -2.1445430e{-}05 & 5.0765505e{-}03 \\
6.5748799e{-}03 & -2.3793801e{-}05 & 5.0098317e{-}03 \\
6.5121915e{-}03 & -2.6142172e{-}05 & 4.9431129e{-}03 \\
6.4495031e{-}03 & -2.8490544e{-}05 & 4.8763941e{-}03 \\
6.3868147e{-}03 & -3.0838915e{-}05 & 4.8096753e{-}03 \\
6.3241263e{-}03 & -3.3187286e{-}05 & 4.7429564e{-}03 \\
6.2614379e{-}03 & -3.5535657e{-}05 & 4.6762376e{-}03 \\
6.1987495e{-}03 & -3.7884028e{-}05 & 4.6095188e{-}03 \\
6.1360611e{-}03 & -4.0232400e{-}05 & 4.5428000e{-}03 \\
6.0733727e{-}03 & -4.2580771e{-}05 & 4.4760812e{-}03 \\
6.0106843e{-}03 & -4.4929142e{-}05 & 4.4093624e{-}03 \\
5.9479959e{-}03 & -4.7277513e{-}05 & 4.3426436e{-}03 \\
5.8853075e{-}03 & -4.9625885e{-}05 & 4.2759247e{-}03 \\
5.8226191e{-}03 & -5.1974256e{-}05 & 4.2092059e{-}03 \\
5.7599307e{-}03 & -5.4322627e{-}05 & 4.1424871e{-}03 \\
5.6972423e{-}03 & -5.6670998e{-}05 & 4.0757683e{-}03 \\
5.6345539e{-}03 & -5.9019369e{-}05 & 4.0090495e{-}03 \\
5.5718655e{-}03 & -6.1367741e{-}05 & 3.9423307e{-}03 \\
5.5091771e{-}03 & -6.3716112e{-}05 & 3.8756119e{-}03 \\
5.4464887e{-}03 & -6.6064483e{-}05 & 3.8088930e{-}03 \\
5.3838003e{-}03 & -6.8412854e{-}05 & 3.7421742e{-}03 \\
5.3211119e{-}03 & -7.0761226e{-}05 & 3.6754554e{-}03 \\
5.2584235e{-}03 & -7.3109597e{-}05 & 3.6087366e{-}03 \\
5.1957351e{-}03 & -7.5457968e{-}05 & 3.5420178e{-}03 \\
5.1330467e{-}03 & -7.7806339e{-}05 & 3.4752990e{-}03 \\
5.0703583e{-}03 & -8.0154710e{-}05 & 3.4085802e{-}03 \\
5.0076699e{-}03 & -8.2503082e{-}05 & 3.3418613e{-}03 \\
4.9449815e{-}03 & -8.4851453e{-}05 & 3.2751425e{-}03 \\
4.8822931e{-}03 & -8.7199824e{-}05 & 3.2084237e{-}03 \\
4.8196047e{-}03 & -8.9548195e{-}05 & 3.1417049e{-}03 \\
4.7569163e{-}03 & -9.1896566e{-}05 & 3.0749861e{-}03 \\
4.6942279e{-}03 & -9.4244938e{-}05 & 3.0082673e{-}03 \\
4.6315395e{-}03 & -9.6593309e{-}05 & 2.9415485e{-}03 \\
4.5688511e{-}03 & -9.8941680e{-}05 & 2.8748296e{-}03 \\
4.5061627e{-}03 & -1.0129005e{-}04 & 2.8081108e{-}03 \\
4.4434743e{-}03 & -1.0363842e{-}04 & 2.7413920e{-}03 \\
4.3807859e{-}03 & -1.0598679e{-}04 & 2.6746732e{-}03 \\
4.3180975e{-}03 & -1.0833516e{-}04 & 2.6079544e{-}03 \\
4.2554091e{-}03 & -1.1068354e{-}04 & 2.5412356e{-}03 \\
4.1927207e{-}03 & -1.1303191e{-}04 & 2.4745168e{-}03 \\
4.1300323e{-}03 & -1.1538028e{-}04 & 2.4077979e{-}03 \\
4.0673439e{-}03 & -1.1772865e{-}04 & 2.3410791e{-}03 \\
4.0046555e{-}03 & -1.2007702e{-}04 & 2.2743603e{-}03 \\
3.9419671e{-}03 & -1.2242539e{-}04 & 2.2076415e{-}03 \\
3.8792787e{-}03 & -1.2477376e{-}04 & 2.1409227e{-}03 \\
3.8165903e{-}03 & -1.2712213e{-}04 & 2.0742039e{-}03
\end{bmatrix}$$

$$RD = \begin{bmatrix}
2.5417382e{-}04 & 3.0307471e{-}05 & -1.5361632e{-}04 \\
2.7572098e{-}04 & 2.9925193e{-}05 & -1.5577968e{-}04 \\
2.9726815e{-}04 & 2.9542914e{-}05 & -1.5794303e{-}04 \\
3.1881531e{-}04 & 2.9160635e{-}05 & -1.6010639e{-}04 \\
3.4036248e{-}04 & 2.8778356e{-}05 & -1.6226974e{-}04 \\
3.6190964e{-}04 & 2.8396077e{-}05 & -1.6443310e{-}04 \\
3.8345681e{-}04 & 2.8013799e{-}05 & -1.6659645e{-}04 \\
4.0500398e{-}04 & 2.7631520e{-}05 & -1.6875981e{-}04 \\
4.2655114e{-}04 & 2.7249241e{-}05 & -1.7092316e{-}04 \\
4.4809831e{-}04 & 2.6866962e{-}05 & -1.7308652e{-}04 \\
4.6964547e{-}04 & 2.6484683e{-}05 & -1.7524987e{-}04 \\
4.9119264e{-}04 & 2.6102404e{-}05 & -1.7741323e{-}04 \\
5.1273980e{-}04 & 2.5720126e{-}05 & -1.7957658e{-}04 \\
5.3428697e{-}04 & 2.5337847e{-}05 & -1.8173994e{-}04 \\
5.5583413e{-}04 & 2.4955568e{-}05 & -1.8390329e{-}04 \\
5.7738130e{-}04 & 2.4573289e{-}05 & -1.8606665e{-}04 \\
5.9892847e{-}04 & 2.4191010e{-}05 & -1.8823000e{-}04 \\
6.2047563e{-}04 & 2.3808732e{-}05 & -1.9039336e{-}04 \\
6.4202280e{-}04 & 2.3426453e{-}05 & -1.9255671e{-}04 \\
6.6356996e{-}04 & 2.3044174e{-}05 & -1.9472007e{-}04 \\
6.8511713e{-}04 & 2.2661895e{-}05 & -1.9688342e{-}04 \\
7.0666429e{-}04 & 2.2279616e{-}05 & -1.9904678e{-}04 \\
7.2821146e{-}04 & 2.1897338e{-}05 & -2.0121013e{-}04 \\
7.4975862e{-}04 & 2.1515059e{-}05 & -2.0337349e{-}04 \\
7.7130579e{-}04 & 2.1132780e{-}05 & -2.0553684e{-}04 \\
7.9285296e{-}04 & 2.0750501e{-}05 & -2.0770020e{-}04 \\
8.1440012e{-}04 & 2.0368222e{-}05 & -2.0986355e{-}04 \\
8.3594729e{-}04 & 1.9985943e{-}05 & -2.1202691e{-}04 \\
8.5749445e{-}04 & 1.9603665e{-}05 & -2.1419026e{-}04 \\
8.7904162e{-}04 & 1.9221386e{-}05 & -2.1635362e{-}04 \\
9.0058878e{-}04 & 1.8839107e{-}05 & -2.1851697e{-}04 \\
9.2213595e{-}04 & 1.8456828e{-}05 & -2.2068033e{-}04 \\
9.4368311e{-}04 & 1.8074549e{-}05 & -2.2284368e{-}04 \\
9.6523028e{-}04 & 1.7692271e{-}05 & -2.2500704e{-}04 \\
9.8677745e{-}04 & 1.7309992e{-}05 & -2.2717039e{-}04 \\
1.0083246e{-}03 & 1.6927713e{-}05 & -2.2933375e{-}04 \\
1.0298718e{-}03 & 1.6545434e{-}05 & -2.3149710e{-}04 \\
1.0514189e{-}03 & 1.6163155e{-}05 & -2.3366046e{-}04 \\
1.0729661e{-}03 & 1.5780876e{-}05 & -2.3582381e{-}04 \\
1.0945133e{-}03 & 1.5398598e{-}05 & -2.3798717e{-}04 \\
1.1160604e{-}03 & 1.5016319e{-}05 & -2.4015052e{-}04 \\
1.1376076e{-}03 & 1.4634040e{-}05 & -2.4231388e{-}04 \\
1.1591548e{-}03 & 1.4251761e{-}05 & -2.4447723e{-}04 \\
1.1807019e{-}03 & 1.3869482e{-}05 & -2.4664059e{-}04 \\
1.2022491e{-}03 & 1.3487204e{-}05 & -2.4880395e{-}04 \\
1.2237963e{-}03 & 1.3104925e{-}05 & -2.5096730e{-}04 \\
1.2453434e{-}03 & 1.2722646e{-}05 & -2.5313066e{-}04 \\
1.2668906e{-}03 & 1.2340367e{-}05 & -2.5529401e{-}04 \\
1.2884378e{-}03 & 1.1958088e{-}05 & -2.5745737e{-}04 \\
1.3099849e{-}03 & 1.1575809e{-}05 & -2.5962072e{-}04 \\
1.3315321e{-}03 & 1.1193531e{-}05 & -2.6178408e{-}04 \\
1.3530793e{-}03 & 1.0811252e{-}05 & -2.6394743e{-}04 \\
1.3746264e{-}03 & 1.0428973e{-}05 & -2.6611079e{-}04 \\
1.3961736e{-}03 & 1.0046694e{-}05 & -2.6827414e{-}04 \\
1.4177208e{-}03 & 9.6644154e{-}06 & -2.7043750e{-}04 \\
1.4392679e{-}03 & 9.2821366e{-}06 & -2.7260085e{-}04 \\
1.4608151e{-}03 & 8.8998578e{-}06 & -2.7476421e{-}04 \\
1.4823623e{-}03 & 8.5175790e{-}06 & -2.7692756e{-}04 \\
1.5039094e{-}03 & 8.1353002e{-}06 & -2.7909092e{-}04 \\
1.5254566e{-}03 & 7.7530213e{-}06 & -2.8125427e{-}04 \\
1.5470038e{-}03 & 7.3707425e{-}06 & -2.8341763e{-}04 \\
1.5685509e{-}03 & 6.9884637e{-}06 & -2.8558098e{-}04 \\
1.5900981e{-}03 & 6.6061849e{-}06 & -2.8774434e{-}04 \\
1.6116452e{-}03 & 6.2239061e{-}06 & -2.8990769e{-}04 \\
1.6331924e{-}03 & 5.8416273e{-}06 & -2.9207105e{-}04 \\
1.6547396e{-}03 & 5.4593484e{-}06 & -2.9423440e{-}04 \\
1.6762867e{-}03 & 5.0770696e{-}06 & -2.9639776e{-}04 \\
1.6978339e{-}03 & 4.6947908e{-}06 & -2.9856111e{-}04 \\
1.7193811e{-}03 & 4.3125120e{-}06 & -3.0072447e{-}04 \\
1.7409282e{-}03 & 3.9302332e{-}06 & -3.0288782e{-}04 \\
1.7624754e{-}03 & 3.5479544e{-}06 & -3.0505118e{-}04 \\
1.7840226e{-}03 & 3.1656755e{-}06 & -3.0721453e{-}04 \\
1.8055697e{-}03 & 2.7833967e{-}06 & -3.0937789e{-}04 \\
1.8271169e{-}03 & 2.4011179e{-}06 & -3.1154124e{-}04 \\
1.8486641e{-}03 & 2.0188391e{-}06 & -3.1370460e{-}04 \\
1.8702112e{-}03 & 1.6365603e{-}06 & -3.1586795e{-}04 \\
1.8917584e{-}03 & 1.2542815e{-}06 & -3.1803131e{-}04 \\
1.9133056e{-}03 & 8.7200265e{-}07 & -3.2019466e{-}04 \\
1.9348527e{-}03 & 4.8972383e{-}07 & -3.2235802e{-}04 \\
1.9563999e{-}03 & 1.0744502e{-}07 & -3.2452137e{-}04 \\
1.9779471e{-}03 & -2.7483380e{-}07 & -3.2668473e{-}04 \\
1.9994942e{-}03 & -6.5711262e{-}07 & -3.2884808e{-}04 \\
2.0210414e{-}03 & -1.0393914e{-}06 & -3.3101144e{-}04 \\
2.0425886e{-}03 & -1.4216702e{-}06 & -3.3317479e{-}04 \\
2.0641357e{-}03 & -1.8039491e{-}06 & -3.3533815e{-}04 \\
2.0856829e{-}03 & -2.1862279e{-}06 & -3.3750150e{-}04 \\
2.1072301e{-}03 & -2.5685067e{-}06 & -3.3966486e{-}04 \\
2.1287772e{-}03 & -2.9507855e{-}06 & -3.4182821e{-}04 \\
2.1503244e{-}03 & -3.3330643e{-}06 & -3.4399157e{-}04 \\
2.1718716e{-}03 & -3.7153431e{-}06 & -3.4615492e{-}04 \\
2.1934187e{-}03 & -4.0976220e{-}06 & -3.4831828e{-}04 \\
2.2149659e{-}03 & -4.4799008e{-}06 & -3.5048163e{-}04 \\
2.2365131e{-}03 & -4.8621796e{-}06 & -3.5264499e{-}04 \\
2.2580602e{-}03 & -5.2444584e{-}06 & -3.5480834e{-}04 \\
2.2796074e{-}03 & -5.6267372e{-}06 & -3.5697170e{-}04 \\
2.3011545e{-}03 & -6.0090160e{-}06 & -3.5913505e{-}04 \\
2.3227017e{-}03 & -6.3912949e{-}06 & -3.6129841e{-}04 \\
2.3442489e{-}03 & -6.7735737e{-}06 & -3.6346176e{-}04 \\
2.3657960e{-}03 & -7.1558525e{-}06 & -3.6562512e{-}04 \\
2.3873432e{-}03 & -7.5381313e{-}06 & -3.6778847e{-}04 \\
2.4088904e{-}03 & -7.9204101e{-}06 & -3.6995183e{-}04
\end{bmatrix}$$

Chapter 3

Impacts of Different Resistance Mechanisms on Tumor Recurrence

3.1 Background

We investigate the biological phenomenon in which a population with negative net growth rate escapes certain extinction via the creation of new genetic variants. In the context of cancer, this corresponds to the situation in which a population of drug-sensitive cells undergoing treatment evolves resistance to therapy. This phenomenon is quite common in cancers treated with molecularly targeted therapies [4]. For example, this behavior is commonly observed in patients with EGFR-mutant non-small cell lung cancer taking erlotinib or gefitinib [65]. In these cases, patients usually develop resistance and disease progression within 12-18 months of starting treatment [5].

During cancer treatment, resistance to therapy may emerge via a variety of mechanisms. In EGFR-mutant non-small cell lung cancer, for example, resistance to erlotinib usually arises due to either a T790M point mutation or amplification of the MET gene [66]. The first of these resistance mechanisms arises via a mutation within a single gene, whereas the second corresponds to an increase in the copy number of the given gene. In this chapter, we define and analyze two separate branching process models of drug

resistance, mirroring these two biological processes of gene mutation and amplification. We then use our models to investigate tumor recurrence time, or the amount of time it takes a tumor to rebound and reach its initial size at detection once again. Because a typical solid tumor has between 10^7 and 10^9 cancer cells per cubic centimeter [67], we focus on characterizing the tumor recurrence time in the large population limit.

Previous works by Foo and Leder [18] and by Foo, Leder, and Zhu [68] have used a similar modeling approach to study the stochastic time at which the resistant cell population begins to dominate the tumor, which the authors refer to as the crossover time. In this chapter, we build on these previous works by using a similar model of resistance driven by gene mutation to investigate the stochastic tumor recurrence time instead. The gene amplification model presented in this paper along with its corresponding analysis is also a novel contribution to this body of work which previously only focused on the case where resistance arises due to a single point mutation.

The remainder of the chapter is organized as follows. In Section 3.2, we introduce the models for both gene mutation and amplification, and provide formulas for some quantities we will use throughout the chapter. In Section 3.3, we analyze the tumor recurrence time in both models. Theorem 1 gives a law of large numbers result regarding the convergence of the stochastic recurrence time in the gene mutation model, and Theorem 2 gives the analogous result in the gene amplification model. We then use our results to draw comparisons between these two models. Section 3.4 provides justification for a specific parameter choice. In Section 3.5, we provide proofs of the main results. Throughout this chapter, we use the following standard Landau notation for asymptotic behavior of non-negative functions:

$$f(t) \sim g(t) \text{ if } f(t)/g(t) \to 1 \text{ as } t \to \infty.$$

3.2 Models and Preliminaries

Both models start with an initial population of n drug-sensitive cells and zero resistant cells at time $t = 0$. The population $X_s(t)$ of sensitive cells is modeled using a subcritical Markovian branching process that declines during treatment with birth rate r_s, death rate d_s, and net growth rate $\lambda_s = r_s - d_s < 0$. Since $\lambda_s < 0$, the sensitive cell population

goes extinct with probability 1. We approximate this extinction time as $t_n = -\frac{1}{\lambda_s}\log n$.

3.2.1 Gene Mutation Model

In the mutation model, a sensitive cell may acquire a single gene mutation, giving rise to a new resistant cell. These mutations occur at rate $\mu_n X_s(t)$, where $\mu_n = \mu n^{-\alpha}$ for $\mu > 0$ and $0 < \alpha < 1$. Each mutant cell gives rise to a supercritical Markovian branching process with birth rate r_m, death rate d_m, and net growth rate $\lambda_m = r_m - d_m > 0$. The total population of mutant cells is denoted by $X_m(t)$. In the following, all probability and expectation operators are conditioned on the initial conditions $X_s(0) = n$ and $X_m(0) = 0$.

Using the transition probabilities of these processes together with the moment generating function, we derive a system of ODE's governing the first and second moments, which we then use to calculate the mean and variance of $X_s(t)$ and $X_m(t)$. For $i = s, m$, let $\phi_i(t) = \mathbb{E}[X_i(t)]$ and let $\psi_i(t) = \mathrm{Var}[X_i(t)]$. Then we have

$$\begin{aligned}
\phi_s(zt_n) &= n^{1-z}, \\
\phi_m(zt_n) &= \frac{\mu n^{1-\alpha}}{\lambda_m - \lambda_s}\left(n^{-\lambda_m z/\lambda_s} - n^{-z}\right), \\
\psi_s(zt_n) &= n^{1-z}\left(\frac{r_s + d_s}{-\lambda_s}\right)\left(1 - n^{-z}\right), \\
\psi_m(zt_n) &\sim \frac{2r_m\mu}{\lambda_m(2\lambda_m - \lambda_s)} \cdot n^{1-\alpha-2\lambda_m z/\lambda_s}.
\end{aligned}$$

3.2.2 Gene Amplification Model

In the amplification model, sensitive cells each have two copies of the gene whose amplification is associated with drug resistance. For this reason and for ease of notation, let a subscript of s be equivalent to a subscript of 2. Let $X_k(t)$, $k = 2, 3, 4, ..., M$, represent the population of type k cells with birth rate r_k, death rate d_k, and net growth rate $\lambda_k = r_k - d_k$. Type k cells have k gene copies and M is the maximum number of gene copies a cell can have. In this model, a type $k-1$ cell may gain a single gene copy, giving rise to a new type k cell. These amplification steps occur at rate $\nu_n X_{k-1}(t)$, where $\nu_n = \nu n^{-\beta}$ for $\nu > 0$ and $0 < \beta < \frac{1}{M-2}$.

We have already seen the formula for the mean of the sensitive cells in the previous section. Now we examine the means of the other populations.

Lemma 1. *For $k = 3, 4, ...,$*

$$\mathbb{E}[X_k(t)] = \nu^{k-2} n^{1-(k-2)\beta} (-1)^k S_k(t),$$

where

$$S_k(t) = \sum_{i=2}^{k} \frac{e^{\lambda_i t}}{P_{i,k}}, \qquad P_{i,k} = \prod_{j=2, j\neq i}^{k} (\lambda_j - \lambda_i).$$

The proof of this lemma can be found in Section 3.5. Since type M cells contain the maximum number of gene copies, they are resistant to treatment and hence $\lambda_M > 0$. With each additional gene copy, cells gain a fitness advantage. More specifically, we define

$$\lambda_k = \lambda_2 + (k-2)m, \qquad m = \frac{\lambda_M - \lambda_2}{M-2}.$$

For $i = 2, 3, ...,$ let $\phi_i(t) = \mathbb{E}[X_i(t)]$. We already have that $\phi_2(t) = \phi_s(t)$. For $k = 3, 4, ...,$

$$\phi_k(zt_n) = \frac{\mu^{k-2}(-1)^k}{m^{k-2}} n^{1-(k-2)\alpha} \tilde{S}_k(z),$$

where

$$\tilde{S}_k(z) = \sum_{i=2}^{k} \frac{n^{-\lambda_i z/\lambda_2}}{\tilde{P}_{i,k}}, \qquad \tilde{P}_{i,k} = \prod_{j=2, j\neq i}^{k} (j - i).$$

Note that, for fixed z and n sufficiently large,

$$\max_{2\leq k\leq M} \phi_k(zt_n) \in \{\phi_2(zt_n), \phi_M(zt_n)\}.$$

3.3 Results

To compare these two resistance mechanisms, we analyze the tumor recurrence time in both models. Tumor recurrence time is defined intuitively as the amount of time it takes from the beginning of treatment until the total number of cancer cells surpasses

the initial population size n, neglecting possible brief instances of this early on due to the stochasticity of the processes. A more precise mathematical definition of recurrence time will be given below.

3.3.1 Recurrence Time in Gene Mutation Model

To obtain an estimate of the stochastic recurrence time, we start with the following proposition, whose proof can be found in Section 3.5.

Proposition 1. *There exists a unique $\tilde{u}_n > 0$ satisfying $\phi_s(\tilde{u}_n t_n) + \phi_m(\tilde{u}_n t_n) = n$. Moreover, $a_n < \tilde{u}_n < A_n$ where:*

$$a_n = \frac{1}{\lambda_m}\left(-\lambda_s\alpha + \frac{1}{t_n}\log\left(\frac{-\lambda_s}{\mu}\right)\right),$$
$$A_n = \frac{1}{\lambda_m}\left(-\lambda_s\alpha + \frac{1}{t_n}\log\left(\frac{\lambda_m - \lambda_s}{\mu}\right)\right).$$

Hence $\tilde{u}_n \to \frac{-\lambda_s\alpha}{\lambda_m}$ as $n \to \infty$.

Let $u_n = \tilde{u}_n t_n$ represent our estimate of the tumor recurrence time. We now state our main law of large numbers result regarding the convergence of the stochastic recurrence time in the gene mutation model:

Theorem 1. *Define the recurrence time in the gene mutation model mathematically as*

$$\tau_n = \inf\{t \geq ct_n : X_s(t) + X_m(t) > n\},$$

where

$$c = \frac{\alpha\lambda_s(\lambda_s - 2\lambda_m)}{2\lambda_m(\lambda_m - \lambda_s)}.$$

Then, for all $\epsilon > 0$,

$$\lim_{n\to\infty} \mathbb{P}\left(|\tau_n - u_n| > \epsilon\right) = 0.$$

In other words, the stochastic recurrence time and its estimate converge to each other in probability as $n \to \infty$. The proof of this result is located in Section 3.5.

For ease of notation, given $\epsilon > 0$, define

$$u_n^-(\epsilon) = \frac{u_n - \epsilon}{t_n},$$
$$u_n^+(\epsilon) = \frac{u_n + \epsilon}{t_n}.$$

We will now state a proposition pertaining to the fluctuations of the sensitive and resistant cell populations about their means.

Proposition 2. *For $\delta > 0$ and $i \in \{s, m\}$,*

$$\lim_{n\to\infty} \mathbb{P}\left(\sup_{z\in[c,u_n^+(\epsilon)]} n^{\alpha+\lambda_m z/\lambda_s - 1} \left| X_i(zt_n) - \phi_i(zt_n) \right| > \delta \right) = 0.$$

The proof of this proposition can be found in Section 3.5.

Next we will prove with high probability that there are no permanent recurrence events in the time interval $[0, ct_n]$, meaning that either the number of cancer cells does not surpass n during this time or it surpasses n only briefly before subsequently falling to n or lower once again. To show this, we will prove with high probability that the sum of sensitive and resistant cells is not greater than n at time ct_n.

Lemma 2.

$$\lim_{n\to\infty} \mathbb{P}\left(X_s(ct_n) + X_m(ct_n) - n \le 0 \right) = 1.$$

Proof. Since $\mathbb{P}(X_s(ct_n) + X_m(ct_n) - n \le 0) = 1 - \mathbb{P}(X_s(ct_n) + X_m(ct_n) - n > 0)$, it suffices to show

$$\lim_{n\to\infty} \mathbb{P}(X_s(ct_n) + X_m(ct_n) - n > 0) = 0.$$

Note that

$$\begin{aligned}
&\mathbb{P}(X_s(ct_n) + X_m(ct_n) - n > 0) \\
&\qquad = \mathbb{P}\Big(n^{\alpha+\lambda_m c/\lambda_s - 1}(X_s(ct_n) - \phi_s(ct_n) + \phi_s(ct_n) - n \\
&\qquad\qquad + \phi_m(ct_n) - \phi_m(ct_n) + X_m(ct_n)) > 0 \Big) \\
&\qquad = \mathbb{P}(\bar{A}_1(n) + \bar{A}_2(n) + \bar{A}_3(n) > 0),
\end{aligned}$$

where

$$\begin{aligned}
\bar{A}_1(n) &= n^{\alpha+\lambda_m c/\lambda_s-1}(X_s(ct_n) - \phi_s(ct_n)),\\
\bar{A}_2(n) &= n^{\alpha+\lambda_m c/\lambda_s-1}(\phi_s(ct_n) + \phi_m(ct_n) - n),\\
\bar{A}_3(n) &= n^{\alpha+\lambda_m c/\lambda_s-1}(X_m(ct_n) - \phi_m(ct_n)).
\end{aligned}$$

We will consider each of these three terms separately, starting with the first. Note that

$$\begin{aligned}
\left|\bar{A}_1(n)\right| &= n^{\alpha+\lambda_m c/\lambda_s-1}\left|X_s(ct_n) - \phi_s(ct_n)\right|\\
&\leq \sup_{z\in[c,u_n^+(\epsilon)]} n^{\alpha+\lambda_m z/\lambda_s-1}\left|X_s(zt_n) - \phi_s(zt_n)\right|,
\end{aligned}$$

which converges to zero in probability by Proposition 2. Similarly,

$$\begin{aligned}
\left|\bar{A}_3(n)\right| &= n^{\alpha+\lambda_m c/\lambda_s-1}\left|X_m(ct_n) - \phi_m(ct_n)\right|\\
&\leq \sup_{z\in[c,u_n^+(\epsilon)]} n^{\alpha+\lambda_m z/\lambda_s-1}\left|X_m(zt_n) - \phi_m(zt_n)\right|,
\end{aligned}$$

which also converges to zero in probability by Proposition 2. Now we just need to show that $\bar{A}_2(n)$ is negative in the large population limit. By the definitions of ϕ_s and ϕ_m,

$$\begin{aligned}
\bar{A}_2(n) &= n^{\alpha+\lambda_m c/\lambda_s-1}\left(n^{1-c} + \frac{\mu n^{1-\alpha}}{\lambda_m-\lambda_s}\left(n^{-\lambda_m c/\lambda_s} - n^{-c}\right) - n\right)\\
&= n^{\alpha+\frac{\lambda_m}{\lambda_s}\cdot\frac{\alpha\lambda_s(\lambda_s-2\lambda_m)}{2\lambda_m(\lambda_m-\lambda_s)}}\left(n^{-c} + \frac{\mu}{\lambda_m-\lambda_s}\left(n^{\frac{\lambda_m}{-\lambda_s}\cdot\frac{\alpha\lambda_s(\lambda_s-2\lambda_m)}{2\lambda_m(\lambda_m-\lambda_s)}-\alpha} - n^{-\alpha-c}\right) - 1\right)\\
&= n^{\alpha\left(1-\frac{2\lambda_m-\lambda_s}{2\lambda_m-2\lambda_s}\right)}\left(n^{-c} + \frac{\mu}{\lambda_m-\lambda_s}\left(n^{\alpha\left(\frac{2\lambda_m-\lambda_s}{2\lambda_m-2\lambda_s}-1\right)} - n^{-\alpha-c}\right) - 1\right).
\end{aligned}$$

Clearly, $\bar{A}_2(n) < 0$ since the first term in the product above is positive and the second term is negative for large n. Furthermore, we can see from the above display that $\bar{A}_2(n) \to -\infty$ as $n \to \infty$. Putting this all together, we have that $\mathbb{P}(\bar{A}_1(n) + \bar{A}_2(n) +$

$\bar{A}_3(n) > 0) \to 0$ as $n \to \infty$.

□

We have just proved that with high probability the sum of sensitive and resistant cells is less than or equal to n at time ct_n. This implies that permanent recurrence occurs at time ct_n or later with high probability.

3.3.2 Recurrence Time in Gene Amplification Model

To obtain an estimate of the stochastic recurrence time, we start with the following proposition, whose proof can be found in Section 3.5.

Proposition 3. *There exists a unique $\tilde{v}_n > 0$ satisfying $\sum_{k=2}^{M} \phi_k(\tilde{v}_n t_n) = n$. Moreover, $b_n < \tilde{v}_n < B_n$ where:*

$$b_n = \frac{1}{\lambda_M}\left[-\lambda_2\beta(M-2) - \frac{1}{t_n}\log\left[\frac{\nu^{M-2}(-1)^M}{m^{M-2}\tilde{P}_{M,M}}\left(1-\frac{\lambda_M}{\lambda_2}\right)\right]\right],$$
$$B_n = \frac{1}{\lambda_M}\left[-\lambda_2\beta(M-2) - \frac{1}{t_n}\log\left[\frac{\nu^{M-2}(-1)^M}{m^{M-2}\tilde{P}_{M,M}}\right]\right].$$

Hence $\tilde{v}_n \to -\frac{\lambda_2}{\lambda_M}\beta(M-2)$ as $n \to \infty$.

Let $v_n = \tilde{v}_n t_n$ represent our estimate of the tumor recurrence time. We now state our main law of large numbers result regarding the convergence of the stochastic recurrence time in the gene amplification model:

Theorem 2. *Define the recurrence time in the gene amplification model mathematically as*

$$\omega_n = \inf\left\{t \geq dt_n : \sum_{k=2}^{M} X_k(t) > n\right\},$$

where

$$\frac{-\lambda_2\beta(M-2)}{\lambda_M - \lambda_2} < d < \frac{-\lambda_2\beta(M-2)}{\lambda_M}. \tag{3.1}$$

Then, for all $\epsilon > 0$,

$$\lim_{n\to\infty} \mathbb{P}\left(|\omega_n - v_n| > \epsilon\right) = 0.$$

In other words, the stochastic recurrence time and its estimate converge to each other in probability as $n \to \infty$. The proof of this result is located in Section 3.5.

For ease of notation, given $\epsilon > 0$, define

$$v_n^-(\epsilon) = \frac{v_n - \epsilon}{t_n},$$
$$v_n^+(\epsilon) = \frac{v_n + \epsilon}{t_n}.$$

We will now state a proposition pertaining to the fluctuations of these populations about their means.

Proposition 4. *For $\delta > 0$ and $2 \leq k \leq M$,*

$$\lim_{n\to\infty} \mathbb{P}\left(\sup_{z\in[d,v_n^+(\epsilon)]} n^{\beta(M-2)+\lambda_M z/\lambda_2 - 1} \left| X_k(zt_n) - \phi_k(zt_n) \right| > \delta \right) = 0.$$

The proof of this proposition can be found in Section 3.5.

Next we will prove with high probability that there are no permanent recurrence events in the time interval $[0, dt_n]$, meaning that either the number of cancer cells does not surpass n during this time or it surpasses n only briefly before subsequently falling to n or lower once again. To show this, we will prove with high probability that the total number of cancer cells is not greater than n at time dt_n.

Lemma 3.

$$\lim_{n\to\infty} \mathbb{P}\left(\sum_{k=2}^{M} X_k(dt_n) - n \leq 0 \right) = 1.$$

Proof. Since $\mathbb{P}\left(\sum_{k=2}^{M} X_k(dt_n) - n \leq 0\right) = 1 - \mathbb{P}\left(\sum_{k=2}^{M} X_k(dt_n) - n > 0\right)$, it suffices to show

$$\lim_{n\to\infty} \mathbb{P}\left(\sum_{k=2}^{M} X_k(dt_n) - n > 0 \right) = 0.$$

Note that

$$\begin{aligned}
&\mathbb{P}\left(\sum_{k=2}^{M} X_k(dt_n) - n > 0\right) \\
&\quad = \mathbb{P}\left(n^{\beta(M-2)+\lambda_M d/\lambda_2 - 1}\left(\sum_{k=2}^{M} X_k(dt_n) + \sum_{k=2}^{M}\phi_k(dt_n) - \sum_{k=2}^{M}\phi_k(dt_n) - n\right) > 0\right) \\
&\quad = \mathbb{P}\left(\sum_{k=2}^{M} \hat{A}_k(n) + \hat{A}_\phi(n) > 0\right),
\end{aligned}$$

where

$$\begin{aligned}
\hat{A}_k(n) &= n^{\beta(M-2)+\lambda_M d/\lambda_2 - 1}\left(X_k(dt_n) - \phi_k(dt_n)\right), \\
\hat{A}_\phi(n) &= n^{\beta(M-2)+\lambda_M d/\lambda_2 - 1}\left(\sum_{k=2}^{M}\phi_k(dt_n) - n\right).
\end{aligned}$$

Note that

$$\begin{aligned}
\left|\hat{A}_k(n)\right| &= n^{\beta(M-2)+\lambda_M d/\lambda_2 - 1}\left|X_k(dt_n) - \phi_k(dt_n)\right| \\
&\leq \sup_{z\in[d,v_n^+(\epsilon)]} n^{\beta(M-2)+\lambda_M z/\lambda_2 - 1}\left|X_k(zt_n) - \phi_k(zt_n)\right|,
\end{aligned}$$

which converges to zero in probability by Proposition 4. Now we just need to show that $\hat{A}_\phi(n)$ is negative in the large population limit. By the definitions of ϕ_2 and ϕ_k, $k \geq 3$,

$$\begin{aligned}
\hat{A}_\phi(n) &= n^{\beta(M-2)+\lambda_M d/\lambda_2 - 1}\left(n^{1-d} + \sum_{k=3}^{M}\frac{\nu^{k-2}(-1)^k}{m^{k-2}} n^{1-(k-2)\beta}\tilde{S}_k(d) - n\right) \\
&= n^{\beta(M-2)+\lambda_M d/\lambda_2}\left(n^{-d} + \sum_{k=3}^{M}\frac{\nu^{k-2}(-1)^k}{m^{k-2}} n^{-\beta(k-2)}\tilde{S}_k(d) - 1\right) \\
&\sim n^{\beta(M-2)+\lambda_M d/\lambda_2}\left(\sum_{k=3}^{M}\frac{\nu^{k-2}(-1)^k}{m^{k-2}}\cdot\frac{n^{-\beta(k-2)-\lambda_k d/\lambda_2}}{\tilde{P}_{k,k}} - 1\right).
\end{aligned}$$

For $3 \leq k < M$, we obviously have $k-2 < M-2$. Since $d > -\lambda_2\beta\frac{M-2}{\lambda_M-\lambda_2} = \frac{-\lambda_2\beta}{m}$ by (3.1), this means that $md/\lambda_2 < -\beta$, and hence $\beta + md/\lambda_2 < 0$. Therefore, for all $3 \leq k < M$,

$$\begin{aligned}
-(k-2)(\beta + md/\lambda_2) &< -(M-2)(\beta + md/\lambda_2) \\
-d - \beta(k-2) - (k-2)md/\lambda_2 &< -d - \beta(M-2) - (M-2)md/\lambda_2 \\
-\beta(k-2) - [\lambda_2 + (k-2)m]d/\lambda_2 &< -\beta(M-2) - [\lambda_2 + (M-2)m]d/\lambda_2 \\
-\beta(k-2) - \lambda_k d/\lambda_2 &< -\beta(M-2) - \lambda_M d/\lambda_2.
\end{aligned}$$

This implies that

$$\begin{aligned}
\hat{A}_\phi(n) &\sim n^{\beta(M-2)+\lambda_M d/\lambda_2}\left(\frac{\nu^{M-2}(-1)^M}{m^{M-2}\tilde{P}_{M,M}} n^{-\beta(M-2)-\lambda_M d/\lambda_2} - 1\right) \\
&= \frac{\nu^{M-2}(-1)^M}{m^{M-2}\tilde{P}_{M,M}} - n^{\beta(M-2)+\lambda_M d/\lambda_2}.
\end{aligned}$$

Since $d < \frac{-\lambda_2\beta(M-2)}{\lambda_M}$ by (3.1), we have that $\lambda_M d/\lambda_2 > -\beta(M-2)$, and therefore $n^{\beta(M-2)+\lambda_M d/\lambda_2} \to \infty$ as $n \to \infty$. Therefore, $\hat{A}_\phi(n)$ is definitely negative in the large population limit. Putting this all together, we have: $\mathbb{P}\left(\sum_{k=2}^{M} \hat{A}_k(n) + \hat{A}_\phi(n) > 0\right) \to 0$ as $n \to \infty$.

□

We have just proved that with high probability the total number of cancer cells is less than or equal to n at time dt_n. This implies that permanent recurrence occurs at time dt_n or later with high probability.

3.3.3 Comparisons

To gain a better understanding of the complexity of the gene amplification model in comparison with the point mutation model, we investigate the impact of the growth rates on tumor composition. Figure 3.1 shows the average simulated tumor composition by copy number at the time of recurrence for $M = 7$ when λ_7 is varied from 1 to 30. From

this figure, we see that, as the step size for λ_k increases, the recurrent tumor shifts from being dominated by the type 7 population to being dominated by the type 2 and 3 cells. This agrees with our intuition because, when the step size for λ_k is large, the growth rates of the type 2 and 3 cell populations are high enough to drive recurrence and hence the population does not evolve clones with higher copy numbers before recurrence occurs.

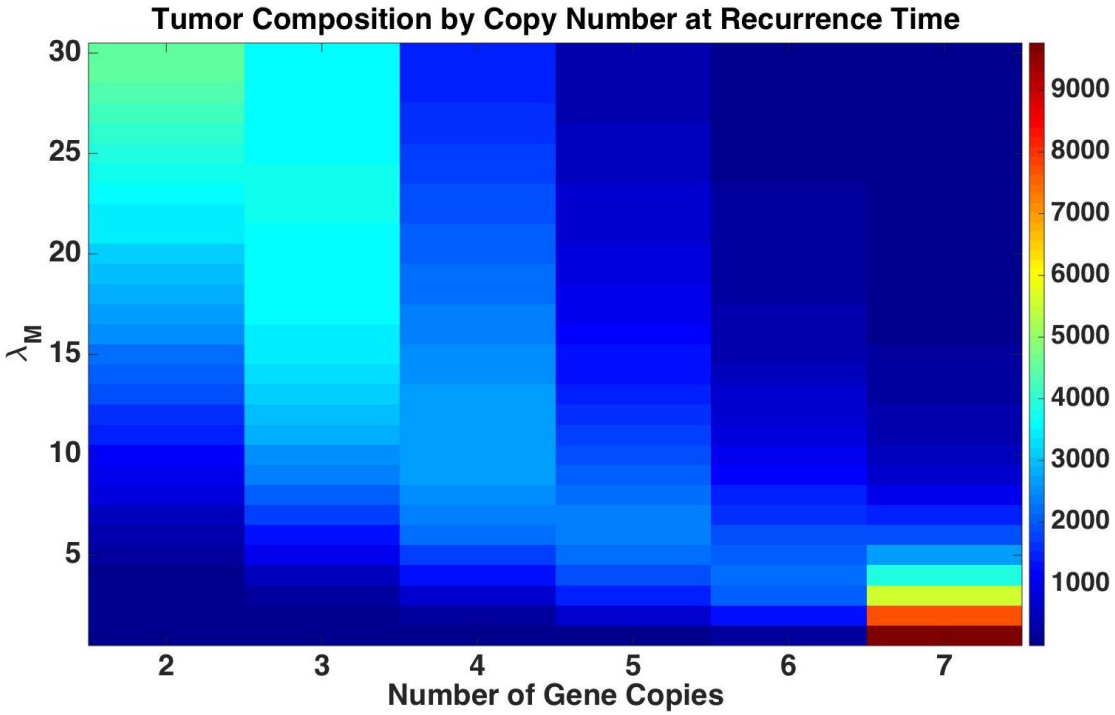

Figure 3.1: **Tumor composition by copy number at recurrence time.** The tumor was simulated up to recurrence time using the gene amplification model with $M = 7$. We used an initial population of 10^4 type 2 cells with $\nu = 5$ and $\alpha = 0.1$. The death rate for all populations was $d_k = 3$. The birth rate of the type 2 cells was $r_2 = 1$ and the birth rate of the type 7 cells varied from $r_7 = 4$ to $r_7 = 33$. Simulations were run repeatedly until the sample means were within 20 cells of the actual means with probability 0.95. The results plotted are the averages of the simulation results.

Figure 3.2 shows the tumor composition breakdown in greater detail for 3 different values of λ_M (small, medium, and large). When λ_M is small (Figure 3.2a), the recurrent tumor is comprised mostly of type 7 cells, and resistance is driven more by mutation than by growth. On the other hand, when λ_M is large (Figure 3.2c), the recurrent tumor

is comprised mostly of type 2 and 3 cells, and resistance is driven more by growth than by mutation. When λ_M is somewhere in the middle (Figure 3.2b), however, we see a more even distribution in the tumor composition, and resistance seems to be driven by a combination of growth and mutation.

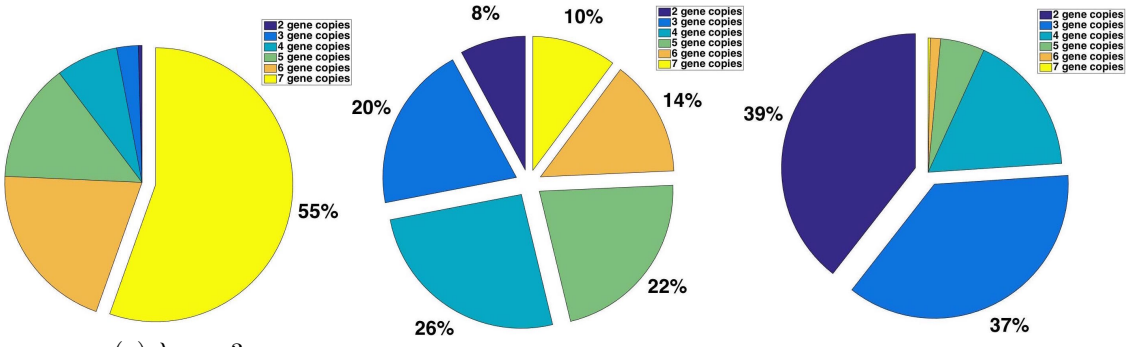

(a) $\lambda_M = 3$ (b) $\lambda_M = 8$ (c) $\lambda_M = 25$

Figure 3.2: **Tumor composition by copy number at recurrence time for specific λ_M.** The composition of the simulated tumor from Figure 3.1 is shown specifically for a small λ_M, a medium λ_M, and a large λ_M.

To compare the two models, we investigate the ratio of recurrence time in the point mutation model to recurrence time in the gene amplification model (u_n/v_n) in the large population limit. Figure 3.3 shows this ratio plotted as both α and β are varied simultaneously, using biologically relevant values for all other parameters. This figure suggests that, in general, recurrence takes longer to develop in tumors where resistance is driven by point mutations than in tumors where resistance is driven by gene amplification. This phenomenon is especially apparent when α is large and β is small, which is the biologically relevant parameter regime.

Figure 3.4 shows the same ratio of the recurrence times plotted as both M and λ_m are varied simultaneously. Note that this ratio is the largest when both M and λ_m are small and smallest when both M and λ_m are large. When λ_m is small, the resistant cell population grows slower and hence the tumor will take longer to recur (causing u_n to be large). When M is small, that means that very few mutations are required to reach the maximum growth rate λ_M, and hence the tumor will recur quite quickly (causing v_n to be small). On the other hand, when λ_m is large, the resistant cell population grows faster and hence the tumor will recur more quickly (causing u_n to be small). And

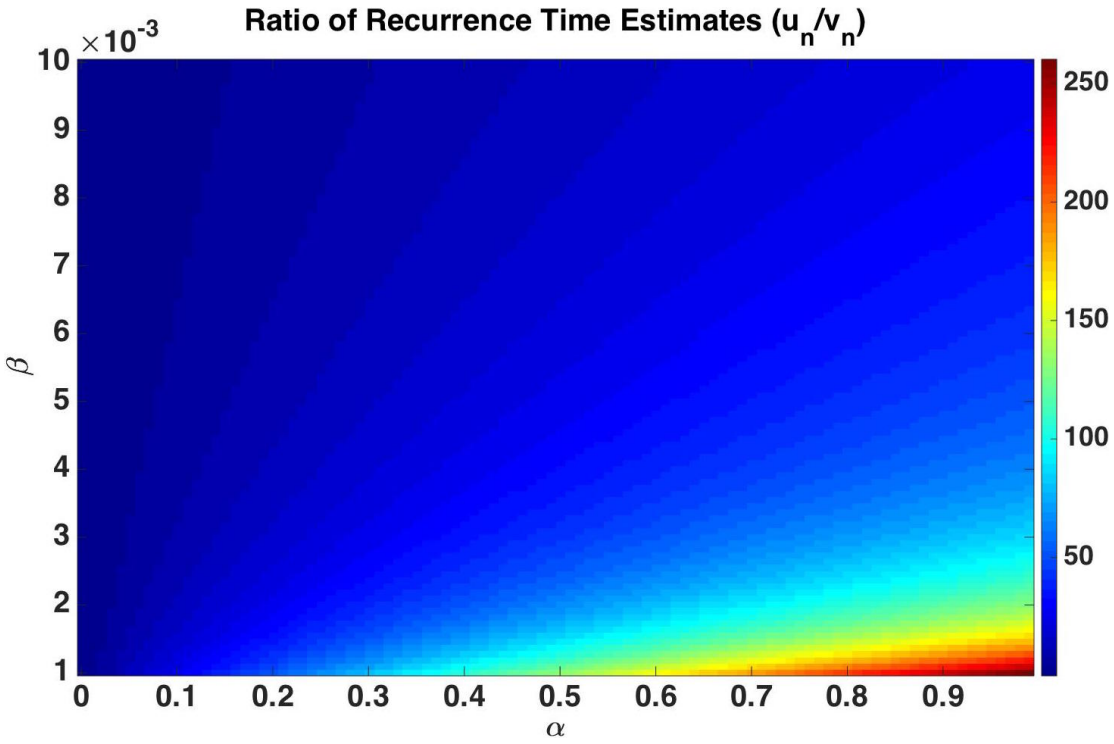

Figure 3.3: **Ratio of recurrence time estimates when α and β are varied.** The ratio of the recurrence time estimates (u_n/v_n) is plotted in the large population limit for varying values of α and β. In the calculation, we use $\lambda_m = 0.0159$ and $\lambda_M = 0.0209$. We also assume $M = 7$.

when M is large, the cells must undergo many mutations before reaching the maximum growth rate λ_M, and hence the tumor will take a long time to recur (causing v_n to be large).

3.4 A Note on Parameter Choice

The threshold on β in the gene amplification model is necessary to control the fluctuations between the cell populations and their means. By Proposition 3, we know that there always exists a unique positive solution $\tilde{v}_n$ to the equation $\sum_{k=2}^{M} \phi_k(\tilde{v}_n t_n) = n$. This means that, at the estimate for the recurrence time, the sum of the means is always equal to n. Recall, however, that, as β increases, the mutation rate decreases. In particular, when β is large, the mutation rate may decrease to the point where very

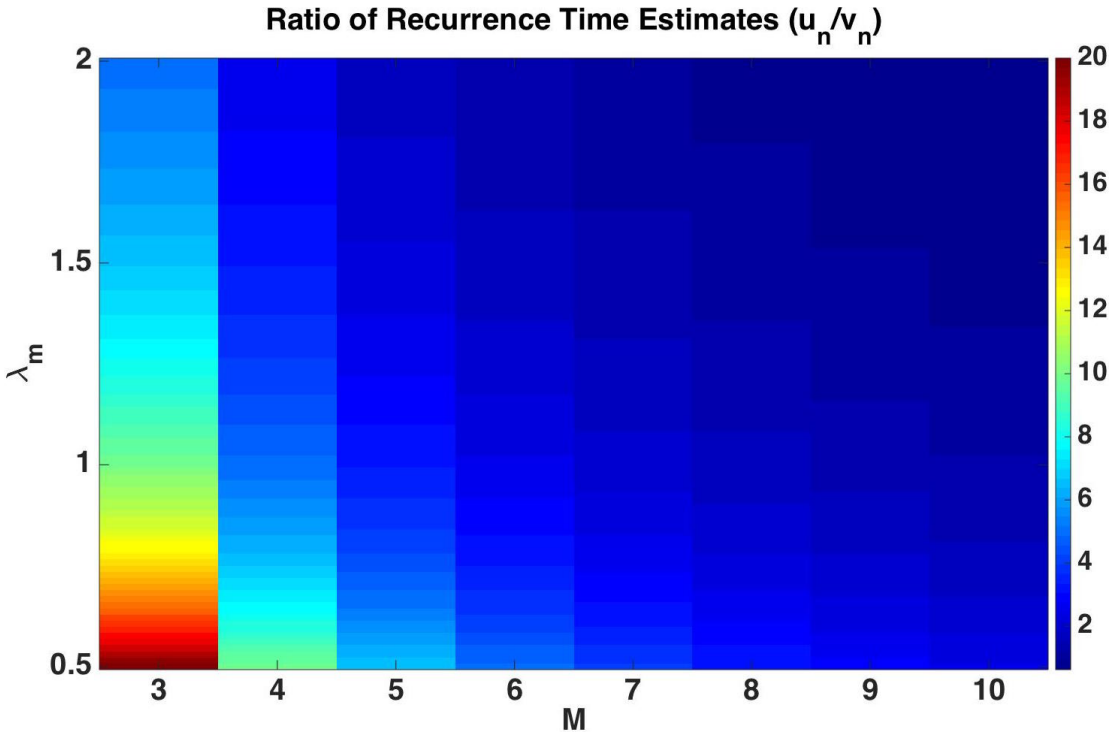

Figure 3.4: **Ratio of recurrence time estimates when M and λ_M are varied.** The ratio of the recurrence time estimates (u_n/v_n) is plotted in the large population limit for varying values of M and λ_m. In the calculation, we use $\alpha = 0.5$ and $\beta = 0.1$. We also assume $\lambda_M = 2$.

few mutations are actually generated, resulting in the entire population of cancer cells dying out before a resistant clone becomes established and hence preventing recurrence altogether. In this case, the total number of cells at the recurrence time estimate would be zero, causing the fluctuations between the actual populations and their means to become infinitely large in the large population limit. On the other hand, by placing a threshold on β, we guarantee that the mutation rate is large enough to generate enough mutations in order to drive recurrence. Thus the fluctuations between the cell populations and their means are controlled in this parameter regime.

The specific threshold on β of $\frac{1}{M-2}$ guarantees that, as M increases, β decreases and hence the mutation rate increases. Recall that the growth rates λ_k are defined to increase linearly with copy number, where $\lambda_2 < 0$ and $\lambda_M > 0$. In particular, it may be the case that multiple mutations are needed before cells have gained enough of a

fitness advantage to have a positive net growth rate. Requiring the threshold on β to be inversely proportional to M ensures that the mutation rate increases as maximum copy number increases. Essentially, the more mutations that are required for cells to attain the maximum net growth rate (the larger M is), the higher the mutation rate must be (the smaller β is) to compensate. Below, we provide evidence to support the assumption of this threshold via simulation.

To gain a better understanding of what is actually happening with these populations of cells in each scenario, we have simulated this process using a wide variety of different values for β. Specifically, when $M = 7$, we would like to argue that we must have $\beta < 0.2$ in order to get recurrence in the large population limit. Let's start by simply looking at two example simulations. Figure 3.5 shows the results of two example simulations – one where we use a $\beta < 0.2$ and one where we use a $\beta > 0.2$. The primary thing to note here is that, in the case where the restriction is satisfied, the mutation rate is sufficiently high to generate a substantial type 7 cell population and hence drive recurrence. However, in the case where the restriction is not satisfied, the subsequent cell populations are never established, and hence the tumor dies out completely before recurrence ever occurs. But obviously, these two simulations do not necessarily reflect the behavior of these processes in general.

To get a better sense of how these processes behave in general, we ran these two simulations along with four others corresponding to increasing values of n, 100 times each. The histograms representing the simulated scaled recurrence time results are shown in Table 3.1. The mean of these results is plotted as a black line, along with the lower bound on the estimate (red line) and the upper bound on the estimate (green line). First, note that the recurrence time is always positive when $\beta = 0.01$. On the other hand, when $\beta = 0.3$, the recurrence time is almost always zero (a recurrence time of zero corresponds to recurrence never occurring). Furthermore, when $\beta = 0.01$, the mean from the simulations and the estimate converge as n increases, whereas this is definitely not the case when $\beta = 0.3$.

However, we have still only examined two values of β. In Table 3.2, we perform a more thorough investigation of this parameter space. Since we are interested in the difference between when $\beta < \frac{1}{M-2}$ and when $\beta > \frac{1}{M-2}$, we investigate values of β approaching 0.2 from above and below. Since we are really interested in what happens

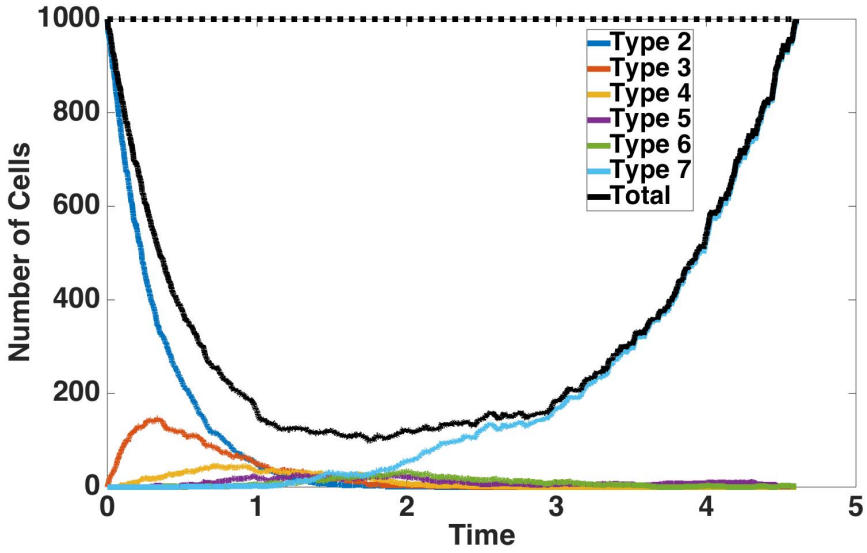

(a) $\beta = 0.01$

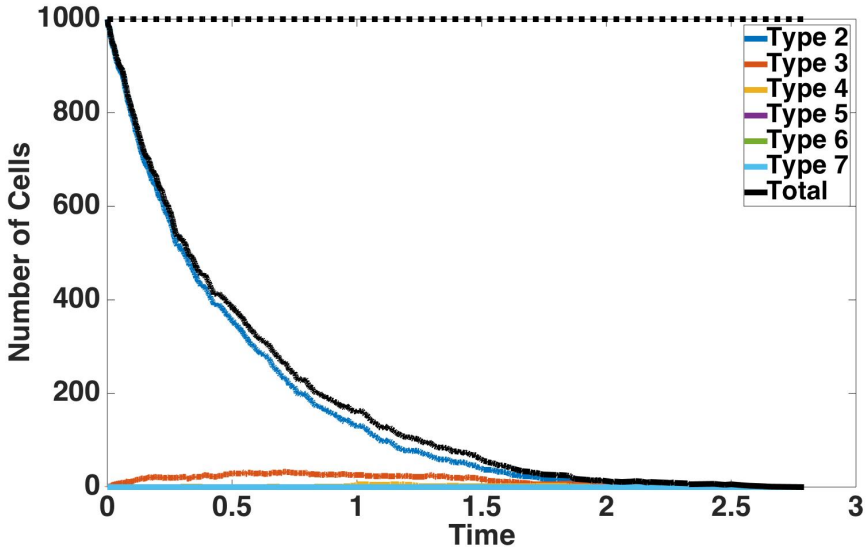

(b) $\beta = 0.3$

Figure 3.5: **Example simulations for $\beta = 0.01$ and $\beta = 0.3$.** Example simulations demonstrating the difference between when the restriction on β is satisfied and not. The tumor is simulated using the following parameters: $n = 10^3$, $r_2 = 1$, $r_3 = 8/5$, $r_4 = 11/5$, $r_5 = 14/5$, $r_6 = 17/5$, $r_7 = 4$, $d_k = 3$, and $\nu = 1$. Results are shown for $\beta = 0.01$ (a) and $\beta = 0.3$ (b).

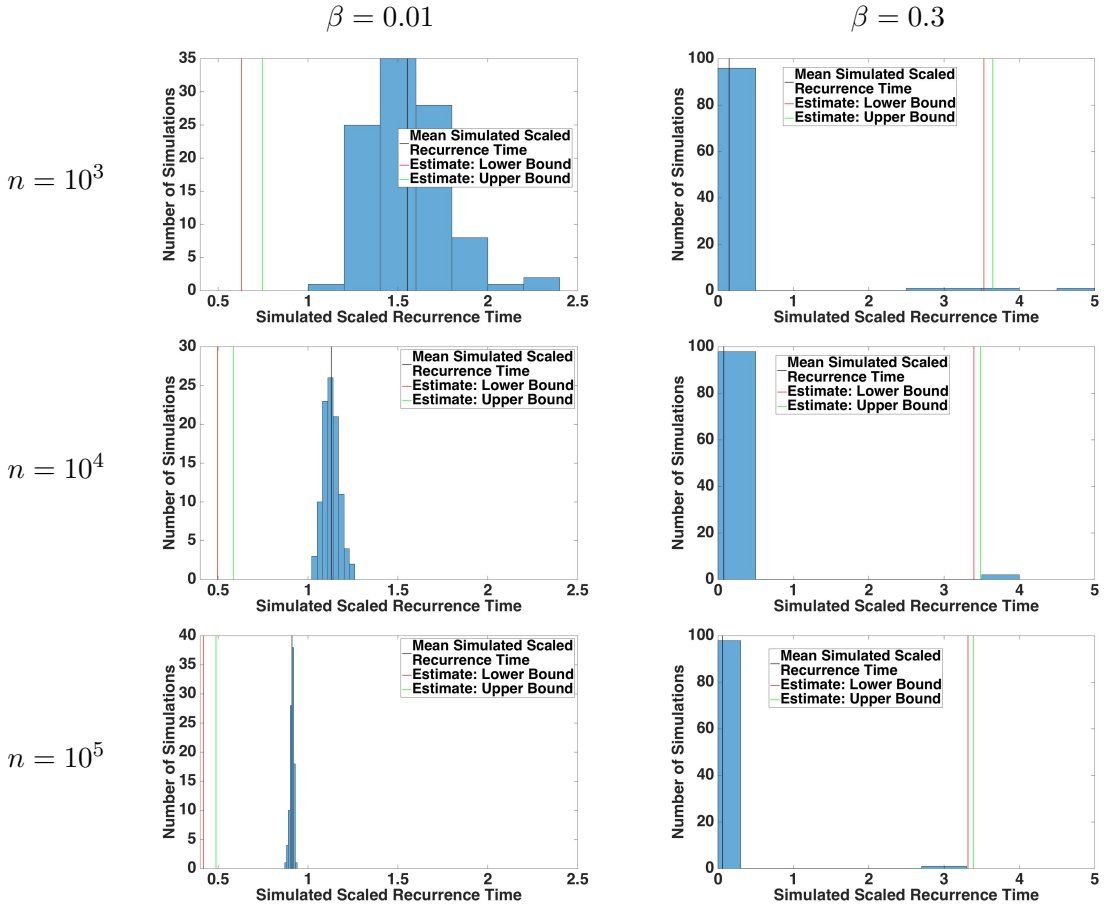

Table 3.1: **Comparison of $\beta = 0.01$ and $\beta = 0.3$.** Histograms showing simulation results when the restriction on β is satisfied and not. The tumor is simulated using the following parameters: $r_2 = 1$, $r_3 = 8/5$, $r_4 = 11/5$, $r_5 = 14/5$, $r_6 = 17/5$, $r_7 = 4$, $d_k = 3$, and $\nu = 1$. Results are shown for $\beta = 0.01$ (left column) and $\beta = 0.3$ (right column), as well as for increasing values of n. For each value of n and β, the corresponding histogram represents the simulated scaled recurrence time results from 100 simulations. The mean of these recurrence times is also plotted, along with the lower and upper bounds of the estimate.

in the large population limit, we use an initial population of 10^5 for all simulations in Table 3.2. The column on the left shows simulation results as $\beta \to 0.2$ from below, whereas the column on the right shows simulation results as $\beta \to 0.2$ from above. Note that, when $\beta = 0.15$, recurrence occurs in all 100 simulations. However, as $\beta \to 0.2$ from below, we see a handful of simulations result in a recurrence time of 0 (recurrence does

not occur). Similarly, when $\beta = 0.25$, recurrence only occurs in a few of the simulations. But as $\beta \to 0.2$ from above, the split between simulations that do and do not result in recurrence becomes more even.

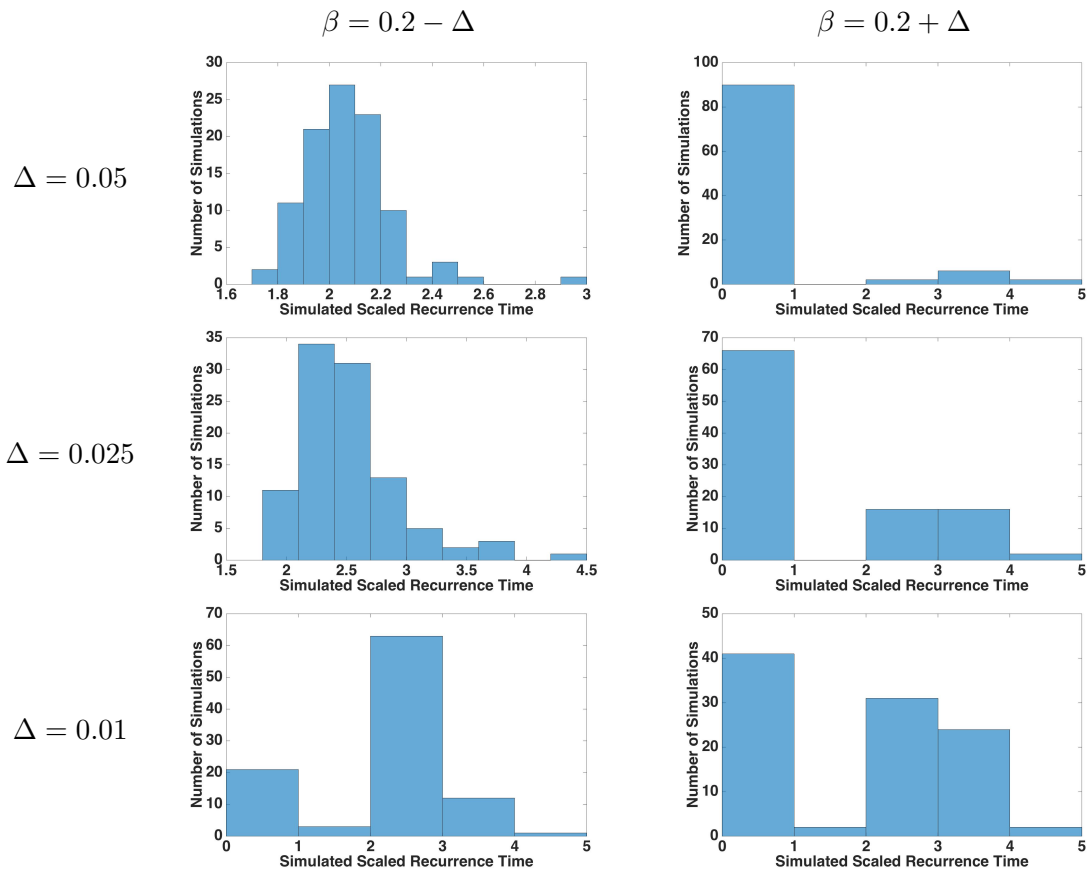

Table 3.2: **Recurrence time results as $\beta \to 0.2$.** Histograms showing simulation results for varying values of β. The tumor is simulated using the following parameters: $n = 10^5$, $r_2 = 1$, $r_3 = 8/5$, $r_4 = 11/5$, $r_5 = 14/5$, $r_6 = 17/5$, $r_7 = 4$, $d_k = 3$, and $\nu = 1$. Results are shown for values of β less than 0.2 in the left column and greater than 0.2 in the left column. Each histogram represents the simulated scaled recurrence time results from 100 simulations.

3.5 Proofs of Main Results

3.5.1 Proof of Lemma 1

Proof. We will prove this by induction. Let's start by proving the base case: $k = 3$. We need to show that

$$\mathbb{E}[X_3(t)] = \nu n^{1-\beta}\left(\frac{e^{\lambda_2 t}}{\lambda_2 - \lambda_3} - \frac{e^{\lambda_3 t}}{\lambda_2 - \lambda_3}\right).$$

Because $X_3(t)$ is a birth-death process with mutation, its mean is governed by the following ODE:

$$\frac{d}{dt}\mathbb{E}[X_3(t)] = \lambda_3 \mathbb{E}[X_3(t)] + \nu n^{-\beta}\mathbb{E}[X_2(t)].$$

Sure enough, plugging $\mathbb{E}[X_2(t)]$ and $\mathbb{E}[X_3(t)]$ into the above ODE yields

$$\frac{d}{dt}\left[\nu n^{1-\beta}\left(\frac{e^{\lambda_2 t}}{\lambda_2 - \lambda_3} - \frac{e^{\lambda_3 t}}{\lambda_2 - \lambda_3}\right)\right] = \lambda_3 \nu n^{1-\beta}\left(\frac{e^{\lambda_2 t}}{\lambda_2 - \lambda_3} - \frac{e^{\lambda_3 t}}{\lambda_2 - \lambda_3}\right) + \nu n^{-\beta} n e^{\lambda_2 t}$$

$$\nu n^{1-\beta}\left(\frac{\lambda_2 e^{\lambda_2 t}}{\lambda_2 - \lambda_3} - \frac{\lambda_3 e^{\lambda_3 t}}{\lambda_2 - \lambda_3}\right) = \nu n^{1-\beta}\left(\frac{\lambda_3 e^{\lambda_2 t}}{\lambda_2 - \lambda_3} - \frac{\lambda_3 e^{\lambda_3 t}}{\lambda_2 - \lambda_3} + \frac{(\lambda_2 - \lambda_3)e^{\lambda_2 t}}{\lambda_2 - \lambda_3}\right),$$

which is clearly true. So we do indeed have $\mathbb{E}[X_3(t)] = \nu n^{1-\beta}\left(\frac{e^{\lambda_2 t}}{\lambda_2 - \lambda_3} - \frac{e^{\lambda_3 t}}{\lambda_2 - \lambda_3}\right)$, as desired. Now assume

$$\mathbb{E}[X_l(t)] = \nu^{l-2} n^{1-(l-2)\beta}(-1)^l S_l(t).$$

We want to show that

$$\mathbb{E}[X_{l+1}(t)] = \nu^{l-1} n^{1-(l-1)\beta}(-1)^{l+1} S_{l+1}(t).$$

Because $X_{l+1}(t)$ is a birth-death process with mutation, its mean is governed by the following ODE:

$$\frac{d}{dt}\mathbb{E}[X_{l+1}(t)] = \lambda_{l+1}\mathbb{E}[X_{l+1}(t)] + \nu n^{-\beta}\mathbb{E}[X_l(t)].$$

Plugging $\mathbb{E}[X_l(t)]$ and $\mathbb{E}[X_{l+1}(t)]$ into the above ODE yields

$$\frac{d}{dt}\left[\nu^{l-1}n^{1-(l-1)\beta}(-1)^{l+1}S_{l+1}(t)\right] = \lambda_{l+1}\nu^{l-1}n^{1-(l-1)\beta}(-1)^{l+1}S_{l+1}(t) + \nu n^{-\beta}\nu^{l-2}n^{1-(l-2)\beta}(-1)^{l}S_l(t)$$
$$\nu^{l-1}n^{1-(l-1)\beta}(-1)^{l+1}\lambda_i S_{l+1}(t) = \nu^{l-1}n^{1-(l-1)\beta}(-1)^{l+1}\left[\lambda_{l+1}S_{l+1}(t) - S_l(t)\right].$$

Dividing both sides by $\nu^{l-1}n^{1-(l-1)\beta}(-1)^{l+1}$, we get

$$\begin{aligned}\lambda_i S_{l+1}(t) &= \lambda_{l+1}S_{l+1}(t) - S_l(t)\\ &= \sum_{i=2}^{l}\frac{\lambda_{l+1}e^{\lambda_i t}}{P_{i,l+1}} + \frac{\lambda_{l+1}e^{\lambda_{l+1}t}}{P_{l+1,l+1}} - \sum_{i=2}^{l}\frac{(\lambda_{l+1}-\lambda_i)e^{\lambda_i t}}{P_{i,l+1}},\end{aligned}$$

which is clearly true. So we have shown the desired result.

□

3.5.2 Proof of Proposition 1

Proof. Let $\bar{f}_n(z) = n^{z-1}(\phi_s(zt_n) + \phi_m(zt_n) - n)$. Using the definitions of ϕ_s and ϕ_m, we see that

$$\begin{aligned}\bar{f}_n(z) &= n^{z-1}\left(n^{1-z} + \frac{\mu n^{1-\alpha}}{\lambda_m - \lambda_s}\left(n^{-\lambda_m z/\lambda_s} - n^{-z}\right) - n\right)\\ &= 1 + \frac{\mu}{n^\alpha(\lambda_m-\lambda_s)}n^{z(1-\lambda_m/\lambda_s)} - \frac{\mu}{n^\alpha(\lambda_m-\lambda_s)} - n^z.\end{aligned}$$

Taking the derivative with respect to z yields

$$\begin{aligned}\bar{f}_n'(z) &= \frac{\mu}{n^\alpha(\lambda_m-\lambda_s)}\frac{\lambda_s-\lambda_m}{\lambda_s}n^{z(1-\lambda_m/\lambda_s)}\log n - n^z\log n\\ &= n^z\log n\left(\frac{-\mu}{n^\alpha\lambda_s}n^{-\lambda_m z/\lambda_s} - 1\right).\end{aligned}$$

Next we set $\bar{f}_n'(z) = 0$ and solve for z to find any local maxima or minima of $\bar{f}_n(z)$.

Since $n^z > 0$ and $\log n > 0$ for sufficiently large n, we have that

$$\begin{aligned} \bar{f}_n'(z) = 0 &\implies \frac{-\mu}{n^\alpha \lambda_s} n^{-\lambda_m z/\lambda_s} = 1 \\ &\implies -\frac{\lambda_m}{\lambda_s} z \log n = \log\left(\frac{n^\alpha \lambda_s}{-\mu}\right). \end{aligned}$$

Solving the above equation for z yields

$$\begin{aligned} z &= \frac{-\lambda_s}{\lambda_m} \cdot \frac{\log(-n^\alpha \lambda_s/\mu)}{\log n} \\ &= \frac{-\lambda_s}{\lambda_m}\left(\alpha + \frac{\log(-\lambda_s/\mu)}{\log n}\right) \\ &= \frac{1}{\lambda_m}\left(-\lambda_s \alpha + \frac{1}{t_n}\log\left(\frac{-\lambda_s}{\mu}\right)\right). \end{aligned}$$

Hence $a_n = \frac{1}{\lambda_m}\left(-\lambda_s\alpha + \frac{1}{t_n}\log(-\lambda_s/\mu)\right)$ is the only maximum or minimum of $\bar{f}_n(z)$. Moreover, we have that $a_n > 0$ for sufficiently large n.

Next note that $\bar{f}_n'(a_n - 1) = n^{a_n - 1}\log n\left(\frac{-\mu}{n^\alpha \lambda_s} n^{-\lambda_m(a_n-1)/\lambda_s} - 1\right)$. Since $n^{a_n-1} > 0$ and $\log n > 0$ for sufficiently large n and

$$\begin{aligned} \frac{-\mu}{n^\alpha \lambda_s} n^{-\lambda_m(a_n-1)/\lambda_s} - 1 &= \frac{-\mu}{n^\alpha \lambda_s} n^{\frac{\lambda_m}{-\lambda_s}\cdot\frac{1}{\lambda_m}(-\lambda_s\alpha + \frac{1}{t_n}\log(\frac{-\lambda_s}{\mu}) - \lambda_m)} - 1 \\ &= \frac{-\mu}{n^\alpha \lambda_s} n^{\alpha + \frac{1}{\log n}\log(\frac{-\lambda_s}{\mu}) + \lambda_m/\lambda_s} - 1 \\ &= n^{\lambda_m/\lambda_s} - 1 \\ &< 0 \text{ for sufficiently large } n, \end{aligned}$$

we have that $\bar{f}_n'(a_n - 1) < 0$ for sufficiently large n. Hence $\bar{f}_n(z)$ is monotonically decreasing for $z < a_n$. Similarly, $\bar{f}_n'(a_n + 1) = n^{a_n+1}\log n\left(\frac{-\mu}{n^\alpha \lambda_s} n^{-\lambda_m(a_n+1)/\lambda_s} - 1\right)$. Since $n^{a_n+1} > 0$ and $\log n > 0$ for sufficiently large n and

$$\begin{aligned}\frac{-\mu}{n^\alpha\lambda_s}n^{-\lambda_m(a_n+1)/\lambda_s}-1 &= \frac{-\mu}{n^\alpha\lambda_s}n^{\frac{\lambda_m}{-\lambda_s}\cdot\frac{1}{\lambda_m}(-\lambda_s\alpha+\frac{1}{t_n}\log(\frac{-\lambda_s}{\mu})+\lambda_m)}-1\\ &= \frac{-\mu}{n^\alpha\lambda_s}n^{\alpha+\frac{1}{\log n}\log(\frac{-\lambda_s}{\mu})-\lambda_m/\lambda_s}-1\\ &= n^{-\lambda_m/\lambda_s}-1\\ &> 0 \text{ for sufficiently large } n,\end{aligned}$$

we have that $\bar{f}_n'(a_n+1) > 0$ for sufficiently large n. Hence $\bar{f}_n(z)$ is monotonically increasing for $z > a_n$.

Now let $A_n = \frac{1}{\lambda_m}\left(-\lambda_s\alpha + \frac{1}{t_n}\log((\lambda_m-\lambda_s)/\mu)\right)$. Then

$$\begin{aligned}\bar{f}_n(A_n) &= 1+\frac{\mu n^{-\alpha}}{\lambda_m-\lambda_s}\left(n^{A_n(1-\lambda_m/\lambda_s)}-1\right)-n^{A_n}\\ &= 1+\frac{\mu n^{-\alpha}}{\lambda_m-\lambda_s}\left(n^{\frac{\lambda_m-\lambda_s}{-\lambda_s\lambda_m}\left(-\lambda_s\alpha+\frac{1}{t_n}\log\left(\frac{\lambda_m-\lambda_s}{\mu}\right)\right)}-1\right)-n^{\frac{1}{\lambda_m}\left(-\lambda_s\alpha+\frac{1}{t_n}\log\left(\frac{\lambda_m-\lambda_s}{\mu}\right)\right)}\\ &= 1+\frac{\mu n^{-\alpha}}{\lambda_m-\lambda_s}\left(n^{\alpha\left(1-\frac{\lambda_s}{\lambda_m}\right)}n^{\frac{\lambda_m-\lambda_s}{\lambda_m\log n}\log\left(\frac{\lambda_m-\lambda_s}{\mu}\right)}-1\right)-n^{\frac{\lambda_s\alpha}{-\lambda_m}}n^{\frac{-\lambda_s}{\lambda_m\log n}\log\left(\frac{\lambda_m-\lambda_s}{\mu}\right)}\\ &= 1+\frac{\mu n^{-\alpha}}{\lambda_m-\lambda_s}\left(n^{\alpha\left(1-\frac{\lambda_s}{\lambda_m}\right)}\left(\frac{\lambda_m-\lambda_s}{\mu}\right)^{1-\frac{\lambda_s}{\lambda_m}}-1\right)-n^{\frac{\lambda_s\alpha}{-\lambda_m}}\left(\frac{\lambda_m-\lambda_s}{\mu}\right)^{\frac{-\lambda_s}{\lambda_m}}\\ &= 1+n^{\frac{\lambda_s\alpha}{-\lambda_m}}\left(\frac{\lambda_m-\lambda_s}{\mu}\right)^{\frac{-\lambda_s}{\lambda_m}}-\frac{\mu n^{-\alpha}}{\lambda_m-\lambda_s}-n^{\frac{\lambda_s\alpha}{-\lambda_m}}\left(\frac{\lambda_m-\lambda_s}{\mu}\right)^{\frac{-\lambda_s}{\lambda_m}}\\ &= 1-\frac{\mu n^{-\alpha}}{\lambda_m-\lambda_s}\\ &> 0 \text{ for sufficiently large } n.\end{aligned}$$

Note that since $\bar{f}_n(0) = 0$ and $\bar{f}_n(z)$ is decreasing for all $z \in (0, a_n)$, we have that $\bar{f}_n(a_n) < 0$. But $\bar{f}_n(z)$ is increasing for $z > a_n$ and we have that $\bar{f}_n(A_n) > 0$. Therefore, there exists a unique $\tilde{u}_n \in (a_n, A_n)$ such that $\bar{f}_n(\tilde{u}_n) = 0$ by monotonicity. Using the definition of $\bar{f}_n(z)$ and the fact that $n^{z-1} > 0$, this implies that there is a unique $\tilde{u}_n > 0$ such that $a_n < \tilde{u}_n < A_n$ and $\phi_s(\tilde{u}_n t_n) + \phi_m(\tilde{u}_n t_n) = n$. Furthermore, $\lim_{n\to\infty} a_n = \lim_{n\to\infty} A_n = \frac{-\lambda_s\alpha}{\lambda_m}$. Hence $\tilde{u}_n \to \frac{-\lambda_s\alpha}{\lambda_m}$ as $n \to \infty$.

□

3.5.3 Proof of Theorem 1

Proof. In order to show the desired result, we must show

$$\lim_{n\to\infty} \mathbb{P}(\tau_n > u_n + \epsilon) + \lim_{n\to\infty} \mathbb{P}(\tau_n < u_n - \epsilon) = 0.$$

Let's start by proving that $\mathbb{P}(\tau_n < u_n - \epsilon) \to 0$ as $n \to \infty$. Note that

$$\begin{aligned}
\mathbb{P}\left(\tau_n < u_n - \epsilon\right) &= \mathbb{P}\left(\frac{\tau_n}{t_n} < u_n^-(\epsilon)\right) \\
&\leq \mathbb{P}\left(\sup_{z\in[c,u_n^-(\epsilon)]} (X_s(zt_n) + X_m(zt_n) - n) > 0\right) \\
&= \mathbb{P}\Bigg(\sup_{z\in[c,u_n^-(\epsilon)]} n^{\alpha+\lambda_m z/\lambda_s - 1}(X_s(zt_n) - \phi_s(zt_n) + \phi_s(zt_n) - n \\
&\qquad\qquad + \phi_m(zt_n) - \phi_m(zt_n) + X_m(zt_n)) > 0\Bigg) \\
&\leq \mathbb{P}\left(\bar{B}_1(n,\epsilon) + \bar{B}_2(n,\epsilon) + \bar{B}_3(n,\epsilon) > 0\right),
\end{aligned}$$

where

$$\begin{aligned}
\bar{B}_1(n,\epsilon) &= \sup_{z\in[c,u_n^-(\epsilon)]} n^{\alpha+\lambda_m z/\lambda_s - 1}(X_s(zt_n) - \phi_s(zt_n)), \\
\bar{B}_2(n,\epsilon) &= \sup_{z\in[c,u_n^-(\epsilon)]} n^{\alpha+\lambda_m z/\lambda_s - 1}(\phi_s(zt_n) + \phi_m(zt_n) - n), \\
\bar{B}_3(n,\epsilon) &= \sup_{z\in[c,u_n^-(\epsilon)]} n^{\alpha+\lambda_m z/\lambda_s - 1}(X_m(zt_n) - \phi_m(zt_n)).
\end{aligned}$$

Note that, for $i \in \{s, m\}$,

$$\begin{aligned}
&\sup_{z\in[c,u_n^-(\epsilon)]} \left| n^{\alpha+\lambda_m z/\lambda_s - 1}\left(X_i(zt_n) - \phi_i(zt_n)\right)\right| \\
&\qquad \leq \sup_{z\in[c,u_n^+(\epsilon)]} n^{\alpha+\lambda_m z/\lambda_s - 1}\left|X_i(zt_n) - \phi_i(zt_n)\right|,
\end{aligned}$$

which converges to zero in probability by Proposition 2. Now we just need to show that $\bar{B}_2(n,\epsilon)$ is negative in the large population limit. Define a function given by $\bar{g}_n(z) = n^{\alpha+\lambda_m z/\lambda_s - 1}\left(\phi_s(zt_n) + \phi_m(zt_n) - n\right)$. Using the definitions of ϕ_s and ϕ_m, we see that

$$\begin{aligned}\bar{g}_n(z) &= n^{\alpha+\lambda_m z/\lambda_s-1}\left(n^{1-z} + \frac{\mu n^{1-\alpha}}{\lambda_m-\lambda_s}\left(n^{-\lambda_m z/\lambda_s} - n^{-z}\right) - n\right)\\ &= n^{\alpha+z(\lambda_m/\lambda_s-1)} + \frac{\mu}{\lambda_m-\lambda_s} - \frac{\mu}{\lambda_m-\lambda_s}n^{z(\lambda_m/\lambda_s-1)} - n^{\alpha+\lambda_m z/\lambda_s}.\end{aligned}$$

Taking the derivative with respect to z yields

$$\begin{aligned}\bar{g}_n'(z) &= \frac{\lambda_m-\lambda_s}{\lambda_s}n^{\alpha+z(\lambda_m/\lambda_s-1)}\log n - \frac{\mu}{\lambda_s}n^{z(\lambda_m/\lambda_s-1)}\log n - \frac{\lambda_m}{\lambda_s}n^{\alpha+\lambda_m z/\lambda_s}\log n\\ &= \frac{-1}{\lambda_s}n^{\alpha+z(\lambda_m/\lambda_s-1)}\log n\left[-\lambda_m+\lambda_s+\mu n^{-\alpha}+\lambda_m n^z\right].\end{aligned}$$

Next we set $\bar{g}_n'(z) = 0$ and solve for z to find any local maxima or minima of $\bar{g}_n(z)$. Since $-1/\lambda_s > 0$ and $n^{\alpha - z(1-\lambda_m/\lambda_s)} > 0$ and $\log n > 0$ for sufficiently large n, we have that

$$\begin{aligned}\bar{g}_n'(z) = 0 &\implies \lambda_m n^z = \lambda_m - \lambda_s - \mu n^{-\alpha}\\ &\implies z\log n = \log\left(\frac{\lambda_m-\lambda_s-\mu n^{-\alpha}}{\lambda_m}\right)\\ &\implies z = \frac{1}{\log n}\log\left(\frac{\lambda_m-\lambda_s-\mu n^{-\alpha}}{\lambda_m}\right).\end{aligned}$$

Hence $\bar{q}_n = \frac{1}{\log n}\log\left(\frac{\lambda_m-\lambda_s-\mu n^{-\alpha}}{\lambda_m}\right)$ is the only maximum or minimum of $\bar{g}_n(z)$. Next note that $\bar{g}_n'(\bar{q}_n+1) = \frac{-1}{\lambda_s}n^{\alpha-(\bar{q}_n+1)(1-\lambda_m/\lambda_s)}\log n\left[-\lambda_m+\lambda_s+\mu n^{-\alpha}+\lambda_m n^{\bar{q}_n+1}\right]$. Since $-1/\lambda_s > 0$ and $n^{\alpha-(\bar{q}_n+1)(1-\lambda_m/\lambda_s)} > 0$ and $\log n > 0$ for sufficiently large n and

$$\begin{aligned}
-\lambda_m + \lambda_s + \mu n^{-\alpha} + \lambda_m n^{\bar{q}_n+1} &= \lambda_m n \cdot n^{\frac{1}{\log n}\log\left(\frac{\lambda_m-\lambda_s-\mu n^{-\alpha}}{\lambda_m}\right)} - \lambda_m + \lambda_s + \mu n^{-\alpha} \\
&= \lambda_m n \left(\frac{\lambda_m - \lambda_s - \mu n^{-\alpha}}{\lambda_m}\right) - \lambda_m + \lambda_s + \mu n^{-\alpha} \\
&= (n-1)\left(\lambda_m - \lambda_s - \mu n^{-\alpha}\right) \\
&> 0 \text{ for sufficiently large } n,
\end{aligned}$$

we have that $\bar{g}_n'(\bar{q}_n + 1) > 0$ for sufficiently large n. Hence $\bar{g}_n(z)$ is monotonically increasing for $z > \bar{q}_n$. Note that the only positive solution to $\bar{g}_n(z) = 0$ occurs at $z = \tilde{u}_n$ by Proposition 1. Also note that $\bar{q}_n < c < u_n^-(\epsilon) < \tilde{u}_n$ for sufficiently large n. Therefore, we have that $\bar{B}_2(n,\epsilon) < 0$. Moreover, we may rewrite $\bar{B}_2(n,\epsilon)$ as

$$\bar{B}_2(n,\epsilon) = n^{\alpha+\lambda_m u_n^-(\epsilon)/\lambda_s - 1}\left(\phi_s\left(u_n^-(\epsilon)t_n\right) + \phi_m\left(u_n^-(\epsilon)t_n\right) - n\right).$$

Then by the definitions of ϕ_s and ϕ_m, we have

$$\begin{aligned}
\bar{B}_2(n,\epsilon) &= n^{\alpha+\lambda_m u_n^-(\epsilon)/\lambda_s - 1}\left(n^{1-u_n^-(\epsilon)} + \frac{\mu n^{1-\alpha}}{\lambda_m - \lambda_s}\left(n^{-\lambda_m u_n^-(\epsilon)/\lambda_s} - n^{-u_n^-(\epsilon)}\right) - n\right) \\
&= n^{\alpha - u_n^-(\epsilon)(1-\lambda_m/\lambda_s)} + \frac{\mu}{\lambda_m - \lambda_s} - \frac{\mu}{\lambda_m - \lambda_s} n^{-u_n^-(\epsilon)(1-\lambda_m/\lambda_s)} - n^{\alpha+\lambda_m u_n^-(\epsilon)/\lambda_s}.
\end{aligned}$$

Note that

$$\begin{aligned}
n^{\alpha+\lambda_m u_n^-(\epsilon)/\lambda_s} &= n^\alpha n^{\frac{\epsilon\lambda_m}{\log n}} n^{\tilde{u}_n(\lambda_m/\lambda_s)} \\
&= e^{\epsilon\lambda_m} n^{\alpha+\tilde{u}_n(\lambda_m/\lambda_s)} \\
&\geq e^{\epsilon\lambda_m} n^{\alpha+A_n(\lambda_m/\lambda_s)} \\
&= e^{\epsilon\lambda_m} n^{\alpha+\frac{\lambda_m}{\lambda_s}\cdot\frac{1}{\lambda_m}\left(-\lambda_s\alpha+\frac{1}{t_n}\log\left(\frac{\lambda_m-\lambda_s}{\mu}\right)\right)} \\
&= e^{\epsilon\lambda_m} n^{\alpha-\alpha-\frac{1}{\log n}\log\left(\frac{\lambda_m-\lambda_s}{\mu}\right)} \\
&= e^{\epsilon\lambda_m}\left(\frac{\mu}{\lambda_m-\lambda_s}\right).
\end{aligned}$$

Therefore, we have that

$$\begin{aligned}\bar{B}_2(n,\epsilon) &\leq n^{\alpha-u_n^-(\epsilon)(1-\lambda_m/\lambda_s)} + \frac{\mu}{\lambda_m-\lambda_s} - \frac{\mu}{\lambda_m-\lambda_s} n^{-u_n^-(\epsilon)(1-\lambda_m/\lambda_s)} - e^{\epsilon\lambda_m}\left(\frac{\mu}{\lambda_m-\lambda_s}\right) \\ &= \frac{\mu}{\lambda_m-\lambda_s}\left(1-e^{\epsilon\lambda_m}\right) + n^{\alpha-u_n^-(\epsilon)(1-\lambda_m/\lambda_s)}\left(1-\frac{\mu n^{-\alpha}}{\lambda_m-\lambda_s}\right). \qquad (3.2)\end{aligned}$$

Clearly, $1-\mu n^{-\alpha}/(\lambda_m-\lambda_s) \to 1$ as $n\to\infty$ since $\alpha>0$. We also have that

$$\begin{aligned}\lim_{n\to\infty} n^{\alpha-u_n^-(\epsilon)(1-\lambda_m/\lambda_s)} &= \lim_{n\to\infty} n^{\alpha} n^{\frac{\epsilon}{t_n}(1-\lambda_m/\lambda_s)} n^{-\tilde{u}_n(1-\lambda_m/\lambda_s)} \\ &= e^{\epsilon(\lambda_m-\lambda_s)} \lim_{n\to\infty} n^{\alpha-\tilde{u}_n(1-\lambda_m/\lambda_s)} \\ &= e^{\epsilon(\lambda_m-\lambda_s)} \lim_{n\to\infty} e^{[\alpha-\tilde{u}_n(1-\lambda_m/\lambda_s)]\log n} \\ &= 0\end{aligned}$$

since $\tilde{u}_n \to -\alpha\lambda_s/\lambda_m$ as $n\to\infty$ by Proposition 1. Therefore, the right-hand side of equation (3.2) converges to $\frac{\mu}{\lambda_m-\lambda_s}(1-e^{\epsilon\lambda_m}) < 0$. So $\bar{B}_2(n,\epsilon)$ is negative in the large population limit. Putting this all together, we have our desired result: $\mathbb{P}(\bar{B}_1(n,\epsilon) + \bar{B}_2(n,\epsilon) + \bar{B}_3(n,\epsilon) > 0) \to 0$ as $n\to\infty$. Therefore, we have shown $\mathbb{P}(\tau_n < u_n - \epsilon) \to 0$ as $n\to\infty$. The proof that $\mathbb{P}(\tau_n > u_n + \epsilon) \to 0$ as $n\to\infty$ follows using a similar argument.

□

3.5.4 Proof of Proposition 2

Proof. Let's start by proving the $i=s$ case. That is, we want to show that

$$\lim_{n\to\infty} \mathbb{P}\left(\sup_{z\in[c,u_n^+(\epsilon)]} n^{\alpha+\lambda_m z/\lambda_s - 1}\left|X_s(zt_n) - \phi_s(zt_n)\right| > \delta\right) = 0.$$

Because a branching process normalized by its mean is a martingale, we know that $Z_s(z) = n^{\alpha+z-1}\left(X_s(zt_n) - \phi_s(zt_n)\right)$ is a martingale in z. To prove our desired result for $i=s$, we need to show

$$\lim_{n\to\infty} \mathbb{P}\left(\sup_{z\in[c,u_n^+(\epsilon)]} n^{\lambda_m z/\lambda_s - z}|Z_s(z)| > \delta \right) = 0.$$

Note that

$$\begin{aligned}\sup_{z\in[c,u_n^+(\epsilon)]} n^{\lambda_m z/\lambda_s - z}|Z_s(z)| &\leq \sup_{z\in[c,u_n^+(\epsilon)]} n^{\lambda_m z/\lambda_s - z} \cdot \sup_{z\in[c,u_n^+(\epsilon)]} |Z_s(z)| \\ &= n^{\lambda_m c/\lambda_s - c} \cdot \sup_{z\in[c,u_n^+(\epsilon)]} |Z_s(z)|.\end{aligned}$$

Therefore, we have that

$$\begin{aligned}\mathbb{P}\left(\sup_{z\in[c,u_n^+(\epsilon)]} n^{\lambda_m z/\lambda_s - z}|Z_s(z)| > \delta \right) &\leq \mathbb{P}\left(n^{\lambda_m c/\lambda_s - c} \cdot \sup_{z\in[c,u_n^+(\epsilon)]} |Z_s(z)| > \delta \right) \\ &= \mathbb{P}\left(\sup_{z\in[c,u_n^+(\epsilon)]} |Z_s(z)| > \delta \cdot n^{c-\lambda_m c/\lambda_s} \right) \\ &\leq \frac{1}{\delta^2} n^{2\lambda_m c/\lambda_s - 2c} \cdot \mathbb{E}\left[\left(Z_s(u_n^+(\epsilon)) \right)^2 \right]\end{aligned}$$

by Doob's Martingale Inequality. Note that

$$\begin{aligned}\mathbb{E}\left[\left(Z_s(u_n^+(\epsilon)) \right)^2 \right] &= \mathbb{E}\left[\left(n^{\alpha+u_n^+(\epsilon)-1} X_s(u_n^+(\epsilon)t_n) - n^{\alpha+u_n^+(\epsilon)-1}\phi_s(u_n^+(\epsilon)t_n) \right)^2 \right] \\ &= \mathrm{Var}\left[n^{\alpha+u_n^+(\epsilon)-1} X_s(u_n^+(\epsilon)t_n) \right].\end{aligned}$$

Therefore, now we have

$$\begin{aligned}
&\mathbb{P}\left(\sup_{z\in[c,u_n^+(\epsilon)]} n^{\lambda_m z/\lambda_s - z}|Z_s(z)| > \delta\right) \\
&\quad\leq \frac{1}{\delta^2} n^{2\lambda_m c/\lambda_s - 2c} \cdot \mathrm{Var}\left[n^{\alpha+u_n^+(\epsilon)-1} X_s(u_n^+(\epsilon)t_n)\right] \\
&\quad= \frac{1}{\delta^2} n^{2\lambda_m c/\lambda_s - 2c} n^{2\alpha+2u_n^+(\epsilon)-2} n^{1-u_n^+(\epsilon)} \left(\frac{r_s+d_s}{-\lambda_s}\right)\left(1-n^{-u_n^+(\epsilon)}\right) \\
&\quad= \frac{1}{\delta^2}\left(\frac{r_s+d_s}{-\lambda_s}\right)\left(1-n^{-u_n^+(\epsilon)}\right) n^{2\alpha+2c(\lambda_m/\lambda_s-1)+u_n^+(\epsilon)-1}.
\end{aligned}$$

Clearly, $\frac{1}{\delta^2}\left(\frac{r_s+d_s}{-\lambda_s}\right)$ is just a finite constant. Note that

$$\begin{aligned}
\lim_{n\to\infty}\left(1-n^{-u_n^+(\epsilon)}\right) &= 1 - \lim_{n\to\infty} n^{-\epsilon/t_n} n^{-\tilde{u}_n} \\
&= 1 - e^{\epsilon\lambda_s} \lim_{n\to\infty} e^{-\tilde{u}_n \log n} \\
&= 1
\end{aligned}$$

since $\tilde{u}_n \to -\lambda_s\alpha/\lambda_m$ as $n\to\infty$ by Proposition 1. We also have that

$$\begin{aligned}
\lim_{n\to\infty} n^{2\alpha+2c(\lambda_m/\lambda_s-1)+u_n^+(\epsilon)-1} &= \lim_{n\to\infty} n^{2\alpha+\frac{\alpha\lambda_s(\lambda_s-2\lambda_m)}{\lambda_m(\lambda_m-\lambda_s)}\cdot\frac{\lambda_m-\lambda_s}{\lambda_s}-1} n^{\tilde{u}_n} n^{\epsilon/t_n} \\
&= e^{-\epsilon\lambda_s} \lim_{n\to\infty} n^{2\alpha+\alpha(\lambda_s-2\lambda_m)/\lambda_m-1+\tilde{u}_n} \\
&= e^{-\epsilon\lambda_s} \lim_{n\to\infty} e^{[\tilde{u}_n+\alpha\lambda_s/\lambda_m-1]\log n} \\
&= 0
\end{aligned}$$

since $\tilde{u}_n \to -\lambda_s\alpha/\lambda_m$ as $n\to\infty$ by Proposition 1. So we are done with the $i=s$ case.

Next, let's prove the desired result for $i=m$. As a reminder, we want to show that

$$\lim_{n\to\infty}\mathbb{P}\left(\sup_{z\in[c,u_n^+(\epsilon)]} n^{\alpha+\lambda_m z/\lambda_s-1}\,|X_m(zt_n)-\phi_m(zt_n)| > \delta\right) = 0.$$

Note that

$$\begin{aligned}\phi_m(zt_n) &= \int_0^{zt_n} \mu n^{-\alpha} n e^{\lambda_s s} e^{\lambda_m (zt_n - s)}\, ds \\ &= \mu n^{1-\lambda_m z/\lambda_s - \alpha} \int_0^{zt_n} e^{(\lambda_s - \lambda_m)s}\, ds.\end{aligned}$$

Therefore,

$$\begin{aligned}&n^{\alpha+\lambda_m z/\lambda_s - 1} \left(X_m(zt_n) - \phi_m(zt_n)\right) \\ &\quad = n^{\alpha+\lambda_m z/\lambda_s - 1} X_m(zt_n) - \mu \int_0^{zt_n} e^{(\lambda_s-\lambda_m)s}\, ds \\ &\quad = n^{\alpha+\lambda_m z/\lambda_s - 1} X_m(zt_n) - \frac{\mu}{n} \int_0^{zt_n} X_s(s) e^{-\lambda_m s}\, ds \\ &\qquad\qquad + \frac{\mu}{n} \int_0^{zt_n} \left(X_s(s) - n e^{\lambda_s s}\right) e^{-\lambda_m s}\, ds.\end{aligned}$$

Taking the absolute value of both sides and using the triangle inequality, we get

$$\begin{aligned}&n^{\alpha+\lambda_m z/\lambda_s - 1} \left|X_m(zt_n) - \phi_m(zt_n)\right| \\ &\quad \le \left| n^{\alpha+\lambda_m z/\lambda_s - 1} X_m(zt_n) - \frac{\mu}{n} \int_0^{zt_n} X_s(s) e^{-\lambda_m s}\, ds \right| \\ &\qquad\qquad + \frac{\mu}{n} \int_0^{zt_n} \left| X_s(s) - n e^{\lambda_s s} \right| e^{-\lambda_m s}\, ds.\end{aligned}$$

This implies that

$$\begin{aligned}&\sup_{z \in [c, u_n^+(\epsilon)]} n^{\alpha+\lambda_m z/\lambda_s - 1} \left|X_m(zt_n) - \phi_m(zt_n)\right| \\ &\quad \le \sup_{z \in [c, u_n^+(\epsilon)]} \left| n^{\alpha+\lambda_m z/\lambda_s - 1} X_m(zt_n) - \frac{\mu}{n} \int_0^{zt_n} X_s(s) e^{-\lambda_m s}\, ds \right| \\ &\qquad\qquad + \sup_{z \in [c, u_n^+(\epsilon)]} \frac{\mu}{n} \int_0^{zt_n} \left| X_s(s) - n e^{\lambda_s s} \right| e^{-\lambda_m s}\, ds.\end{aligned}$$

Hence

$$\mathbb{P}\left(\sup_{z\in[c,u_n^+(\epsilon)]} n^{\alpha+\lambda_m z/\lambda_s-1}\left|X_m(zt_n)-\phi_m(zt_n)\right|>\delta\right)$$
$$\leq \mathbb{P}\left(\sup_{z\in[c,u_n^+(\epsilon)]}\left|n^{\alpha+\lambda_m z/\lambda_s-1}X_m(zt_n)-\frac{\mu}{n}\int_0^{zt_n}X_s(s)e^{-\lambda_m s}\,ds\right|>\delta/2\right)$$
$$+\mathbb{P}\left(\sup_{z\in[c,u_n^+(\epsilon)]}\frac{\mu}{n}\int_0^{zt_n}\left|X_s(s)-ne^{\lambda_s s}\right|e^{-\lambda_m s}\,ds>\delta/2\right).$$

The process in the second term of the above sum is monotonically increasing in z. So we may simplify the expression above to

$$\mathbb{P}\left(\sup_{z\in[c,u_n^+(\epsilon)]} n^{\alpha+\lambda_m z/\lambda_s-1}\left|X_m(zt_n)-\phi_m(zt_n)\right|>\delta\right)$$
$$\leq \mathbb{P}\left(\sup_{z\in[c,u_n^+(\epsilon)]}\left|n^{\alpha+\lambda_m z/\lambda_s-1}X_m(zt_n)-\frac{\mu}{n}\int_0^{zt_n}X_s(s)e^{-\lambda_m s}\,ds\right|>\delta/2\right)$$
$$+\mathbb{P}\left(\frac{\mu}{n}\int_0^{u_n^+(\epsilon)t_n}\left|X_s(s)-ne^{\lambda_s s}\right|e^{-\lambda_m s}\,ds>\delta/2\right).$$

By Lemma 1 in [69], we know that

$$e^{-\lambda_m t}X_m(t)-\int_0^t \mu n^{-\alpha}e^{-\lambda_m s}X_s(s)\,ds$$

is a martingale. Setting $t=zt_n=\frac{z}{-\lambda_s}\log n$, we get that

$$n^{\lambda_m z/\lambda_s}X_m(zt_n)-\frac{\mu}{n^\alpha}\int_0^{zt_n}e^{-\lambda_m s}X_s(s)\,ds$$

is a martingale in z. Since linear combinations of martingales are also martingales,

$$n^{\alpha+\lambda_m z/\lambda_s-1}X_m(zt_n)-\frac{\mu}{n}\int_0^{zt_n}e^{-\lambda_m s}X_s(s)\,ds$$

is also a martingale in z. Therefore,

$$\left|n^{\alpha+\lambda_m z/\lambda_s-1}X_m(zt_n)-\frac{\mu}{n}\int_0^{zt_n}X_s(s)e^{-\lambda_m s}\,ds\right|$$

is a non-negative submartingale in z, so we can apply Doob's Martingale Inequality to get

$$\begin{aligned}\mathbb{P}\left(\sup_{z\in[c,u_n^+(\epsilon)]} n^{\alpha+\lambda_m z/\lambda_s-1}\left|X_m(zt_n)-\phi_m(zt_n)\right|>\delta\right)\\ \leq \frac{4}{\delta^2}\cdot\mathbb{E}\left[\left(n^{\alpha+\lambda_m u_n^+(\epsilon)/\lambda_s-1}X_m(u_n+\epsilon)-\frac{\mu}{n}\int_0^{u_n+\epsilon}X_s(s)e^{-\lambda_m s}\,ds\right)^2\right]\\ +\mathbb{P}\left(\frac{\mu}{n}\int_0^{u_n+\epsilon}\left|X_s(s)-ne^{\lambda_s s}\right|e^{-\lambda_m s}\,ds>\delta/2\right).\end{aligned} \tag{3.3}$$

Let us start by showing that the second term in (3.3) converges to zero. Since convergence in mean implies convergence in probability (by Markov's Inequality), it suffices to show that

$$\lim_{n\to\infty}\mathbb{E}\left[\frac{\mu}{n}\int_0^{u_n+\epsilon}\left|X_s(s)-ne^{\lambda_s s}\right|e^{-\lambda_m s}\,ds\right]=0,$$

or, equivalently,

$$\lim_{n\to\infty}\frac{\mu}{n}\int_0^{u_n+\epsilon}\mathbb{E}\left[\left|X_s(s)-ne^{\lambda_s s}\right|\right]e^{-\lambda_m s}\,ds=0.$$

By the Cauchy-Schwarz Inequality, we know

$$\begin{aligned}\mathbb{E}\left[\left|X_s(s)-ne^{\lambda_s s}\right|\right]&\leq\sqrt{\mathbb{E}\left[\left|X_s(s)-ne^{\lambda_s s}\right|^2\right]}\\ &\leq\sqrt{\mathrm{Var}\left[X_s(s)\right]}\\ &=n^{1/2}\left[\left(\frac{r_s+d_s}{\lambda_s}\right)\left(e^{2\lambda_s s}-e^{\lambda_s s}\right)\right]^{1/2}.\end{aligned}$$

Multiplying both sides by $\frac{\mu}{n}e^{-\lambda_m s}$ and integrating yields

$$\begin{aligned}
&\frac{\mu}{n}\int_0^{u_n+\epsilon}\mathbb{E}\left[\left|X_s(s)-ne^{\lambda_s s}\right|\right]e^{-\lambda_m s}\,ds\\
&\quad\le\frac{\mu}{n^{1/2}}\int_0^{u_n+\epsilon}\left[\left(\frac{r_s+d_s}{\lambda_s}\right)\left(e^{2\lambda_s s}-e^{\lambda_s s}\right)\right]^{1/2}e^{-\lambda_m s}\,ds\\
&\quad=\mu\left(\frac{r_s+d_s}{-\lambda_s n}\right)^{1/2}\int_0^{u_n+\epsilon}\left(1-e^{\lambda_s s}\right)^{1/2}e^{\lambda_s s/2}e^{-\lambda_m s}\,ds\\
&\quad\le\mu\left(\frac{r_s+d_s}{-\lambda_s n}\right)^{1/2}\int_0^{u_n+\epsilon}e^{(\lambda_s/2-\lambda_m)s}\,ds\\
&\quad=\frac{\mu}{\lambda_s/2-\lambda_m}\left(\frac{r_s+d_s}{-\lambda_s n}\right)^{1/2}\left(e^{(\lambda_s/2-\lambda_m)(u_n+\epsilon)}-1\right).
\end{aligned}$$

Note that, since $u_n=\tilde{u}_n t_n=\frac{\tilde{u}_n}{-\lambda_s}\log n$,

$$\begin{aligned}
e^{(\lambda_s/2-\lambda_m)(u_n+\epsilon)}&=e^{(\lambda_s/2-\lambda_m)\frac{\tilde{u}_n}{-\lambda_s}\log n}e^{(\lambda_s/2-\lambda_m)\epsilon}\\
&=n^{(\lambda_m/\lambda_s-1/2)\tilde{u}_n}e^{(\lambda_s/2-\lambda_m)\epsilon},
\end{aligned}$$

which converges to zero since $\tilde{u}_n\to\frac{-\lambda_s\alpha}{\lambda_m}$ as $n\to\infty$ by Proposition 1. Therefore,

$$\lim_{n\to\infty}\frac{\mu}{n}\int_0^{u_n+\epsilon}\mathbb{E}\left[\left|X_s(s)-ne^{\lambda_s s}\right|\right]e^{-\lambda_m s}\,ds=0,$$

as desired. Next, we will show the first term in (3.3) converges to zero as well.

$$\begin{aligned}
&\mathbb{E}\left[\left(n^{\alpha+\lambda_m u_n^+(\epsilon)/\lambda_s-1}X_m(u_n+\epsilon)-\frac{\mu}{n}\int_0^{u_n+\epsilon}X_s(s)e^{-\lambda_m s}\,ds\right)^2\right]\\
&\quad=n^{2(\alpha+\lambda_m u_n^+(\epsilon)/\lambda_s-1)}\mathbb{E}\left[X_m(u_n+\epsilon)^2\right]\\
&\qquad-2\mu n^{\alpha+\lambda_m u_n^+(\epsilon)/\lambda_s-2}\int_0^{u_n+\epsilon}\mathbb{E}\left[X_s(s)X_m(u_n+\epsilon)\right]e^{-\lambda_m s}\,ds\\
&\qquad+\left(\frac{\mu}{n}\right)^2\int_0^{u_n+\epsilon}\int_0^{u_n+\epsilon}\mathbb{E}\left[X_s(s)X_s(y)\right]e^{-\lambda_m s}e^{-\lambda_m y}\,ds\,dy.
\end{aligned}$$

From Lemma 1 in [18], we know that

$$\mathbb{E}\left[X_m(u_n+\epsilon)^2\right] = \left(\frac{\mu}{n^\alpha}\right)^2 \int_0^{u_n+\epsilon}\int_0^{u_n+\epsilon} \mathbb{E}\left[X_s(s)X_s(y)\right] e^{\lambda_m(2u_n+2\epsilon-s-y)}\,ds\,dy$$
$$+ \left(\frac{\mu}{n^\alpha}\right) \int_0^{u_n+\epsilon} \mathbb{E}\left[X_s(s)\right]\mathbb{E}\left[\tilde{X}_m(u_n+\epsilon-s)^2\right]\,ds,$$
$$\mathbb{E}\left[X_s(s)X_m(u_n+\epsilon)\right] = \left(\frac{\mu}{n^\alpha}\right) \int_0^{u_n+\epsilon} \mathbb{E}\left[X_s(y)X_s(s)\right] e^{\lambda_m(u_n+\epsilon-y)}\,dy,$$

where $\tilde{X}_m$ is a binary branching process starting from size one with birth rate r_m and death rate d_m. Substituting these expressions into our equation yields

$$\mathbb{E}\left[\left(n^{\alpha+\lambda_m u_n^+(\epsilon)/\lambda_s-1}X_m(u_n+\epsilon) - \frac{\mu}{n}\int_0^{u_n+\epsilon} X_s(s)e^{-\lambda_m s}\,ds\right)^2\right]$$
$$= \mu^2 n^{2(\lambda_m u_n^+(\epsilon)/\lambda_s-1)} \int_0^{u_n+\epsilon}\int_0^{u_n+\epsilon} \mathbb{E}\left[X_s(s)X_s(y)\right] e^{\lambda_m(2u_n+2\epsilon-s-y)}\,ds\,dy$$
$$+ \mu n^{\alpha+2(\lambda_m u_n^+(\epsilon)/\lambda_s-1)} \int_0^{u_n+\epsilon} \mathbb{E}\left[X_s(s)\right]\mathbb{E}\left[\tilde{X}_m(u_n+\epsilon-s)^2\right]\,ds$$
$$- 2\mu^2 n^{\lambda_m u_n^+(\epsilon)/\lambda_s-2} \int_0^{u_n+\epsilon}\int_0^{u_n+\epsilon} \mathbb{E}\left[X_s(s)X_s(y)\right] e^{\lambda_m(u_n+\epsilon-s-y)}\,ds\,dy$$
$$+ \mu^2 n^{-2} \int_0^{u_n+\epsilon}\int_0^{u_n+\epsilon} \mathbb{E}\left[X_s(s)X_s(y)\right] e^{-\lambda_m(s+y)}\,ds\,dy.$$

Then, by the definition of $u_n^+(\epsilon)$,

$$
\begin{aligned}
&\mathbb{E}\left[\left(n^{\alpha+\lambda_m u_n^+(\epsilon)/\lambda_s-1}X_m(u_n+\epsilon)-\frac{\mu}{n}\int_0^{u_n+\epsilon}X_s(s)e^{-\lambda_m s}\,ds\right)^2\right]\\
&\quad=\mu^2 n^{-2\left(\frac{\lambda_m(u_n+\epsilon)}{\log n}+1\right)}\int_0^{u_n+\epsilon}\int_0^{u_n+\epsilon}\mathbb{E}\left[X_s(s)X_s(y)\right]e^{\lambda_m(2u_n+2\epsilon-s-y)}\,ds\,dy\\
&\qquad+\mu n^{\alpha-2\left(\frac{\lambda_m(u_n+\epsilon)}{\log n}+1\right)}\int_0^{u_n+\epsilon}\mathbb{E}\left[X_s(s)\right]\mathbb{E}\left[\tilde{X}_m(u_n+\epsilon-s)^2\right]\,ds\\
&\quad-2\mu^2 n^{-\frac{\lambda_m(u_n+\epsilon)}{\log n}-2}\int_0^{u_n+\epsilon}\int_0^{u_n+\epsilon}\mathbb{E}\left[X_s(s)X_s(y)\right]e^{\lambda_m(u_n+\epsilon-s-y)}\,ds\,dy\\
&\qquad+\mu^2 n^{-2}\int_0^{u_n+\epsilon}\int_0^{u_n+\epsilon}\mathbb{E}\left[X_s(s)X_s(y)\right]e^{-\lambda_m(s+y)}\,ds\,dy\\
&\quad=\left(\frac{\mu}{n}\right)^2\int_0^{u_n+\epsilon}\int_0^{u_n+\epsilon}\mathbb{E}\left[X_s(s)X_s(y)\right]e^{-\lambda_m(s+y)}\,ds\,dy\\
&\qquad+\mu n^{\alpha-2}e^{-2\lambda_m(u_n+\epsilon)}\int_0^{u_n+\epsilon}\mathbb{E}\left[X_s(s)\right]\mathbb{E}\left[\tilde{X}_m(u_n+\epsilon-s)^2\right]\,ds\\
&\qquad-2\left(\frac{\mu}{n}\right)^2\int_0^{u_n+\epsilon}\int_0^{u_n+\epsilon}\mathbb{E}\left[X_s(s)X_s(y)\right]e^{-\lambda_m(s+y)}\,ds\,dy\\
&\qquad+\left(\frac{\mu}{n}\right)^2\int_0^{u_n+\epsilon}\int_0^{u_n+\epsilon}\mathbb{E}\left[X_s(s)X_s(y)\right]e^{-\lambda_m(s+y)}\,ds\,dy\\
&\quad=\mu n^{\alpha-2}e^{-2\lambda_m(u_n+\epsilon)}\int_0^{u_n+\epsilon}\mathbb{E}\left[X_s(s)\right]\mathbb{E}\left[\tilde{X}_m(u_n+\epsilon-s)^2\right]\,ds.
\end{aligned}
$$

Note that

$$
\begin{aligned}
\mathbb{E}\left[X_s(t)\right]&=ne^{\lambda_s t},\\
\mathbb{E}\left[\tilde{X}_m(t)^2\right]&=\frac{2r_m}{\lambda_m}e^{2\lambda_m t}-\frac{r_m+d_m}{\lambda_m}e^{\lambda_m t}.
\end{aligned}
$$

Substituting these into the above expression yields

$$
\begin{aligned}
&\mathbb{E}\left[\left(n^{\alpha+\lambda_m u_n^+(\epsilon)/\lambda_s-1}X_m(u_n+\epsilon)-\frac{\mu}{n}\int_0^{u_n+\epsilon}X_s(s)e^{-\lambda_m s}\,ds\right)^2\right] \\
&\quad=\mu n^{\alpha-2}e^{-2\lambda_m(u_n+\epsilon)}\int_0^{u_n+\epsilon}ne^{\lambda_s s}\left(\frac{2r_m}{\lambda_m}e^{2\lambda_m(u_n+\epsilon-s)}-\frac{r_m+d_m}{\lambda_m}e^{\lambda_m(u_n+\epsilon-s)}\right)ds \\
&\quad=\frac{2r_m\mu n^{\alpha-1}}{\lambda_m}\int_0^{u_n+\epsilon}e^{(\lambda_s-2\lambda_m)s}\,ds \\
&\qquad-\frac{\mu n^{\alpha-1}(r_m+d_m)}{\lambda_m}e^{-\lambda_m(u_n+\epsilon)}\int_0^{u_n+\epsilon}e^{(\lambda_s-\lambda_m)s}\,ds \\
&\quad=\frac{2r_m\mu n^{\alpha-1}}{\lambda_m(\lambda_s-2\lambda_m)}\left(e^{(\lambda_s-2\lambda_m)(u_n+\epsilon)}-1\right) \\
&\qquad-\frac{\mu n^{\alpha-1}(r_m+d_m)}{\lambda_m(\lambda_s-\lambda_m)}\left(e^{(\lambda_s-2\lambda_m)(u_n+\epsilon)}-e^{-\lambda_m(u_n+\epsilon)}\right).
\end{aligned}
$$

Since $u_n=\tilde{u}_n t_n$ and $t_n=\frac{-1}{\lambda_s}\log n$, the expression above is equivalent to

$$
\begin{aligned}
\frac{\mu n^{\alpha-1}}{\lambda_m}\Bigg[&e^{(\lambda_s-2\lambda_m)(\tilde{u}_n\frac{-1}{\lambda_s}\log n+\epsilon)}\left(\frac{2r_m}{\lambda_s-2\lambda_m}-\frac{r_m+d_m}{\lambda_s-\lambda_m}\right) \\
&-\frac{2r_m}{\lambda_s-2\lambda_m}+\frac{r_m+d_m}{\lambda_s-\lambda_m}e^{-\lambda_m(\tilde{u}_n\frac{-1}{\lambda_s}\log n+\epsilon)}\Bigg].
\end{aligned}
$$

Because $\tilde{u}_n\to\frac{-\lambda_s\alpha}{\lambda_m}$ as $n\to\infty$, $e^{(\lambda_s-2\lambda_m)(\tilde{u}_n\frac{-1}{\lambda_s}\log n+\epsilon)}\to 0$ and $e^{-\lambda_m(\tilde{u}_n\frac{-1}{\lambda_s}\log n+\epsilon)}\to 0$. Therefore, the entire expression above converges to zero since $\alpha<1$, so we are done.

□

3.5.5 Proof of Proposition 3

Proof. Let $\hat{f}_n(z)=\sum_{k=2}^{M}\phi_k(zt_n)-n$. Taking the first derivative of ϕ_2 with respect to z, we get

$$\frac{d}{dz}\phi_2(zt_n)=-n^{1-z}\log n.$$

Taking a second derivative yields

$$\begin{aligned}\frac{d^2}{dz^2}\phi_2(zt_n) &= (\log n)^2 n^{1-z} \\ &> 0.\end{aligned}$$

Hence $\phi_2(zt_n)$ is concave up everywhere. Now for $k > 2$, we have

$$\phi_k(zt_n) = \frac{\nu^{k-2}(-1)^k}{m^{k-2}} n^{1-(k-2)\beta} \tilde{S}_k(z).$$

Taking the first derivative of this equation with respect to z, we get

$$\frac{d}{dz}\phi_k(zt_n) = \frac{\nu^{k-2}(-1)^k}{m^{k-2}} n^{1-(k-2)\beta} \log n \left(-\frac{\lambda_i}{\lambda_2}\right) \tilde{S}_k(z).$$

Taking a second derivative yields

$$\begin{aligned}\frac{d^2}{dz^2}\phi_k(zt_n) &= \frac{\nu^{k-2}(-1)^k}{m^{k-2}} n^{1-(k-2)\beta} (\log n)^2 \left(\frac{\lambda_i}{\lambda_2}\right)^2 \tilde{S}_k(z) \\ &\sim \frac{\nu^{k-2}(-1)^k}{m^{k-2}} n^{1-(k-2)\beta} (\log n)^2 \frac{(\lambda_k/\lambda_2)^2 n^{-\lambda_k z/\lambda_2}}{\tilde{P}_{k,k}} \\ &> 0.\end{aligned}$$

So $\phi_k(zt_n)$ is concave up in the large population limit for all $k \geq 2$. Therefore, $\sum_{k=2}^{M} \phi_k(zt_n)$ is concave up since a sum of concave up functions is always concave up. Hence $\hat{f}_n(z)$ is concave up as well. Since $\hat{f}_n(z)$ is clearly differentiable everywhere, this implies that either $\hat{f}_n(z)$ is monotonically increasing everywhere, or $\hat{f}_n(z)$ is decreasing on the first part of its domain and then increasing on the rest of its domain. Note that $\hat{f}_n(0) = 0$. We also have that

$$\begin{aligned}
\hat{f}_n(b_n) &= n^{1-b_n} + \sum_{k=3}^{M} \frac{\nu^{k-2}(-1)^k}{m^{k-2}} n^{1-(k-2)\beta} \tilde{S}_k(b_n) - n \\
&= n\Bigg[n^{\frac{\lambda_2}{\lambda_M}\beta(M-2)} n^{\frac{1}{\lambda_M t_n}\log\left[\frac{\nu^{M-2}(-1)^M}{m^{M-2}\tilde{P}_{M,M}}\left(\frac{\lambda_2-\lambda_M}{\lambda_2}\right)\right]} \\
&\quad + \sum_{k=3}^{M} \frac{\nu^{k-2}(-1)^k}{m^{k-2}} \sum_{i=2}^{k} \frac{n^{-\beta(k-2)} n^{\frac{\lambda_i}{\lambda_M}\beta(M-2)} n^{\frac{\lambda_i}{\lambda_M\lambda_2 t_n}\log\left[\frac{\nu^{M-2}(-1)^M}{m^{M-2}\tilde{P}_{M,M}}\left(\frac{\lambda_2-\lambda_M}{\lambda_2}\right)\right]}}{\tilde{P}_{i,k}} - 1 \Bigg] \\
&\sim n\left[\sum_{k=3}^{M} \frac{\nu^{k-2}(-1)^k}{m^{k-2}} \cdot \frac{n^{\beta[\lambda_k(M-2)/\lambda_M-(k-2)]}\left[\frac{\nu^{M-2}(-1)^M}{m^{M-2}\tilde{P}_{M,M}}\left(\frac{\lambda_2-\lambda_M}{\lambda_2}\right)\right]^{-\lambda_k/\lambda_M}}{\tilde{P}_{k,k}} - 1 \right] \\
&= n\Bigg[\sum_{k=3}^{M-1} \frac{\nu^{k-2}(-1)^k}{m^{k-2}} \cdot \frac{n^{\beta[\lambda_k(M-2)/\lambda_M-(k-2)]}\left[\frac{\nu^{M-2}(-1)^M}{m^{M-2}\tilde{P}_{M,M}}\left(\frac{\lambda_2-\lambda_M}{\lambda_2}\right)\right]^{-\lambda_k/\lambda_M}}{\tilde{P}_{k,k}} \\
&\qquad\qquad + \frac{\lambda_2}{\lambda_2-\lambda_M} - 1 \Bigg].
\end{aligned}$$

Note that

$$\begin{aligned}
&\left[\frac{\lambda_k(M-2)}{\lambda_M} - (k-2)\right] \\
&\quad = \frac{\left[\lambda_2 + (k-2)\frac{\lambda_M-\lambda_2}{M-2}\right](M-2) - \left[\lambda_2 + (M-2)\frac{\lambda_M-\lambda_2}{M-2}\right](k-2)}{\lambda_M} \\
&\quad = \frac{\lambda_2(M-2) + (k-2)(\lambda_M-\lambda_2) - \lambda_2(k-2) - (k-2)(\lambda_M-\lambda_2)}{\lambda_M} \\
&\quad = \frac{\lambda_2}{\lambda_M}(M-k),
\end{aligned}$$

so we can substitute this to get

$$\begin{aligned}\hat{f}_n(b_n) &\sim n\left[\sum_{k=3}^{M-1}\frac{\nu^{k-2}(-1)^k\left[\frac{\nu^{M-2}(-1)^M}{m^{M-2}\tilde{P}_{M,M}}\left(\frac{\lambda_2-\lambda_M}{\lambda_2}\right)\right]^{\frac{-\lambda_k}{\lambda_M}}}{m^{k-2}\tilde{P}_{k,k}}n^{\beta\lambda_2(M-k)/\lambda_M}+\frac{\lambda_2}{\lambda_2-\lambda_M}-1\right]\\ &\sim n\left(\frac{\lambda_2}{\lambda_2-\lambda_M}-1\right)\\ &<0.\end{aligned}$$

So $\hat{f}_n(b_n)<0$ in the large population limit. Similarly,

$$\begin{aligned}\hat{f}_n(B_n) &= n^{1-B_n}+\sum_{k=3}^{M}\frac{\nu^{k-2}(-1)^k}{m^{k-2}}n^{1-(k-2)\beta}\tilde{S}_k(B_n)-n\\ &= n\Bigg[n^{\frac{\lambda_2}{\lambda_M}\beta(M-2)}n^{\frac{1}{\lambda_M t_n}\log\left[\frac{\nu^{M-2}(-1)^M}{m^{M-2}\tilde{P}_{M,M}}\right]}\\ &\quad+\sum_{k=3}^{M}\frac{\nu^{k-2}(-1)^k}{m^{k-2}}\sum_{i=2}^{k}\frac{n^{-\beta(k-2)}n^{\frac{\lambda_i}{\lambda_M}\beta(M-2)}n^{\frac{\lambda_i}{\lambda_M\lambda_2 t_n}\log\left[\frac{\nu^{M-2}(-1)^M}{m^{M-2}\tilde{P}_{M,M}}\right]}}{\tilde{P}_{i,k}}-1\Bigg]\\ &\sim n\left[\sum_{k=3}^{M}\frac{\nu^{k-2}(-1)^k}{m^{k-2}}\cdot\frac{n^{\beta[\lambda_k(M-2)/\lambda_M-(k-2)]}\left[\frac{\nu^{M-2}(-1)^M}{m^{M-2}\tilde{P}_{M,M}}\right]^{-\lambda_k/\lambda_M}}{\tilde{P}_{k,k}}-1\right]\\ &= n\left[\sum_{k=3}^{M-1}\frac{\nu^{k-2}(-1)^k\left[\frac{\nu^{M-2}(-1)^M}{m^{M-2}\tilde{P}_{M,M}}\right]^{-\lambda_k/\lambda_M}}{m^{k-2}\tilde{P}_{k,k}}n^{\beta\lambda_2(M-k)/\lambda_M}\right]\\ &>0.\end{aligned}$$

So $\hat{f}_n(B_n)>0$ in the large population limit. Therefore, we know that $\hat{f}_n(z)$ must be monotonically decreasing on the first part of its domain and monotonically increasing on the rest of its domain. This implies that there exists one and only one positive solution $\tilde{v}_n$ to the equation $\hat{f}_n(z)=0$. And since $\hat{f}_n(b_n)<0$ and $\hat{f}_n(B_n)>0$ in the large population limit, we must have $b_n<\tilde{v}_n<B_n$. Lastly, because $\lim_{n\to\infty}b_n=\lim_{n\to\infty}B_n=-\frac{\lambda_2}{\lambda_M}\beta(M-2)$, the solution $\tilde{v}_n\to-\frac{\lambda_2}{\lambda_M}\beta(M-2)$ as $n\to\infty$ as well.

□

3.5.6 Proof of Theorem 2

Proof. In order to show the desired result, we must show

$$\lim_{n\to\infty} \mathbb{P}(\omega_n > v_n + \epsilon) + \lim_{n\to\infty} \mathbb{P}(\omega_n < v_n - \epsilon) = 0.$$

Let's start by proving that $\mathbb{P}(\omega_n < v_n - \epsilon) \to 0$ as $n \to \infty$. Note that

$$\begin{aligned}
\mathbb{P}(\omega_n < v_n - \epsilon) &= \mathbb{P}\left(\frac{\omega_n}{t_n} < v_n^-(\epsilon)\right) \\
&\leq \mathbb{P}\left(\sup_{z\in[d,v_n^-(\epsilon)]} \left(\sum_{k=2}^{M} X_k(zt_n) - n\right) > 0\right) \\
&= \mathbb{P}\Bigg(\sup_{z\in[d,v_n^-(\epsilon)]} n^{\beta(M-2)+\lambda_M z/\lambda_2 - 1}\Bigg(\sum_{k=2}^{M} X_k(zt_n) \\
&\qquad + \sum_{k=2}^{M} \phi_k(zt_n) - \sum_{k=2}^{M} \phi_k(zt_n) - n\Bigg) > 0\Bigg) \\
&\leq \mathbb{P}\left(\sum_{k=2}^{M} \hat{B}_k(n,\epsilon) + \hat{B}_\phi(n,\epsilon) > 0\right),
\end{aligned}$$

where

$$\begin{aligned}
\hat{B}_k(n,\epsilon) &= \sup_{z\in[d,v_n^-(\epsilon)]} n^{\beta(M-2)+\lambda_M z/\lambda_2 - 1} \left(X_k(zt_n) - \phi_k(zt_n)\right), \\
\hat{B}_\phi(n,\epsilon) &= \sup_{z\in[d,v_n^-(\epsilon)]} n^{\beta(M-2)+\lambda_M z/\lambda_2 - 1} \left(\sum_{k=2}^{M} \phi_k(zt_n) - n\right).
\end{aligned}$$

Note that

$$\begin{aligned}
&\sup_{z\in[d,v_n^-(\epsilon)]} \left| n^{\beta(M-2)+\lambda_M z/\lambda_2 - 1} \left(X_k(zt_n) - \phi_k(zt_n)\right)\right| \\
&\qquad \leq \sup_{z\in[d,v_n^+(\epsilon)]} n^{\beta(M-2)+\lambda_M z/\lambda_2 - 1} \left|X_k(zt_n) - \phi_k(zt_n)\right|,
\end{aligned}$$

which converges to zero in probability by Proposition 4. Now we just need to show that $\hat{B}_\phi(n,\epsilon)$ is negative in the large population limit. Define a function given by $\hat{g}_n(z) = n^{\beta(M-2)+\lambda_M z/\lambda_2 - 1}\left(\sum_{k=2}^M \phi_k(zt_n) - n\right)$. Using the definitions of ϕ_2 and ϕ_k for $k > 2$, we see that

$$\begin{aligned}
\hat{g}_n(z) &= n^{\beta(M-2)+\lambda_M z/\lambda_2 - 1}\left(n^{1-z} + \sum_{k=3}^M \frac{\nu^{k-2}(-1)^k}{m^{k-2}} n^{1-(k-2)\beta}\tilde{S}_k(z) - n\right) \\
&= n^{\beta(M-2)+z\left(\frac{\lambda_M}{\lambda_2}-1\right)} + \sum_{k=3}^M \frac{\nu^{k-2}(-1)^k}{m^{k-2}} \sum_{i=2}^k \frac{n^{\beta(M-k)+\frac{\lambda_M-\lambda_i}{\lambda_2}z}}{\tilde{P}_{i,k}} - n^{\beta(M-2)+\frac{\lambda_M}{\lambda_2}z} \\
&= n^{(M-2)\left(\beta+\frac{mz}{\lambda_2}\right)} + \sum_{k=3}^M \frac{\nu^{k-2}(-1)^k}{m^{k-2}} \sum_{i=2}^k \frac{n^{\beta(M-k)+\frac{(M-i)mz}{\lambda_2}}}{\tilde{P}_{i,k}} - n^{(M-2)\left(\beta+\frac{mz}{\lambda_2}\right)+z}.
\end{aligned}$$

Taking the derivative with respect to z yields

$$\begin{aligned}
\hat{g}_n'(z) &= n^{(M-2)(\beta+mz/\lambda_2)}\log n \cdot \frac{(M-2)m}{\lambda_2} \\
&\quad + \sum_{k=3}^M \frac{\nu^{k-2}(-1)^k}{m^{k-2}} \sum_{i=2}^k \frac{n^{\beta(M-k)+(M-i)mz/\lambda_2}\log n \cdot \frac{(M-i)m}{\lambda_2}}{\tilde{P}_{i,k}} \\
&\quad - n^{(M-2)(\beta+mz/\lambda_2)+z}\log n \cdot \left(\frac{(M-2)m}{\lambda_2} + 1\right) \\
&= \frac{\log n}{\lambda_2}\Bigg[(M-2)m \cdot n^{(M-2)(\beta+mz/\lambda_2)} \\
&\quad + \sum_{k=3}^M \frac{\nu^{k-2}(-1)^k}{m^{k-2}} \sum_{i=2}^k \frac{(M-i)m}{\tilde{P}_{i,k}} n^{\beta(M-k)+(M-i)mz/\lambda_2} - \lambda_M n^{(M-2)(\beta+mz/\lambda_2)+z}\Bigg] \\
&\sim \frac{\log n}{\lambda_2}\left[\sum_{k=3}^M \frac{\nu^{k-2}(-1)^k(M-k)}{m^{k-3}\tilde{P}_{k,k}} n^{(M-k)(\beta+mz/\lambda_2)} - \lambda_M n^{(M-2)(\beta+mz/\lambda_2)+z}\right].
\end{aligned}$$

When $z \geq d$, we have that $z > -\lambda_2\beta\frac{M-2}{\lambda_M-\lambda_2} = -\lambda_2\beta/m$ by (3.1). Therefore, $mz/\lambda_2 < -\beta$, and hence $\beta + mz/\lambda_2 < 0$. This implies that, when $z \geq d$,

$$\begin{aligned}\hat{g}_n'(z) &\sim \frac{\log n}{\lambda_2}\left[\frac{\nu^{M-2}(-1)^M(M-M)}{m^{M-3}\tilde{P}_{M,M}}n^{(M-M)(\beta+mz/\lambda_2)} - \lambda_M n^{(M-2)(\beta+mz/\lambda_2)+z}\right] \\ &= \frac{\lambda_M \log n}{-\lambda_2} n^{(M-2)(\beta+mz/\lambda_2)+z} \\ &> 0 \text{ for sufficiently large } n.\end{aligned}$$

Hence $\hat{g}_n(z)$ is monotonically increasing in the large population limit for all $z \geq d$. Specifically, $\hat{g}_n(z)$ is monotonically increasing on the interval $[d, v_n^-(\epsilon)]$. Therefore, we may rewrite $\hat{B}_\phi(n,\epsilon)$ as

$$\hat{B}_\phi(n,\epsilon) = n^{\beta(M-2)+\lambda_M v_n^-(\epsilon)/\lambda_2 - 1}\left(\sum_{k=2}^{M}\phi_k(v_n^-(\epsilon)t_n) - n\right).$$

Then by the definitions of ϕ_2 and ϕ_k for $k > 2$, we have

$$\begin{aligned}\hat{B}_\phi(n,\epsilon) &= n^{\beta(M-2)+\lambda_M v_n^-(\epsilon)/\lambda_2 - 1}\left(n^{1-v_n^-(\epsilon)} + \sum_{k=3}^{M}\frac{\nu^{k-2}(-1)^k}{m^{k-2}}n^{1-(k-2)\beta}\tilde{S}_k(v_n^-(\epsilon)) - n\right) \\ &= n^{(M-2)(\beta+mv_n^-(\epsilon)/\lambda_2)+v_n^-(\epsilon)-1}\Bigg(n^{1-v_n^-(\epsilon)} \\ &\quad + \sum_{k=3}^{M}\frac{\nu^{k-2}(-1)^k}{m^{k-2}}n^{1-(k-2)\beta}\sum_{i=2}^{k}\frac{n^{-v_n^-(\epsilon)-(i-2)mv_n^-(\epsilon)/\lambda_2}}{\tilde{P}_{i,k}} - n\Bigg) \\ &\sim n^{(M-2)(\beta+mv_n^-(\epsilon)/\lambda_2)}\left(\sum_{k=3}^{M}\frac{\nu^{k-2}(-1)^k}{m^{k-2}}\cdot\frac{n^{-(k-2)(\beta+mv_n^-(\epsilon)/\lambda_2)}}{\tilde{P}_{k,k}} - n^{v_n^-(\epsilon)}\right).\end{aligned}$$

Since $v_n^-(\epsilon) > d$, we have that $v_n^-(\epsilon) > -\lambda_2\beta\frac{M-2}{\lambda_M-\lambda_2} = -\lambda_2\beta/m$ by (3.1). Therefore, $mv_n^-(\epsilon)/\lambda_2 < -\alpha$, and hence $\alpha + mv_n^-(\epsilon)/\lambda_2 < 0$. This implies that

$$\begin{aligned}\hat{B}_\phi(n,\epsilon) &\sim n^{(M-2)(\beta+mv_n^-(\epsilon)/\lambda_2)}\left(\frac{\nu^{M-2}(-1)^M}{m^{M-2}\tilde{P}_{M,M}}n^{-(M-2)(\beta+mv_n^-(\epsilon)/\lambda_2)} - n^{v_n^-(\epsilon)}\right) \\ &= \frac{\nu^{M-2}(-1)^M}{m^{M-2}\tilde{P}_{M,M}} - n^{\beta(M-2)+\lambda_M v_n^-(\epsilon)/\lambda_2}.\end{aligned}$$

Note that

$$\begin{aligned}
n^{\beta(M-2)+\lambda_M v_n^-(\epsilon)/\lambda_2} &= n^{\beta(M-2)} n^{\frac{\epsilon\lambda_M}{\log n}} n^{\lambda_M \tilde{v}_n/\lambda_2} \\
&= e^{\epsilon\lambda_M} n^{\beta(M-2)+\lambda_M \tilde{v}_n/\lambda_2} \\
&\geq e^{\epsilon\lambda_M} n^{\beta(M-2)+\lambda_M B_n/\lambda_2} \\
&= e^{\epsilon\lambda_M} n^{\beta(M-2)+\frac{\lambda_M}{\lambda_2}\cdot\frac{1}{\lambda_M}\left[-\lambda_2\beta(M-2)-\frac{1}{t_n}\log\left[\frac{\nu^{M-2}(-1)^M}{m^{M-2}\tilde{P}_{M,M}}\right]\right]} \\
&= e^{\epsilon\lambda_M} n^{\beta(M-2)-\beta(M-2)+\frac{1}{\log n}\log\left[\frac{\nu^{M-2}(-1)^M}{m^{M-2}\tilde{P}_{M,M}}\right]} \\
&= e^{\epsilon\lambda_M} \frac{\nu^{M-2}(-1)^M}{m^{M-2}\tilde{P}_{M,M}}.
\end{aligned}$$

Therefore, we have that

$$\begin{aligned}
\hat{B}_\phi(n,\epsilon) &\sim \frac{\nu^{M-2}(-1)^M}{m^{M-2}\tilde{P}_{M,M}} - n^{\beta(M-2)+\lambda_M v_n^-(\epsilon)/\lambda_2} \\
&\leq \frac{\nu^{M-2}(-1)^M}{m^{M-2}\tilde{P}_{M,M}} - e^{\epsilon\lambda_M}\frac{\nu^{M-2}(-1)^M}{m^{M-2}\tilde{P}_{M,M}} \\
&= \frac{\nu^{M-2}(-1)^M}{m^{M-2}\tilde{P}_{M,M}}\left(1-e^{\epsilon\lambda_M}\right).
\end{aligned}$$

So $\hat{B}_\phi(n,\epsilon)$ is definitely negative in the large population limit. Putting this all together, we have that $\mathbb{P}\left(\sum_{k=2}^M \hat{B}_k(n,\epsilon)+\hat{B}_\phi(n,\epsilon)>0\right)\to 0$ as $n\to\infty$. Therefore, we have shown $\mathbb{P}(\omega_n < v_n-\epsilon)\to 0$ as $n\to\infty$. The proof that $\mathbb{P}(\omega_n > v_n+\epsilon)\to 0$ as $n\to\infty$ follows using a similar argument.

□

3.5.7 Proof of Proposition 4

Proof. Let's start by proving the $k=2$ case. That is, we want to show that

$$\lim_{n\to\infty}\mathbb{P}\left(\sup_{z\in[d,v_n^+(\epsilon)]} n^{\beta(M-2)+\lambda_M z/\lambda_2-1}\left|X_2(zt_n)-\phi_2(zt_n)\right|>\delta\right)=0.$$

Because a branching process normalized by its mean is a martingale, we know that $Z_2(z) = n^{\beta(M-2)+z-1}\left(X_2(zt_n) - \phi_2(zt_n)\right)$ is a martingale in z. To prove our desired result for $k = 2$, we need to show

$$\lim_{n\to\infty} \mathbb{P}\left(\sup_{z\in[d,v_n^+(\epsilon)]} n^{(\lambda_M-\lambda_2)z/\lambda_2}|Z_2(z)| > \delta \right) = 0,$$

or, equivalently,

$$\lim_{n\to\infty} \mathbb{P}\left(\sup_{z\in[d,v_n^+(\epsilon)]} n^{(M-2)mz/\lambda_2}|Z_2(z)| > \delta \right) = 0.$$

Note that

$$\begin{aligned}\sup_{z\in[d,v_n^+(\epsilon)]} n^{(M-2)mz/\lambda_2}|Z_2(z)| &\leq \sup_{z\in[d,v_n^+(\epsilon)]} n^{(M-2)mz/\lambda_2} \cdot \sup_{z\in[d,v_n^+(\epsilon)]} |Z_2(z)| \\ &= n^{(M-2)md/\lambda_2} \cdot \sup_{z\in[d,v_n^+(\epsilon)]} |Z_2(z)|.\end{aligned}$$

Therefore, we have that

$$\begin{aligned}&\mathbb{P}\left(\sup_{z\in[d,v_n^+(\epsilon)]} n^{(M-2)mz/\lambda_2}|Z_2(z)| > \delta \right) \\ &\quad\leq \mathbb{P}\left(n^{(M-2)md/\lambda_2} \cdot \sup_{z\in[d,v_n^+(\epsilon)]} |Z_2(z)| > \delta \right) \\ &\quad= \mathbb{P}\left(\sup_{z\in[d,v_n^+(\epsilon)]} |Z_2(z)| > \delta \cdot n^{(2-M)md/\lambda_2} \right) \\ &\quad\leq \frac{1}{\delta} n^{(M-2)md/\lambda_2} \cdot \mathbb{E}\left[\left| Z_2(v_n^+(\epsilon)) \right| \right] \text{ by Doob's Martingale Inequality} \\ &\quad= \frac{1}{\delta} n^{(M-2)md/\lambda_2} \cdot \mathbb{E}\left[\left| n^{\beta(M-2)+v_n^+(\epsilon)-1}(X_2(v_n^+(\epsilon)t_n) - \phi_2(v_n^+(\epsilon)t_n)) \right| \right] \\ &\quad= \frac{1}{\delta} n^{\beta(M-2)+(M-2)md/\lambda_2+v_n^+(\epsilon)-1} \cdot \mathbb{E}\left[\left| X_2(v_n^+(\epsilon)t_n) - \phi_2(v_n^+(\epsilon)t_n) \right| \right].\end{aligned}$$

Clearly,

$$\begin{aligned}\left|X_2(v_n^+(\epsilon)t_n) - \phi_2(v_n^+(\epsilon)t_n)\right| &\leq \left|X_2(v_n^+(\epsilon)t_n)\right| + \left|\phi_2(v_n^+(\epsilon)t_n)\right| \\ &= X_2(v_n^+(\epsilon)t_n) + \phi_2(v_n^+(\epsilon)t_n).\end{aligned}$$

This implies that

$$\begin{aligned}\mathbb{E}\left[\left|X_2(v_n^+(\epsilon)t_n) - \phi_2(v_n^+(\epsilon)t_n)\right|\right] &\leq \mathbb{E}\left[X_2(v_n^+(\epsilon)t_n) + \phi_2(v_n^+(\epsilon)t_n)\right] \\ &= 2\phi_2(v_n^+(\epsilon)t_n).\end{aligned}$$

And hence

$$\begin{aligned}\mathbb{P}\left(\sup_{z\in[d,v_n^+(\epsilon)]} n^{(M-2)mz/\lambda_2}|Z_2(z)| > \delta\right) &\leq \frac{2}{\delta} n^{\beta(M-2)+(M-2)md/\lambda_2+v_n^+(\epsilon)-1} n^{1-v_n^+(\epsilon)} \\ &= \frac{2}{\delta} n^{(M-2)(\beta+md/\lambda_2)}.\end{aligned}$$

So it suffices to show that $\beta + md/\lambda_2 < 0$. From (3.1), we have that

$$d > -\lambda_2\beta\frac{M-2}{\lambda_M - \lambda_2} = \frac{-\lambda_2\beta}{m},$$

which implies that $md/\lambda_2 < -\beta$, so we are done with the $k = 2$ case.

Next, let's prove the desired result for $k > 2$. Note that

$$\begin{aligned}\phi_k(zt_n) &= \int_0^{zt_n} \nu n^{-\beta}\phi_{k-1}(s)e^{\lambda_k(zt_n-s)}\,ds \\ &= \nu n^{-\beta-\lambda_k z/\lambda_2}\int_0^{zt_n}\phi_{k-1}(s)e^{-\lambda_k s}\,ds.\end{aligned}$$

Therefore,

$$
\begin{aligned}
&n^{\beta(M-2)+\lambda_M z/\lambda_2-1}\left(X_k(zt_n)-\phi_k(zt_n)\right)\\
&\quad= n^{\beta(M-2)+\lambda_M z/\lambda_2-1}X_k(zt_n)-\nu n^{\beta(M-3)+(\lambda_M-\lambda_k)z/\lambda_2-1}\int_0^{zt_n}\phi_{k-1}(s)e^{-\lambda_k s}\,ds\\
&\quad= n^{\beta(M-2)+\lambda_M z/\lambda_2-1}X_k(zt_n)-\nu n^{\beta(M-3)+(M-k)mz/\lambda_2-1}\int_0^{zt_n}\phi_{k-1}(s)e^{-\lambda_k s}\,ds\\
&\quad= n^{\beta(M-2)+\lambda_M z/\lambda_2-1}X_k(zt_n)-\nu n^{\beta(M-3)+(M-k)mz/\lambda_2-1}\int_0^{zt_n}X_{k-1}(s)e^{-\lambda_k s}\,ds\\
&\qquad\qquad+\nu n^{\beta(M-3)+(M-k)mz/\lambda_2-1}\int_0^{zt_n}\left(X_{k-1}(s)-\phi_{k-1}(s)\right)e^{-\lambda_k s}\,ds.
\end{aligned}
$$

Taking the absolute value of both sides and using the triangle inequality, we get

$$
\begin{aligned}
&n^{\beta(M-2)+\lambda_M z/\lambda_2-1}\left|X_k(zt_n)-\phi_k(zt_n)\right|\\
&\quad\le\left|n^{\beta(M-2)+\lambda_M z/\lambda_2-1}X_k(zt_n)-\nu n^{\beta(M-3)+(M-k)mz/\lambda_2-1}\int_0^{zt_n}X_{k-1}(s)e^{-\lambda_k s}\,ds\right|\\
&\qquad\qquad+\nu n^{\beta(M-3)+(M-k)mz/\lambda_2-1}\int_0^{zt_n}\left|X_{k-1}(s)-\phi_{k-1}(s)\right|e^{-\lambda_k s}\,ds.
\end{aligned}
$$

This implies that

$$
\begin{aligned}
&\sup_{z\in[d,v_n^+(\epsilon)]}n^{\beta(M-2)+\lambda_M z/\lambda_2-1}\left|X_k(zt_n)-\phi_k(zt_n)\right|\\
&\quad\le\sup_{z\in[d,v_n^+(\epsilon)]}\left|n^{\beta(M-2)+\lambda_M z/\lambda_2-1}X_k(zt_n)\right.\\
&\qquad\qquad\left.-\nu n^{\beta(M-3)+(M-k)mz/\lambda_2-1}\int_0^{zt_n}X_{k-1}(s)e^{-\lambda_k s}\,ds\right|\\
&\qquad+\sup_{z\in[d,v_n^+(\epsilon)]}\nu n^{\beta(M-3)+(M-k)mz/\lambda_2-1}\int_0^{zt_n}\left|X_{k-1}(s)-\phi_{k-1}(s)\right|e^{-\lambda_k s}\,ds.
\end{aligned}
$$

Hence

$$\begin{aligned}
&\mathbb{P}\left(\sup_{z\in[d,v_n^+(\epsilon)]} n^{\beta(M-2)+\lambda_M z/\lambda_2-1}\left|X_k(zt_n)-\phi_k(zt_n)\right|>\delta\right)\\
&\quad\le \mathbb{P}\Bigg(\sup_{z\in[d,v_n^+(\epsilon)]}\Bigg|n^{\beta(M-2)+\lambda_M z/\lambda_2-1}X_k(zt_n)\\
&\qquad\qquad -\nu n^{\beta(M-3)+(M-k)mz/\lambda_2-1}\int_0^{zt_n} X_{k-1}(s)e^{-\lambda_k s}\,ds\Bigg|>\delta/2\Bigg)\\
&\qquad+\mathbb{P}\left(\sup_{z\in[d,v_n^+(\epsilon)]}\nu n^{\beta(M-3)+\frac{(M-k)mz}{\lambda_2}-1}\int_0^{zt_n}\left|X_{k-1}(s)-\phi_{k-1}(s)\right|e^{-\lambda_k s}\,ds>\delta/2\right).
\end{aligned}\tag{3.4}$$

As a reminder, our goal is to show that (3.4) converges to 0 as $n\to\infty$.

Let's start with the second term. Note that

$$\begin{aligned}
&\sup_{z\in[d,v_n^+(\epsilon)]}\nu n^{\beta(M-3)+(M-k)mz/\lambda_2-1}\int_0^{zt_n}\left|X_{k-1}(s)-\phi_{k-1}(s)\right|e^{-\lambda_k s}\,ds\\
&\quad\le \sup_{z\in[d,v_n^+(\epsilon)]}\nu n^{\beta(M-3)+(M-k)mz/\lambda_2-1}\sup_{z\in[d,v_n^+(\epsilon)]}\int_0^{zt_n}\left|X_{k-1}(s)-\phi_{k-1}(s)\right|e^{-\lambda_k s}\,ds\\
&\quad=\nu n^{\beta(M-3)+(M-k)md/\lambda_2-1}\int_0^{v_n^+(\epsilon)t_n}\left|X_{k-1}(s)-\phi_{k-1}(s)\right|e^{-\lambda_k s}\,ds.
\end{aligned}$$

So, in order to show the second term in (3.4) converges to 0, we must show

$$\lim_{n\to\infty}\mathbb{P}\left(\nu n^{\beta(M-3)+(M-k)md/\lambda_2-1}\int_0^{v_n^+(\epsilon)t_n}\left|X_{k-1}(s)-\phi_{k-1}(s)\right|e^{-\lambda_k s}\,ds>\delta/2\right)=0.$$

Since convergence in mean implies convergence in probability (by Markov's Inequality), it suffices to show that

$$\lim_{n\to\infty}\mathbb{E}\left(\nu n^{\beta(M-3)+(M-k)md/\lambda_2-1}\int_0^{v_n^+(\epsilon)t_n}\left|X_{k-1}(s)-\phi_{k-1}(s)\right|e^{-\lambda_k s}\,ds\right)=0$$

or, equivalently,

$$\lim_{n\to\infty} \nu n^{\beta(M-3)+(M-k)md/\lambda_2-1} \int_0^{v_n+\epsilon} \mathbb{E}\left[|X_{k-1}(s) - \phi_{k-1}(s)|\right] e^{-\lambda_k s}\, ds = 0.$$

Note that

$$\begin{aligned} |X_{k-1}(s) - \phi_{k-1}(s)| &\leq |X_{k-1}(s)| + |\phi_{k-1}(s)| \text{ by the triangle inequality} \\ &= X_{k-1}(s) + \phi_{k-1}(s). \end{aligned}$$

Taking the mean of both sides yields

$$\begin{aligned} \mathbb{E}\left[|X_{k-1}(s) - \phi_{k-1}(s)|\right] &\leq \mathbb{E}\left[X_{k-1}(s) + \phi_{k-1}(s)\right] \\ &= 2\phi_{k-1}(s). \end{aligned}$$

Multiplying both sides by $\nu n^{\beta(M-3)+(M-k)md/\lambda_2-1} e^{-\lambda_k s}$ and integrating gives us the following inequality:

$$\begin{aligned} &\nu n^{\beta(M-3)+(M-k)md/\lambda_2-1} \int_0^{v_n+\epsilon} \mathbb{E}\left[|X_{k-1}(s) - \phi_{k-1}(s)|\right] e^{-\lambda_k s}\, ds \\ &\qquad \leq \nu n^{\beta(M-3)+(M-k)md/\lambda_2-1} \int_0^{v_n+\epsilon} 2\phi_{k-1}(s) e^{-\lambda_k s}\, ds. \end{aligned}$$

So it suffices to show that

$$\lim_{n\to\infty} \nu n^{\beta(M-3)+(M-k)md/\lambda_2-1} \int_0^{v_n+\epsilon} 2\phi_{k-1}(s) e^{-\lambda_k s}\, ds = 0$$

or, equivalently,

$$\lim_{n\to\infty} n^{\beta(M-3)+(M-k)md/\lambda_2-1} \int_0^{v_n+\epsilon} \mathbb{E}\left[X_{k-1}(s)\right] e^{-\lambda_k s}\, ds = 0.$$

Using the definition of $\mathbb{E}\left[X_{k-1}(s)\right]$, we see that

$$
\begin{aligned}
&n^{\beta(M-3)+(M-k)md/\lambda_2-1}\int_0^{v_n+\epsilon}\mathbb{E}\left[X_{k-1}(s)\right]e^{-\lambda_k s}\,ds\\
&\quad=n^{\beta(M-3)+(M-k)md/\lambda_2-1}\int_0^{v_n+\epsilon}\left[\nu^{k-3}n^{1-(k-3)\beta}(-1)^{k-1}S_{k-1}(s)\right]e^{-\lambda_k s}\,ds\\
&\quad=\nu^{k-3}n^{\beta(M-k)+(M-k)md/\lambda_2}(-1)^{k-1}\int_0^{v_n+\epsilon}\sum_{i=2}^{k-1}\frac{e^{(\lambda_i-\lambda_k)s}}{P_{i,k-1}}\,ds\\
&\quad=\left(\frac{\nu}{m}\right)^{k-3}n^{(M-k)(\beta+md/\lambda_2)}(-1)^{k-1}\sum_{i=2}^{k-1}\int_0^{v_n+\epsilon}\frac{e^{(i-k)ms}}{\tilde{P}_{i,k-1}}\,ds\\
&\quad=\frac{\nu^{k-3}}{m^{k-2}}n^{(M-k)(\beta+md/\lambda_2)}(-1)^{k}\sum_{i=2}^{k-1}\frac{1}{\tilde{P}_{i,k}}\left(e^{(i-k)m(v_n+\epsilon)}-1\right).
\end{aligned}
$$

Since $v_n=\tilde{v}_n t_n=-\frac{\tilde{v}_n}{\lambda_2}\log n$,

$$
\begin{aligned}
e^{(i-k)m(v_n+\epsilon)}&=e^{(k-i)m\frac{\tilde{v}_n}{\lambda_2}\log n}e^{(i-k)m\epsilon}\\
&=n^{(k-i)m\tilde{v}_n/\lambda_2}e^{(i-k)m\epsilon}.
\end{aligned}
$$

So we want to show that

$$
\lim_{n\to\infty}\frac{\nu^{k-3}}{m^{k-2}}n^{(M-k)(\beta+md/\lambda_2)}(-1)^{k}\sum_{i=2}^{k-1}\frac{1}{\tilde{P}_{i,k}}\left(n^{(k-i)m\tilde{v}_n/\lambda_2}e^{(i-k)m\epsilon}-1\right)=0
$$

or, equivalently,

$$
\lim_{n\to\infty}n^{(M-k)(\beta+md/\lambda_2)}\sum_{i=2}^{k-1}\frac{1}{\tilde{P}_{i,k}}\left(n^{(k-i)m\tilde{v}_n/\lambda_2}e^{(i-k)m\epsilon}-1\right)=0.
$$

Since $\tilde{v}_n\to-\frac{\lambda_2}{\lambda_M}\beta(M-2)$ as $n\to\infty$, we have that $n^{(k-i)m\tilde{v}_n/\lambda_2}\to 0$ and hence $n^{(k-i)m\tilde{v}_n/\lambda_2}e^{(i-k)m\epsilon}-1\to -1$. Therefore, this problem simplifies to showing that $n^{(M-k)(\beta+md/\lambda_2)}\to 0$ as $n\to\infty$. But we have already seen that $\beta+md/\lambda_2<0$ in the $k=2$ case, so we have the desired result.

Now that we have proved the second term in (3.4) converges to 0 as $n\to\infty$, all we

have left is to show that the first term converges to 0 as well. By Lemma 1 in [69], we know that

$$e^{-\lambda_k t} X_k(t) - \int_0^t \nu n^{-\beta} e^{-\lambda_k s} X_{k-1}(s)\, ds$$

is a martingale. Setting $t = zt_n = -\frac{z}{\lambda_2} \log n$, we get that

$$n^{\lambda_k z/\lambda_2} X_k(zt_n) - \nu n^{-\beta} \int_0^{zt_n} e^{-\lambda_k s} X_{k-1}(s)\, ds$$

is a martingale in z. Since linear combinations of martingales are also martingales,

$$n^{\frac{\lambda_k}{\lambda_2} z + \beta(M-2) + \frac{\lambda_M - \lambda_k}{\lambda_2} z - 1} X_k(zt_n) - \nu n^{-\beta + \beta(M-2) + \frac{\lambda_M - \lambda_k}{\lambda_2} z - 1} \int_0^{zt_n} X_{k-1}(s) e^{-\lambda_k s}\, ds$$

is also a martingale in z. The expression above simplifies to

$$n^{\beta(M-2) + \lambda_M z/\lambda_2 - 1} X_k(zt_n) - \nu n^{\beta(M-3) + (M-k)mz/\lambda_2 - 1} \int_0^{zt_n} X_{k-1}(s) e^{-\lambda_k s}\, ds.$$

Therefore,

$$\left| n^{\beta(M-2) + \lambda_M z/\lambda_2 - 1} X_k(zt_n) - \nu n^{\beta(M-3) + (M-k)mz/\lambda_2 - 1} \int_0^{zt_n} X_{k-1}(s) e^{-\lambda_k s}\, ds \right|$$

is a non-negative submartingale in z, so we can apply Doob's Martingale Inequality to get

$$\mathbb{P}\Bigg(\sup_{z\in[d,v_n^+(\epsilon)]}\Bigg|n^{\beta(M-2)+\lambda_M z/\lambda_2-1}X_k(zt_n) - \nu n^{\beta(M-3)+(M-k)mz/\lambda_2-1}\int_0^{zt_n}X_{k-1}(s)e^{-\lambda_k s}\,ds\Bigg| > \delta/2\Bigg)$$
$$\leq \frac{4}{\delta^2}\cdot\mathbb{E}\Bigg[\Bigg(n^{\beta(M-2)+\lambda_M v_n^+(\epsilon)/\lambda_2-1}X_k(v_n+\epsilon) - \nu n^{\beta(M-3)+(M-k)mv_n^+(\epsilon)/\lambda_2-1}\int_0^{v_n+\epsilon}X_{k-1}(s)e^{-\lambda_k s}\,ds\Bigg)^2\Bigg].$$

Therefore, it suffices to show that

$$\lim_{n\to\infty}\mathbb{E}\Bigg[\Bigg(n^{\beta(M-2)+\lambda_M v_n^+(\epsilon)/\lambda_2-1}X_k(v_n+\epsilon) - \nu n^{\beta(M-3)+(M-k)mv_n^+(\epsilon)/\lambda_2-1}\int_0^{v_n+\epsilon}X_{k-1}(s)e^{-\lambda_k s}\,ds\Bigg)^2\Bigg] = 0.$$

We can expand the quantity above as follows:

$$\mathbb{E}\Bigg[\Bigg(n^{\beta(M-2)+\lambda_M v_n^+(\epsilon)/\lambda_2-1}X_k(v_n+\epsilon) - \nu n^{\beta(M-3)+(M-k)mv_n^+(\epsilon)/\lambda_2-1}\int_0^{v_n+\epsilon}X_{k-1}(s)e^{-\lambda_k s}\,ds\Bigg)^2\Bigg]$$
$$= n^{2\beta(M-2)+2\lambda_M v_n^+(\epsilon)/\lambda_2-2}\mathbb{E}\left[X_k(v_n+\epsilon)^2\right] - 2\nu n^{\beta(2M-5)+(2\lambda_M-\lambda_k)v_n^+(\epsilon)/\lambda_2-2}\int_0^{v_n+\epsilon}\mathbb{E}\left[X_{k-1}(s)X_k(v_n+\epsilon)\right]e^{-\lambda_k s}\,ds$$
$$+\nu^2 n^{2\beta(M-3)+2\frac{\lambda_M-\lambda_k}{\lambda_2}v_n^+(\epsilon)-2}\int_0^{v_n+\epsilon}\int_0^{v_n+\epsilon}\mathbb{E}\left[X_{k-1}(s)X_{k-1}(y)\right]e^{-\lambda_k(s+y)}\,ds\,dy.$$

By making a slight modification to the proof of Lemma 1 in [18], we have that

$$\mathbb{E}\left[X_k(v_n+\epsilon)^2\right] = (\nu n^{-\beta})^2 \int_0^{v_n+\epsilon}\int_0^{v_n+\epsilon} \mathbb{E}\left[X_{k-1}(s)X_{k-1}(y)\right] e^{\lambda_k(2v_n+2\epsilon-s-y)}\,ds\,dy$$
$$+ \nu n^{-\beta}\int_0^{v_n+\epsilon} \mathbb{E}\left[X_{k-1}(s)\right]\mathbb{E}\left[\tilde{X}_k(v_n+\epsilon-s)^2\right]\,ds$$
$$\mathbb{E}\left[X_{k-1}(s)X_k(v_n+\epsilon)\right] = \nu n^{-\beta}\int_0^{v_n+\epsilon} \mathbb{E}\left[X_{k-1}(s)X_{k-1}(y)\right] e^{-\lambda_k(v_n+\epsilon-y)}\,dy$$

where $\tilde{X}_k$ is a binary branching process starting from size one with birth rate r_k and death rate d_k. Substituting these expressions into our equation yields

$$\mathbb{E}\Bigg[\Bigg(n^{\beta(M-2)+\lambda_M v_n^+(\epsilon)/\lambda_2-1}X_k(v_n+\epsilon)$$
$$-\nu n^{\beta(M-3)+(M-k)mv_n^+(\epsilon)/\lambda_2-1}\int_0^{v_n+\epsilon} X_{k-1}(s)e^{-\lambda_k s}\,ds\Bigg)^2\Bigg]$$
$$= \nu^2 n^{2\beta(M-3)+\frac{2\lambda_M v_n^+(\epsilon)}{\lambda_2}-2}\int_0^{v_n+\epsilon}\int_0^{v_n+\epsilon} \mathbb{E}\left[X_{k-1}(s)X_{k-1}(y)\right] e^{\lambda_k(2v_n+2\epsilon-s-y)}\,ds\,dy$$
$$+\nu n^{\beta(2M-5)+\frac{2\lambda_M v_n^+(\epsilon)}{\lambda_2}-2}\int_0^{v_n+\epsilon} \mathbb{E}\left[X_{k-1}(s)\right]\mathbb{E}\left[\tilde{X}_k(v_n+\epsilon-s)^2\right]\,ds$$
$$-2\nu^2 n^{2\beta(M-3)+\frac{(2\lambda_M-\lambda_k)v_n^+(\epsilon)}{\lambda_2}-2}\int_0^{v_n+\epsilon}\int_0^{v_n+\epsilon} \mathbb{E}\left[X_{k-1}(s)X_{k-1}(y)\right] e^{\lambda_k(v_n+\epsilon-s-y)}\,ds\,dy$$
$$+\nu^2 n^{2\beta(M-3)+\frac{2(\lambda_M-\lambda_k)v_n^+(\epsilon)}{\lambda_2}-2}\int_0^{v_n+\epsilon}\int_0^{v_n+\epsilon} \mathbb{E}\left[X_{k-1}(s)X_{k-1}(y)\right] e^{-\lambda_k(s+y)}\,ds\,dy.$$

Then, by definition of $v_n^+(\epsilon)$,

$$
\begin{aligned}
&\mathbb{E}\Bigg[\Bigg(n^{\beta(M-2)+\lambda_M v_n^+(\epsilon)/\lambda_2-1}X_k(v_n+\epsilon)\\
&\quad-\nu n^{\beta(M-3)+(M-k)mv_n^+(\epsilon)/\lambda_2-1}\int_0^{v_n+\epsilon}X_{k-1}(s)e^{-\lambda_k s}\,ds\Bigg)^2\Bigg]\\
&\qquad=\nu^2 n^{2\beta(M-3)-2}e^{-2\lambda_M(v_n+\epsilon)}\int_0^{v_n+\epsilon}\int_0^{v_n+\epsilon}\mathbb{E}\left[X_{k-1}(s)X_{k-1}(y)\right]e^{\lambda_k(2v_n+2\epsilon-s-y)}\,ds\,dy\\
&\qquad\qquad+\nu n^{\beta(2M-5)-2}e^{-2\lambda_M(v_n+\epsilon)}\int_0^{v_n+\epsilon}\mathbb{E}\left[X_{k-1}(s)\right]\mathbb{E}\left[\tilde{X}_k(v_n+\epsilon-s)^2\right]\,ds\\
&\qquad-2\nu^2 n^{2\beta(M-3)-2}e^{(\lambda_k-2\lambda_M)(v_n+\epsilon)}\int_0^{v_n+\epsilon}\int_0^{v_n+\epsilon}\mathbb{E}\left[X_{k-1}(s)X_{k-1}(y)\right]e^{\lambda_k(v_n+\epsilon-s-y)}\,ds\,dy\\
&\qquad\qquad+\nu^2 n^{2\beta(M-3)-2}e^{2(\lambda_k-\lambda_M)(v_n+\epsilon)}\int_0^{v_n+\epsilon}\int_0^{v_n+\epsilon}\mathbb{E}\left[X_{k-1}(s)X_{k-1}(y)\right]e^{-\lambda_k(s+y)}\,ds\,dy\\
&\qquad=\nu^2 n^{2\beta(M-3)-2}e^{2(\lambda_k-\lambda_M)(v_n+\epsilon)}\int_0^{v_n+\epsilon}\int_0^{v_n+\epsilon}\mathbb{E}\left[X_{k-1}(s)X_{k-1}(y)\right]e^{-\lambda_k(s+y)}\,ds\,dy\\
&\qquad\qquad+\nu n^{\beta(2M-5)-2}e^{-2\lambda_M(v_n+\epsilon)}\int_0^{v_n+\epsilon}\mathbb{E}\left[X_{k-1}(s)\right]\mathbb{E}\left[\tilde{X}_k(v_n+\epsilon-s)^2\right]\,ds\\
&\qquad-2\nu^2 n^{2\beta(M-3)-2}e^{2(\lambda_k-\lambda_M)(v_n+\epsilon)}\int_0^{v_n+\epsilon}\int_0^{v_n+\epsilon}\mathbb{E}\left[X_{k-1}(s)X_{k-1}(y)\right]e^{-\lambda_k(s+y)}\,ds\,dy\\
&\qquad\qquad+\nu^2 n^{2\beta(M-3)-2}e^{2(\lambda_k-\lambda_M)(v_n+\epsilon)}\int_0^{v_n+\epsilon}\int_0^{v_n+\epsilon}\mathbb{E}\left[X_{k-1}(s)X_{k-1}(y)\right]e^{-\lambda_k(s+y)}\,ds\,dy\\
&\qquad=\nu n^{\beta(2M-5)-2}e^{-2\lambda_M(v_n+\epsilon)}\int_0^{v_n+\epsilon}\mathbb{E}\left[X_{k-1}(s)\right]\mathbb{E}\left[\tilde{X}_k(v_n+\epsilon-s)^2\right]\,ds.
\end{aligned}
$$

Note that

$$
\begin{aligned}
\mathbb{E}\left[X_{k-1}(s)\right]&=\nu^{k-3}n^{1-(k-3)\beta}(-1)^{k-1}S_{k-1}(s),\\
\mathbb{E}\left[\tilde{X}_k(v_n+\epsilon-s)^2\right]&=\frac{2r_k}{\lambda_k}e^{2\lambda_k(v_n+\epsilon-s)}-\frac{r_k+d_k}{\lambda_k}e^{\lambda_k(v_n+\epsilon-s)}.
\end{aligned}
$$

Substituting these into the above expression yields

$$\mathbb{E}\Bigg[\Bigg(n^{\beta(M-2)+\lambda_M v_n^+(\epsilon)/\lambda_2-1}X_k(v_n+\epsilon)$$
$$-\nu n^{\beta(M-3)+(M-k)mv_n^+(\epsilon)/\lambda_2-1}\int_0^{v_n+\epsilon}X_{k-1}(s)e^{-\lambda_k s}\,ds\Bigg)^2\Bigg]$$
$$=\nu n^{\beta(2M-5)-2}e^{-2\lambda_M(v_n+\epsilon)}\cdot$$
$$\int_0^{v_n+\epsilon}\nu^{k-3}n^{1-(k-3)\beta}(-1)^{k-1}S_{k-1}(s)\left(\frac{2r_k}{\lambda_k}e^{2\lambda_k(v_n+\epsilon-s)}-\frac{r_k+d_k}{\lambda_k}e^{\lambda_k(v_n+\epsilon-s)}\right)ds$$
$$=\nu^{k-2}n^{\beta(2M-k-2)-1}e^{-2\lambda_M(v_n+\epsilon)}(-1)^{k-1}\left[\frac{2r_k}{\lambda_k}e^{2\lambda_k(v_n+\epsilon)}\int_0^{v_n+\epsilon}\sum_{i=2}^{k-1}\frac{e^{(\lambda_i-2\lambda_k)s}}{P_{i,k-1}}\,ds\right.$$
$$\left.-\frac{r_k+d_k}{\lambda_k}e^{\lambda_k(v_n+\epsilon)}\int_0^{v_n+\epsilon}\sum_{i=2}^{k-1}\frac{e^{(\lambda_i-\lambda_k)s}}{P_{i,k-1}}\,ds\right]$$
$$=\nu^{k-2}n^{\beta(2M-k-2)-1}(-1)^{k-1}e^{-2\lambda_M(v_n+\epsilon)}\frac{1}{\lambda_k}\cdot$$
$$\sum_{i=2}^{k-1}\left[\frac{2r_k\left(e^{\lambda_i(v_n+\epsilon)}-e^{2\lambda_k(v_n+\epsilon)}\right)}{(\lambda_i-2\lambda_k)P_{i,k-1}}-\frac{(r_k+d_k)\left(e^{\lambda_i(v_n+\epsilon)}-e^{\lambda_k(v_n+\epsilon)}\right)}{(\lambda_i-\lambda_k)P_{i,k-1}}\right].$$

Now note that

$$\frac{2r_k\left(e^{\lambda_i(v_n+\epsilon)}-e^{2\lambda_k(v_n+\epsilon)}\right)}{(\lambda_i-2\lambda_k)P_{i,k-1}}-\frac{(r_k+d_k)\left(e^{\lambda_i(v_n+\epsilon)}-e^{\lambda_k(v_n+\epsilon)}\right)}{(\lambda_i-\lambda_k)P_{i,k-1}}$$
$$=\frac{2r_k(\lambda_i-\lambda_k)\left(e^{\lambda_i(v_n+\epsilon)}-e^{2\lambda_k(v_n+\epsilon)}\right)-(r_k+d_k)(\lambda_i-2\lambda_k)\left(e^{\lambda_i(v_n+\epsilon)}-e^{\lambda_k(v_n+\epsilon)}\right)}{(\lambda_i-\lambda_k)(\lambda_i-2\lambda_k)P_{i,k-1}}$$
$$=\frac{\lambda_k\left(\lambda_i+2d_k\right)e^{\lambda_i(v_n+\epsilon)}+\left(r_k+d_k\right)\left(\lambda_i-2\lambda_k\right)e^{\lambda_k(v_n+\epsilon)}+2r_k\left(\lambda_k-\lambda_i\right)e^{2\lambda_k(v_n+\epsilon)}}{(\lambda_i-\lambda_k)(\lambda_i-2\lambda_k)P_{i,k-1}}.$$

Substituting this back in, we get

$$
\begin{aligned}
&\mathbb{E}\Bigg[\Bigg(n^{\beta(M-2)+\lambda_M v_n^+(\epsilon)/\lambda_2-1}X_k(v_n+\epsilon)\\
&\quad-\nu n^{\beta(M-3)+(M-k)mv_n^+(\epsilon)/\lambda_2-1}\int_0^{v_n+\epsilon}X_{k-1}(s)e^{-\lambda_k s}\,ds\Bigg)^2\Bigg]\\
&\qquad=\nu^{k-2}n^{\beta(2M-k-2)-1}(-1)^{k-1}e^{-2\lambda_M(v_n+\epsilon)}\frac{1}{\lambda_k}\cdot\\
&\qquad\sum_{i=2}^{k-1}\frac{\lambda_k\left(\lambda_i+2d_k\right)e^{\lambda_i(v_n+\epsilon)}+\left(r_k+d_k\right)\left(\lambda_i-2\lambda_k\right)e^{\lambda_k(v_n+\epsilon)}+2r_k\left(\lambda_k-\lambda_i\right)e^{2\lambda_k(v_n+\epsilon)}}{(\lambda_i-\lambda_k)(\lambda_i-2\lambda_k)P_{i,k-1}}\\
&\qquad\sim\frac{\nu^{k-2}n^{\beta(2M-k-2)-1}(-1)^{k-1}e^{-2\lambda_M(v_n+\epsilon)}}{\lambda_k(\lambda_{k-1}-\lambda_k)(\lambda_{k-1}-2\lambda_k)P_{k-1,k-1}}\cdot\\
&\qquad\left[(r_k+d_k)(\lambda_{k-1}-2\lambda_k)e^{\lambda_k(v_n+\epsilon)}+2r_k(\lambda_k-\lambda_{k-1})e^{2\lambda_k(v_n+\epsilon)}\right].
\end{aligned}
$$

Since $v_n=\tilde{v}_n t_n=-\frac{\tilde{v}_n}{\lambda_2}\log n$,

$$
\begin{aligned}
&\mathbb{E}\Bigg[\Bigg(n^{\beta(M-2)+\lambda_M v_n^+(\epsilon)/\lambda_2-1}X_k(v_n+\epsilon)\\
&\quad-\nu n^{\beta(M-3)+(M-k)mv_n^+(\epsilon)/\lambda_2-1}\int_0^{v_n+\epsilon}X_{k-1}(s)e^{-\lambda_k s}\,ds\Bigg)^2\Bigg]\\
&\qquad\sim\frac{\nu^{k-2}n^{\beta(2M-k-2)-1}(-1)^{k-1}e^{-2\lambda_M\epsilon}e^{\frac{2\lambda_M\tilde{v}_n}{\lambda_2}\log n}}{\lambda_k(\lambda_{k-1}-\lambda_k)(\lambda_{k-1}-2\lambda_k)P_{k-1,k-1}}\cdot\\
&\qquad\left[(r_k+d_k)(\lambda_{k-1}-2\lambda_k)e^{\lambda_k\epsilon}e^{\frac{\lambda_k\tilde{v}_n}{-\lambda_2}\log n}+2r_k(\lambda_k-\lambda_{k-1})e^{2\lambda_k\epsilon}e^{\frac{2\lambda_k\tilde{v}_n}{-\lambda_2}\log n}\right]\\
&\qquad=\frac{\nu^{k-2}(-1)^{k-1}e^{-2\lambda_M\epsilon}}{\lambda_k(\lambda_{k-1}-\lambda_k)(\lambda_{k-1}-2\lambda_k)P_{k-1,k-1}}\cdot\\
&\qquad\Big[(r_k+d_k)(\lambda_{k-1}-2\lambda_k)e^{\lambda_k\epsilon}n^{\beta(2M-k-2)-1+(2\lambda_M-\lambda_k)\tilde{v}_n/\lambda_2}\\
&\qquad\quad+2r_k(\lambda_k-\lambda_{k-1})e^{2\lambda_k\epsilon}n^{\beta(2M-k-2)-1+2(\lambda_M-\lambda_k)\tilde{v}_n/\lambda_2}\Big].
\end{aligned}
$$

Note that

$$\begin{aligned}\frac{2\lambda_M - \lambda_k}{\lambda_2} &= \frac{2(\lambda_2 + (M-2)m) - (\lambda_2 + (k-2)m)}{\lambda_2} \\ &= 1 + \frac{m(2M-k-2)}{\lambda_2}.\end{aligned}$$

Therefore,

$$\begin{aligned}\lim_{n\to\infty} n^{\beta(2M-k-2)-1+(2\lambda_M-\lambda_k)\tilde{v}_n/\lambda_2} &= \lim_{n\to\infty} n^{\beta(2M-k-2)-1+\tilde{v}_n+\frac{m(2M-k-2)}{\lambda_2}\tilde{v}_n} \\ &= \lim_{n\to\infty} e^{\left[\beta(2M-k-2)-1+\tilde{v}_n+\frac{m(2M-k-2)}{\lambda_2}\tilde{v}_n\right]\log n}.\end{aligned}$$

Then, since

$$\begin{aligned}&\lim_{n\to\infty}\left[\beta(2M-k-2)-1+\tilde{v}_n+\frac{m(2M-k-2)}{\lambda_2}\tilde{v}_n\right] \\ &\quad= \beta(2M-k-2)-1-\frac{\lambda_2}{\lambda_M}\beta(M-2)-\frac{m(2M-k-2)}{\lambda_2}\frac{\lambda_2}{\lambda_M}\beta(M-2) \\ &\quad= \beta(2M-k-2)\left(1-\frac{M-2}{\lambda_M}\frac{\lambda_M-\lambda_2}{M-2}\right)-1-\frac{\lambda_2}{\lambda_M}\beta(M-2) \\ &\quad= \frac{\lambda_2}{\lambda_M}\beta(M-k)-1 \\ &\quad< 0,\end{aligned}$$

by Proposition 3, we have that

$$\lim_{n\to\infty} n^{\beta(2M-k-2)-1+(2\lambda_M-\lambda_k)\tilde{v}_n/\lambda_2} = 0.$$

Similarly, note that

$$\begin{aligned}2\frac{\lambda_M - \lambda_k}{\lambda_2} &= 2\frac{(\lambda_2 + (M-2)m) - (\lambda_2 + (k-2)m)}{\lambda_2} \\ &= 2m\frac{M-k}{\lambda_2}.\end{aligned}$$

Therefore,

$$\lim_{n\to\infty} n^{\beta(2M-k-2)-1+2(\lambda_M-\lambda_k)\tilde{v}_n/\lambda_2} = \lim_{n\to\infty} n^{\beta(2M-k-2)-1+2m\frac{M-k}{\lambda_2}\tilde{v}_n}$$
$$= \lim_{n\to\infty} e^{\left[\beta(2M-k-2)-1+2m\frac{M-k}{\lambda_2}\tilde{v}_n\right]\log n}.$$

We also have that

$$\lim_{n\to\infty}\left[\beta(2M-k-2)-1+2m\frac{M-k}{\lambda_2}\tilde{v}_n\right]$$
$$= \beta(2M-k-2)-1-2m\frac{M-k}{\lambda_2}\frac{\lambda_2}{\lambda_M}\beta(M-2) \text{ by Proposition 3}$$
$$= \beta(M-2)+\beta(M-k)-1-2\beta\left(1-\frac{\lambda_2}{\lambda_M}\right)(M-k)$$
$$= \beta(M-2)-1+\beta(M-k)\left(2\frac{\lambda_2}{\lambda_M}-1\right).$$

Since $\beta(M-k)(2\lambda_2/\lambda_M-1)<0$ and $\beta<1/(M-2)$, the above limit is negative, and hence

$$\lim_{n\to\infty} n^{\beta(2M-k-2)-1+2(\lambda_M-\lambda_k)\tilde{v}_n/\lambda_2} = 0.$$

So we are done.

□

References

[1] Charles Sawyers. Targeted cancer therapy. *Nature*, 432(7015):294, 2004.

[2] David E Gerber. Targeted therapies: a new generation of cancer treatments. *American family physician*, 77(3), 2008.

[3] Junjie Li, Feng Chen, Marlein Miranda Cona, Yuanbo Feng, Uwe Himmelreich, Raymond Oyen, Alfons Verbruggen, and Yicheng Ni. A review on various targeted anticancer therapies. *Targeted oncology*, 7(1):69–85, 2012.

[4] Min Huang, Aijun Shen, Jian Ding, and Meiyu Geng. Molecularly targeted cancer therapy: some lessons from the past decade. *Trends in pharmacological sciences*, 35(1):41–50, 2014.

[5] William Pao, Vincent A Miller, Katerina A Politi, Gregory J Riely, Romel Somwar, Maureen F Zakowski, Mark G Kris, and Harold Varmus. Acquired resistance of lung adenocarcinomas to gefitinib or erlotinib is associated with a second mutation in the egfr kinase domain. *PLoS medicine*, 2(3):e73, 2005.

[6] JH Goldie and AJ Coldman. Quantitative model for multiple levels of drug resistance in clinical tumors. *Cancer treatment reports*, 67(10):923–931, 1983.

[7] James H Goldie and Andrew J Coldman. The genetic origin of drug resistance in neoplasms: implications for systemic therapy. *Cancer research*, 44(9):3643–3653, 1984.

[8] Andrew J Coldman and JM Murray. Optimal control for a stochastic model of cancer chemotherapy. *Mathematical biosciences*, 168(2):187–200, 2000.

[9] Yoh Iwasa, Franziska Michor, and Martin A Nowak. Evolutionary dynamics of escape from biomedical intervention. *Proceedings of the Royal Society of London B: Biological Sciences*, 270(1533):2573–2578, 2003.

[10] Natalia L Komarova and Dominik Wodarz. Drug resistance in cancer: principles of emergence and prevention. *Proceedings of the National Academy of Sciences of the United States of America*, 102(27):9714–9719, 2005.

[11] Natalia L Komarova and Dominik Wodarz. Effect of cellular quiescence on the success of targeted cml therapy. *PLoS One*, 2(10):e990, 2007.

[12] Natalia Komarova. Stochastic modeling of drug resistance in cancer. *Journal of theoretical biology*, 239(3):351–366, 2006.

[13] Natalia L Komarova, Allen A Katouli, and Dominik Wodarz. Combination of two but not three current targeted drugs can improve therapy of chronic myeloid leukemia. *PLoS One*, 4(2):e4423, 2009.

[14] Jasmine Foo and Franziska Michor. Evolution of resistance to targeted anti-cancer therapies during continuous and pulsed administration strategies. *PLoS computational biology*, 5(11):e1000557, 2009.

[15] Jasmine Foo and Franziska Michor. Evolution of resistance to anti-cancer therapy during general dosing schedules. *Journal of theoretical biology*, 263(2):179–188, 2010.

[16] Juliann Chmielecki, Jasmine Foo, Geoffrey R Oxnard, Katherine Hutchinson, Kadoaki Ohashi, Romel Somwar, Lu Wang, Katherine R Amato, Maria Arcila, Martin L Sos, et al. Optimization of dosing for egfr-mutant non–small cell lung cancer with evolutionary cancer modeling. *Science translational medicine*, 3(90):90ra59–90ra59, 2011.

[17] Jasmine Foo, Juliann Chmielecki, William Pao, and Franziska Michor. Effects of pharmacokinetic processes and varied dosing schedules on the dynamics of acquired resistance to erlotinib in egfr-mutant lung cancer. *Journal of Thoracic Oncology*, 7(10):1583–1593, 2012.

[18] Jasmine Foo, Kevin Leder, et al. Dynamics of cancer recurrence. *The Annals of Applied Probability*, 23(4):1437–1468, 2013.

[19] Dietmar W Siemann. The unique characteristics of tumor vasculature and preclinical evidence for its selective disruption by tumor-vascular disrupting agents. *Cancer treatment reviews*, 37(1):63–74, 2011.

[20] Shannon M Mumenthaler, Jasmine Foo, Nathan C Choi, Nicholas Heise, Kevin Leder, David B Agus, William Pao, Franziska Michor, and Parag Mallick. The impact of microenvironmental heterogeneity on the evolution of drug resistance in cancer cells. *Cancer informatics*, 14:CIN–S19338, 2015.

[21] Olivier Trédan, Carlos M Galmarini, Krupa Patel, and Ian F Tannock. Drug resistance and the solid tumor microenvironment. *Journal of the National Cancer Institute*, 99(19):1441–1454, 2007.

[22] Lori A Hazlehurst, Terry H Landowski, and William S Dalton. Role of the tumor microenvironment in mediating de novo resistance to drugs and physiological mediators of cell death. *Oncogene*, 22(47):7396, 2003.

[23] Kenneth H Shain, Terry H Landowski, and William S Dalton. The tumor microenvironment as a determinant of cancer cell survival: a possible mechanism for de novo drug resistance. *Current opinion in oncology*, 12(6):557–563, 2000.

[24] William S Dalton. The tumor microenvironment as a determinant of drug response and resistance. *Drug Resistance Updates*, 2(5):285–288, 1999.

[25] Akihiro Tomida and Takashi Tsuruo. Drug resistance mediated by cellular stress response to the microenvironment of solid tumors. *Anti-cancer drug design*, 14(2):169–177, 1999.

[26] Rutger Hermsen, J Barrett Deris, and Terence Hwa. On the rapidity of antibiotic resistance evolution facilitated by a concentration gradient. *Proceedings of the National Academy of Sciences*, 109(27):10775–10780, 2012.

[27] Qiucen Zhang, Guillaume Lambert, David Liao, Hyunsung Kim, Kristelle Robin, Chih-kuan Tung, Nader Pourmand, and Robert H Austin. Acceleration of emergence of bacterial antibiotic resistance in connected microenvironments. *Science*, 333(6050):1764–1767, 2011.

[28] Michael Hockel and Peter Vaupel. Tumor hypoxia: definitions and current clinical, biologic, and molecular aspects. *Journal of the National Cancer Institute*, 93(4):266–276, 2001.

[29] Andrew I Minchinton and Ian F Tannock. Drug penetration in solid tumours. *Nature Reviews Cancer*, 6(8):583, 2006.

[30] Joseph J Casciari, Stratis V Sotirchos, and Robert M Sutherland. Variations in tumor cell growth rates and metabolism with oxygen concentration, glucose concentration, and extracellular ph. *Journal of cellular physiology*, 151(2):386–394, 1992.

[31] RA Gatenby, K Smallbone, PK Maini, F Rose, J Averill, RB Nagle, L Worrall, and RJ Gillies. Cellular adaptations to hypoxia and acidosis during somatic evolution of breast cancer. *British journal of cancer*, 97(5):646, 2007.

[32] Jen Jen Yeh and William Y Kim. Targeting tumor hypoxia with hypoxia-activated prodrugs. *Journal of Clinical Oncology*, 33(13):1505–1508, 2015.

[33] William A Denny. The role of hypoxia-activated prodrugs in cancer therapy. *The lancet oncology*, 1(1):25–29, 2000.

[34] Jessica D Sun, Qian Liu, Jingli Wang, Dharmendra Ahluwalia, Damien Ferraro, Yan Wang, Jian-Xin Duan, W Steve Ammons, John G Curd, Mark D Matteucci, et al. Selective tumor hypoxia targeting by hypoxia-activated prodrug th-302 inhibits tumor growth in preclinical models of cancer. *Clinical cancer research*, 18(3):758–770, 2012.

[35] Jinsong Hu, Damian R Handisides, Els Van Valckenborgh, Hendrik De Raeve, Eline Menu, Isabelle Vande Broek, Qian Liu, Jessica D Sun, Ben Van Camp, Charles P Hart, et al. Targeting the multiple myeloma hypoxic niche with th-302, a hypoxia-activated prodrug. *Blood*, 116(9):1524–1527, 2010.

[36] Roger M Phillips. Targeting the hypoxic fraction of tumours using hypoxia-activated prodrugs. *Cancer chemotherapy and pharmacology*, 77(3):441–457, 2016.

[37] Fanying Meng, James W Evans, Deepthi Bhupathi, Monica Banica, Leslie Lan, Gustavo Lorente, Jian-Xin Duan, Xiaohong Cai, Alexandra M Mowday, Christopher P Guise, et al. Molecular and cellular pharmacology of the hypoxia-activated prodrug th-302. *Molecular cancer therapeutics*, pages molcanther–0634, 2011.

[38] Christopher P Guise, Alexandra M Mowday, Amir Ashoorzadeh, Ran Yuan, Wan-Hua Lin, Dong-Hai Wu, Jeff B Smaill, Adam V Patterson, and Ke Ding. Bioreductive prodrugs as cancer therapeutics: targeting tumor hypoxia. *Chinese journal of cancer*, 33(2):80, 2014.

[39] Shannon M Mumenthaler, Jasmine Foo, Kevin Leder, Nathan C Choi, David B Agus, William Pao, Parag Mallick, and Franziska Michor. Evolutionary modeling of combination treatment strategies to overcome resistance to tyrosine kinase inhibitors in non-small cell lung cancer. *Molecular pharmaceutics*, 8(6):2069–2079, 2011.

[40] Jasmine Foo and Franziska Michor. Evolution of acquired resistance to anti-cancer therapy. *Journal of theoretical biology*, 355:10–20, 2014.

[41] Allen A Katouli and Natalia L Komarova. Optimizing combination therapies with existing and future cml drugs. *PloS one*, 5(8):e12300, 2010.

[42] Ivana Bozic, Johannes G Reiter, Benjamin Allen, Tibor Antal, Krishnendu Chatterjee, Preya Shah, Yo Sup Moon, Amin Yaqubie, Nicole Kelly, Dung T Le, et al. Evolutionary dynamics of cancer in response to targeted combination therapy. *elife*, 2, 2013.

[43] William Pao, Vincent Miller, Maureen Zakowski, Jennifer Doherty, Katerina Politi, Inderpal Sarkaria, Bhuvanesh Singh, Robert Heelan, Valerie Rusch, Lucinda Fulton, et al. Egf receptor gene mutations are common in lung cancers from "never smokers" and are associated with sensitivity of tumors to gefitinib and erlotinib. *Proceedings of the National Academy of Sciences of the United States of America*, 101(36):13306–13311, 2004.

[44] DA Haber, DW Bell, R Sordella, EL Kwak, N Godin-Heymann, SV Sharma, TJ Lynch, and J Settleman. Molecular targeted therapy of lung cancer: Egfr mutations and response to egfr inhibitors. In *Cold Spring Harbor symposia on quantitative biology*, volume 70, pages 419–426. Cold Spring Harbor Laboratory Press, 2005.

[45] Román Pérez-Soler, Abraham Chachoua, Lisa A Hammond, Eric K Rowinsky, Mark Huberman, Daniel Karp, James Rigas, Gary M Clark, Pedro Santabárbara, and Philip Bonomi. Determinants of tumor response and survival with erlotinib in patients with non—small-cell lung cancer. *Journal of clinical oncology*, 22(16):3238–3247, 2004.

[46] Gregory J Riely, Mark G Kris, Binsheng Zhao, Tim Akhurst, Daniel T Milton, Erin Moore, Leslie Tyson, William Pao, Naiyer A Rizvi, Lawrence H Schwartz, et al. Prospective assessment of discontinuation and reinitiation of erlotinib or gefitinib in patients with acquired resistance to erlotinib or gefitinib followed by the addition of everolimus. *Clinical cancer research*, 13(17):5150–5155, 2007.

[47] Andrew J Weickhardt, Benjamin Scheier, Joseph Malachy Burke, Gregory Gan, Xian Lu, Paul A Bunn Jr, Dara L Aisner, Laurie E Gaspar, Brian D Kavanagh, Robert C Doebele, et al. Local ablative therapy of oligoprogressive disease prolongs disease control by tyrosine kinase inhibitors in oncogene-addicted non–small-cell lung cancer. *Journal of Thoracic Oncology*, 7(12):1807–1814, 2012.

[48] Geoffrey R Oxnard, Peter Lo, David Michael Jackman, Mohit Butaney, Stephanie Heon, Bruce E Johnson, Lecia V Sequist, and Pasi A Janne. Delay of chemotherapy through use of post-progression erlotinib in patients with egfr-mutant lung cancer., 2012.

[49] Lu Xu, Eiki Kikuchi, Chunxiao Xu, Hiromichi Ebi, Dalia Ercan, Katherine A Cheng, Robert Padera, Jeffrey A Engelman, Pasi A Jänne, Geoffrey I Shapiro, et al. Combined egfr/met or egfr/hsp90 inhibition is effective in the treatment of lung cancers codriven by mutant egfr containing t790m and met. *Cancer research*, 72(13):3302–3311, 2012.

[50] Lucia Regales, Yixuan Gong, Ronglai Shen, Elisa de Stanchina, Igor Vivanco, Aviva Goel, Jason A Koutcher, Maria Spassova, Ouathek Ouerfelli, Ingo K Mellinghoff, et al. Dual targeting of egfr can overcome a major drug resistance mutation in mouse models of egfr mutant lung cancer. *The Journal of clinical investigation*, 119(10):3000–3010, 2009.

[51] Peter Vaupel, Michael Höckel, and Arnulf Mayer. Detection and characterization of tumor hypoxia using po2 histography. *Antioxidants & redox signaling*, 9(8):1221–1236, 2007.

[52] Hilary A Coller, Konstantin Khrapko, Natalya D Bodyak, Ekaterina Nekhaeva, Pablo Herrero-Jimenez, and William G Thilly. High frequency of homoplasmic mitochondrial dna mutations in human tumors can be explained without selection. *Nature genetics*, 28(2):147, 2001.

[53] David J Araten, David W Golde, Rong H Zhang, Howard T Thaler, Lucia Gargiulo, Rosario Notaro, and Lucio Luzzatto. A quantitative measurement of the human somatic mutation rate. *Cancer research*, 65(18):8111–8117, 2005.

[54] Michael D Prados, Kathleen R Lamborn, Susan Chang, Eric Burton, Nicholas Butowski, Mary Malec, Ami Kapadia, Jane Rabbitt, Margaretta S Page, Ann Fedoroff, et al. Phase 1 study of erlotinib hcl alone and combined with temozolomide in patients with stable or recurrent malignant glioma. *Neuro-oncology*, 8(1):67–78, 2006.

[55] AC Mita, K Papadopoulos, MJA De Jonge, G Schwartz, J Verweij, MM Mita, A Ricart, Q SC Chu, AW Tolcher, L Wood, et al. Erlotinib 'dosing-to-rash': a phase ii intrapatient dose escalation and pharmacologic study of erlotinib in previously treated advanced non-small cell lung cancer. *British journal of cancer*, 105(7):938, 2011.

[56] Glen J Weiss, Jeffrey R Infante, E Gabriela Chiorean, Mitesh J Borad, Johanna C Bendell, Julian R Molina, Raoul Tibes, Ramesh K Ramanathan, Karen Lewandowski, Suzanne F Jones, et al. Phase 1 study of the safety, tolerability, and pharmacokinetics of th-302, a hypoxia-activated prodrug, in patients with advanced solid malignancies. *Clinical cancer research*, 17(9):2997–3004, 2011.

[57] Jasdeep K Saggar and Ian F Tannock. Activity of the hypoxia-activated prodrug th-302 in hypoxic and perivascular regions of solid tumors and its potential to enhance therapeutic effects of chemotherapy. *International journal of cancer*, 134(11):2726–2734, 2014.

[58] Manuel Hidalgo, Lillian L Siu, John Nemunaitis, Jinee Rizzo, Lisa A Hammond, Chris Takimoto, S Gail Eckhardt, Anthony Tolcher, Carolyn D Britten, Louis Denis, et al. Phase i and pharmacologic study of osi-774, an epidermal growth factor receptor tyrosine kinase inhibitor, in patients with advanced solid malignancies. *Journal of clinical oncology*, 19(13):3267–3279, 2001.

[59] Daniel T Milton, Christopher G Azzoli, Robert T Heelan, Ennapadam Venkatraman, Jorge E Gomez, Mark G Kris, Lee M Krug, William Pao, Naiyer A Rizvi, Megan Dunne, et al. A phase i/ii study of weekly high-dose erlotinib in previously treated patients with nonsmall cell lung cancer. *Cancer*, 107(5):1034–1041, 2006.

[60] Marina Konopleva, Damian R Handisides, Mary Ann Richie, Juliana M Benito, Gautam Borthakur, Elias J Jabbour, Stefan H Faderl, Jorge E Cortes, Stewart Kroll, Michael Andreeff, et al. A phase 1 study of th-302, an investigational hypoxia-targeted drug, in patients with advanced leukemias. *Blood*, 122(21):3920–3920, 2013.

[61] Libo Zhang, Paula Marrano, Bing Wu, Sushil Kumar, Paul Thorner, and Sylvain Baruchel. Combined antitumor therapy with metronomic topotecan and hypoxia-activated prodrug, evofosfamide, in neuroblastoma and rhabdomyosarcoma preclinical models. *Clinical Cancer Research*, 22(11):2697–2708, 2016.

[62] Hassan K Awwad, Mervat El Aggar, Nadia Mocktar, and Mohsin Barsoum. Intercapillary distance measurement as an indicator of hypoxia in carcinoma of the cervix uteri. *International Journal of Radiation Oncology* Biology* Physics*, 12(8):1329–1333, 1986.

[63] James W Baish, Triantafyllos Stylianopoulos, Ryan M Lanning, Walid S Kamoun, Dai Fukumura, Lance L Munn, and Rakesh K Jain. Scaling rules for diffusive drug delivery in tumor and normal tissues. *Proceedings of the National Academy of Sciences*, 108(5):1799–1803, 2011.

[64] Alfred Bahnson, Charalambos Athanassiou, Douglas Koebler, Lei Qian, Tongying Shun, Donna Shields, Hui Yu, Hong Wang, Julie Goff, Tao Cheng, et al. Automated measurement of cell motility and proliferation. *BMC Cell Biology*, 6(1):19, 2005.

[65] William Pao and Juliann Chmielecki. Rational, biologically based treatment of egfr-mutant non-small-cell lung cancer. *Nature Reviews Cancer*, 10(11):760, 2010.

[66] Joy Tang, Rasha Salama, Shirish M Gadgeel, Fazlul H Sarkar, and Aamir Ahmad. Erlotinib resistance in lung cancer: current progress and future perspectives. *Frontiers in pharmacology*, 4:15, 2013.

[67] James S Michaelson, Elkan Halpern, and Daniel B Kopans. Breast cancer: computer simulation method for estimating optimal intervals for screening. *Radiology*, 212(2):551–560, 1999.

[68] Jasmine Foo, Kevin Leder, and Junfeng Zhu. Escape times for branching processes with random mutational fitness effects. *Stochastic Processes and Their Applications*, 124(11):3661–3697, 2014.

[69] Richard Durrett and Stephen Moseley. Evolution of resistance and progression to disease during clonal expansion of cancer. *Theoretical population biology*, 77(1):42–48, 2010.